



Developmental osteology of *Ictalurus punctatus* and *Noturus gyrinus* (Siluriformes: Ictaluridae) with a discussion of siluriform bone homologies

Kole M. Kubicek¹

¹ Department of Ecology and Conservation Biology, Texas A&M University, College Station, TX 77843, USA

<http://zoobank.org/94783E0B-0B9C-4DA9-A1EA-4626F05A5450>

Corresponding author: Kole M. Kubicek (kolekubicek@gmail.com)

Academic editor Ralf Britz | Received 1 April 2022 | Accepted 19 July 2022 | Published 12 August 2022

Citation: Kubicek KM (2022) Developmental osteology of *Ictalurus punctatus* and *Noturus gyrinus* (Siluriformes: Ictaluridae) with a discussion of siluriform bone homologies. *Vertebrate Zoology* 72 661–727. <https://doi.org/10.3897/vz.72.e85144>

Abstract

The skeleton of Siluriformes is characterized by several autapomorphies, including secondary absence, extreme modification, and purported fusion of several ossifications. Although well documented in adults, information on skeletal development in catfishes is relatively sparse and typically focused on particular regions of the skeleton (e.g., Weberian apparatus). To further our understanding of the siluriform skeleton, I document the development of the entire skeleton in two ictalurid species, *Ictalurus punctatus* (channel catfish) and *Noturus gyrinus* (tadpole madtom) from five days pre-hatch to adult. I reexamine the homologies of bones previously hypothesized to represent compound elements in catfishes as well as an additional element only known to occur in some ictalurids. Development of the skeleton is complete in *I. punctatus* at 22.4 mm SL and almost complete in *N. gyrinus* (except dorsal- and anal-fin distal radials) at 14.1 mm SL. No signs of ontogenetic fusion were observed in any of the purported compound elements. Previous hypotheses of the homology of these elements and of additional ossifications are reviewed in light of developmental information obtained herein. No dermal parietal component is present at any stage in the so-called parieto-supraoccipital. The bone is the supraoccipital which ossifies from two lateral centers of ossification which later fuse, rather than from a median center. The ‘posttemporo-supracleithrum’ originates from a single center of ossification and represents the supraacleithrum. The posttemporal is present in ictalurids and many other catfishes as a canal-bearing bone between the supraacleithrum and the pterotic, a bone sometimes identified as the extrascapular. The extrascapular is missing in catfishes. Ictalurids have an additional dermal bone above the posttemporal, which is either an independently ossifying fragment of the posttemporal or a neoformation restricted to some members of this family. The single chondral bone of the pectoral girdle originates from a single center of ossification that represents the coracoid. The scapula is missing in catfishes. Dorsal-fin distal radial 2 is absent in catfishes and the foramen of dorsal-fin spine 2 is formed from modifications to the base of the fin-ray itself. Unlike loricarioid catfishes, the urohyal of ictalurids originates solely as an ossification of the sternohyoideus tendons. The anteriormost infraorbital element ossifies from a single center of ossification around the infraorbital sensory canal and represents the lacrimal. The antorbital is missing in catfishes. Finally, skeletal development of *I. punctatus* is compared to that available for other otophysans, including the cypriniforms *Danio rerio* and *Enteromius holotaenia* and the characiform *Salminus brasiliensis*.

Keywords

Catfish, Morphology, Ontogeny, Otophysi, Skeleton, Teleostei

Introduction

The order Siluriformes (catfishes) are a highly diverse (~3900 species, Nelson et al. 2016; Fricke et al. 2022) group of otophysan fishes that are distributed in freshwaters across the globe and have invaded marine coastal waters on two separate occasions (Lundberg et al. 2007). Members of this group are found in both pelagic (Reynolds 1971; Kaatz et al. 2010) and benthic environments (Paxton 1997; Mistri et al. 2018), with some species capable of traversing across land to find more suitable habitat (e.g., *Clarias gariepinus*, Johnels 1957). Catfishes also exhibit a wide diversity of life history and reproductive strategies, ranging from broadcast spawners with little or no parental care (Katano 1988; Machata 2007) to nest guards and mouthbrooders with large eggs, in which males protect developing embryos (Mayden et al. 1980; Barbieri et al. 1992). Given this ecological diversity, it is no surprise that siluriforms also show a remarkable amount of morphological variation in body shape (ranging from anguilliform [e.g., Clariidae; Jansen et al. 2006] to markedly dorsoventrally flattened [e.g., Aspredinidae, Chacidae; Brown and Ferraris 1988; Carvalho and Reis 2020] to thin and elongated, twig-like [e.g., *Farlowella*; Ballen et al. 2016] to shortened and stout bodied [*Corydoras*; Tencatt and Ohara 2016]) and size (ranging from greater than 3 meters in *Siluris glanis* to less than 20 mm in some Neotropical catfishes [e.g., Friel and Lundberg 1996; de Pinna and Winemiller 2000; Copp et al. 2009]).

Despite this remarkable morphological variation, Siluriformes are well characterized as a monophyletic group by several derived skeletal characters, including the secondary absence of several ossifications (e.g., subopercle, intercalar) and the extreme modification of others (e.g., anteriormost pectoral-fin ray, maxilla, metapterygoid) (Fink and Fink 1981). Catfishes also possess several ossifications that have been proposed to be the result of ontogenetic (developmental) fusion of two bones that are separate in other teleosts. For example, the dermal, paired parietals and the chondral, median supraoccipital are thought to fuse during development to form a single bone in the adult, referred to as the parieto-supraoccipital (Arratia 1987). Although some evidence has been presented in favor of this hypothesis (Bamford 1948; Arratia et al. 1978; Arratia and Menu-Marque 1981; Arratia and Gayet 1995), it has been formulated based on the observation of only a small number of developmental stages representing a limited number of species. This is also the case for several other skeletal elements that are hypothesized to represent compound elements, including the posttemporo-supracleithrum (Fink and Fink 1981), the scapulocoracoid (Stark 1930; Arratia 2003b), urohyal (Arratia and Schultze 1990; Geerinckx et al. 2011), and lacrimal (de Pinna et al. 2020). Although the suspected compound nature of these elements appears to be generally accepted among the majority of researchers working with the catfish skeleton (e.g., Geerinckx et al. 2007; Birindelli et al. 2008; Calegari et al. 2019), the homology

of these “compound” bones has yet to be adequately addressed and several independent research groups have adopted different terms for these elements (e.g., de Pinna et al. 2007; Lundberg et al. 2017; Slobodian and Pastana 2018), perhaps due to uncertainty regarding homology or because of difference of opinion.

The highly modified skeleton of catfishes has been the subject of numerous detailed osteological investigations (e.g., Alexander 1966; Lundberg and Baskin 1969; Rao and Lakshmi 1984; Arratia 2003a, b; Huysentruyt and Adriaens 2005; Rodiles-Hernández et al. 2005; Egge 2007; Vigliotta 2008; Britz et al. 2014; Carvalho and Reis 2020); however, the majority of these studies have focused on adult individuals with relatively fewer examining the earliest stages of skeletal development (see below). This is surprising given that one potential way to resolve homology of controversial elements (including the suspected compound ossifications of catfishes) is to follow the ontogenetic trajectory of the elements in question. Typically, elements which are highly modified in adults are conserved in their earliest developmental stages and can be compared to similar developmental stages of other taxa in order to determine their homology (e.g., Britz and Hoffman 2006; Hoffmann and Britz 2006; Hilton and Johnson 2007; Britz and Johnson 2012). In addition to furthering our knowledge of the adult skeleton, studies of development can also reveal novel morphological information for phylogenetic studies (e.g., Johnson 1983; Johnson and Washington 1987; Kubicek and Conway 2016) as well as identify changes in developmental timing (i.e., heterochrony; Mabee and Trendler 1996; Britz and Conway 2009, 2016; Mattox et al. 2016; Conway et al. 2021) that may have played an important role in generating the tremendous morphological diversity that exists among and between the different groups of bony fishes. Though available, studies that have investigated skeletal ontogeny in members of the Siluriformes have focused only on specific regions of the skeleton, such as the cranium (Kindred 1919; Bamford 1948; Geerinckx et al. 2007; Huysentruyt et al. 2011), postcranium (Grande and Shardo 2002), pectoral-fin spine (Reed 1924; Kubicek et al. 2019), or the Weberian apparatus (Coburn and Grubich 1998; Britz and Hoffman 2006; Hoffmann and Britz 2006). To date, no single study has investigated development of the entire skeleton for a single species of catfish.

In order to further our understanding of the catfish skeleton, as well as that of bony fishes more generally, I investigate skeletal development in the ictalurid catfishes *Ictalurus punctatus* and *Noturus gyrinus*. I compile a sequence of ossification for both species, documenting the progression of skeletal development (from the earliest stages of ossification through to later stages), and provide a high-quality photographic atlas illustrating select aspects of skeletal ontogeny for *I. punctatus*. Additionally, the homology of the five bones that have been proposed to represent compound elements in ictalurid catfishes (parieto-supraoccipital, posttemporo-supracleithrum, scapulocoracoid, urohyal, and lacrimal) are discussed in light of developmental information. Finally, a comparison is

made between the ossification sequences produced herein for ictalurid catfishes and those available for other members of the Otophysi.

Methods

Eggs of *Ictalurus punctatus* were obtained from the Texas A&M Aquatic Research and Teaching Facility. Eggs were incubated until hatching, at which point embryos were moved to 5 gal aquaria where they were raised until sampling. Eggs were treated with Paraguard (Seachem Laboratories, Madison, GA) to prevent fungus. Embryos or larvae were sampled daily from 5 days pre-hatch up to 30 days post-hatch (dph) and every third day from 30 dph up to 60 dph. Sampled individuals were euthanized with an overdose of tricaine methanesulfate (MS222) and subsequently fixed in a solution of 10% buffered paraformaldehyde for 24 hr. After fixation, individuals were transferred to a 70% EtOH solution for permanent storage. Adult individuals (N = 8) of *Noturus gyrinus* were collected from the wild (Little Brazos River, Brazos Co., TX, USA) and brought back to the lab where they were sexed and divided (1–2 females per male) between 10 gallon aquaria (pH 7.5–8.0; temperature 26°C ± 1°C). Individuals were fed on a diet of decapsulated brine shrimp eggs, crushed blackworm pellets, and chopped blackworms and maintained for captive spawning. Upon spawning, eggs were collected, incubated, and sampled as described above for *I. punctatus*.

Gross and histological examination

A total of 100 individuals of *Ictalurus punctatus* (7.7 mm notochord length [NL] to 44.9 mm standard length [SL]) and 120 of *Noturus gyrinus* (5.4 mm SL to 26.4 mm SL) were cleared and double-stained (c&s) for bone and cartilage examination. Smaller specimens of *I. punctatus* (< 20 mm SL) were c&s using a modification of the acid-free clearing and staining method of Kimmel and Walker (2007). Under this protocol, specimens were transferred to 90% ETOH solution containing Alizarin red S overnight to stain the bones. Specimens were then rinsed in 70% ETOH, followed by 50% ETOH for 30 minutes each to remove excess Alizarin stain from the tissue. The yolk-sac was removed from larval individuals. Specimens were next stained for cartilage in a solution of 0.02% Alcian Blue/30mM MgCl₂/70% ETOH for 1–8 hrs depending on size before being rinsed overnight in a 30mM MgCl₂/70% ETOH solution. Specimens were next rehydrated through a series of ETOH solutions (50%, 20%) and water before being transferred to a 0.1% trypsin enzyme buffer solution (7:3 ratio of water to saturated borax solution) for clearing. The trypsin enzyme buffer solution has the added benefit of removing the outer layer of skin, the goblet cells in which take up Alcian blue.

Specimens were next bleached in a 0.1% KOH solution with ~5 drops of 30% hydrogen peroxide under strong light until the pigment has been nearly removed. This was followed by a rinse in enzyme buffer solution without trypsin to remove excess bleaching solution. Specimens were next worked through a series of KOH/90% glycerol solutions (30%, 50%, 70%) containing Alizarin red S in order to re-stain any skeletal elements that had lost stain during the c&s process and to ensure no further loss of stain. Finally, specimens were transferred to a 90% glycerol solution for permanent storage. Larger individuals of *I. punctatus* (~20 mm SL and larger) and all specimens of *N. gyrinus* were c&s following the protocol of Taylor and Van Dyke (1985).

Once c&s, specimens were dissected and scored for the presence/absence of 328 (*I. punctatus*) and 286 (*N. gyrinus*) ossified skeletal elements under a ZEISS SteREO Discovery V20 stereomicroscope. For each individual specimen, bones were considered present at the first sign of alizarin red S staining and absent in the absence of alizarin red S staining. In the few cases in which it was not possible to confirm through stereomicroscopy whether a particular bone was stained with alizarin red S, specimens were examined at higher magnification using a Zeiss Primo Star compound microscope. The cartilage staining of Taylor and Van Dyke's (1985) c&s protocol relies on an acidic solution which has previously been reported to negatively affect the staining of bone (Walker and Kimmel 2007), which could hinder the identification of bony elements, particularly during the earliest stages of development. In order to compensate for this as well as ensure that scoring of double-stained individuals was accurate, a small number of individuals of each species (45 *I. punctatus* [8.6 mm NL–21.2 mm SL] and 38 *N. gyrinus* [5.8 mm SL–13.1 mm SL]) were cleared and single stained with alizarin red S following the protocol of Taylor (1967), and scored for the presence and absence of bone. Bone presence/absence data of skeletal elements collected from double- or single-stained specimens were highly congruent and compiled in Microsoft Excel©. The length of the smallest individual in which a particular ossification was observed amongst the sampled individuals (minimum length) and the minimum length at which a particular ossification was observed in all sampled individuals (fixed length) was determined for each bony element to generate the sequence of ossification for the entire skeleton, as well as individual regions of the skeleton (Figs. 1–4; following Cubbage and Mabee 1996; Bird and Mabee 2003; Mattox et al. 2014). Select individuals (and dissected parts thereof) were photographed using a ZEISS Axiocam MRc5 digital camera attached to a ZEISS SteReo Discovery V20 stereomicroscope. Heads were removed from select specimens of *I. punctatus* and prepared for serial sectioning. Dissected heads were decalcified and prepared for embedding in paraffin following the protocol of Pinion et al. (2021). Sagittal sections, 9 µm thick, were cut and affixed to albumenized slides. Slides were stained with Eosin and Hematoxylin (following Kiernan 1990). Select stained sections were photographed using a Zeiss Axiocam MRc5 digital

camera attached to a Zeiss Primo Star compound microscope. The adult stage of *I. punctatus* was examined in three specimens (426 mm SL–441 mm SL) prepared as dry skeletons, dissected and photographed with a Nikon D850 DSLR camera equipped with Nikon AF-S Micro NIKKOR 60mm lens. All images were processed using Adobe Photoshop CS5.1 and Illustrator CS5.1. Terminology of cartilages follows de Beer (1937). Osteological terminology follows that of Egge (2007). Weberian apparatus terminology follows that of Bridge and Hadron (1893) and Chranilov (1927) except that the term *os suspensorium* is used in its original sense as defined by Sørensen (1890) and the terms inner arm of *os suspensorium* and outer arm of *os suspensorium* are used instead of *os suspensorium* and transverse process/parapophysis respectively following Fukushima (1992). Pectoral-fin spine terminology follows that of Kubicek et al. (2019). The caudal-fin skeleton of teleosts, including catfishes, has been extensively studied (Lundberg and Baskin 1969; de Pinna and Ng 2004; Schultze and Arratia 2013; Cumplido et al. 2020); however, the homology of the ural centra relative to that of other teleosts remains unclear. To prevent confusion regarding homology, the two ural centra are referred to as the anterior ural centrum and posterior ural centrum. The term membrane bone here-in follows Patterson (1977) and is used to refer to endoskeletal ossifications that are not preformed in cartilage. Sensory canal pores associated with particular skeletal elements were determined by counting individual pores in branches of the cephalic sensory canal from anterior to posterior. For example, the first anterior most infraorbital sensory canal pore was counted as infraorbital sensory canal pore 1.

Neuromast staining

Variation in the number and position of canal neuromasts was studied in four members of the Ictaluridae (*Ameiurus melas*, *Ictalurus punctatus*, *Noturus gyrinus*, *Pylodictis olivaris*) and other catfishes representing the families Callichthyidae (*Corydoras panda*), Loricariidae (*Ancistrus* sp.), Mochokidae (*Synodontis nigriventris*), Pimelodidae (*Pimelodus pictus*), and Siluridae (*Kryptopterus vitreolus*). Specimens of aforementioned ictalurids were collected from the wild (Little Brazos River, Brazos Co., TX, USA) and members of other families were obtained via the ornamental aquarium fish trade. Canal neuromasts were stained in live individuals following the protocol of Nakae et al. (2012). The staining solution was prepared in 400ml volumes (instead of 800ml as recommended by Nakae et al. 2012). Specimens were euthanized immediately after staining in a solution of aquarium water containing a lethal dose of MS222 and then observed under a ZEISS SteReo Discovery V20 stereomicroscope equipped with a Nightsea Stereo Microscope Fluorescence adapter (royal blue excitation 440–460 nm emission 500 nm LP GFP filter). Resulting images were processed using Adobe Photoshop CS5.1 and Illustrator CS5.1.

Material examined

The following specimens, listed alphabetically by family, genus and species were examined during the course of this study. For each species, the collection numbers along with the total number of individuals from each lot examined and the size range of those specimens are listed. Individuals examined are whole mount c&s unless otherwise denoted. Institutional abbreviations follow Sabaj (2020).

Amblycipitidae: *Amblyceps cerinum*, UMMZ 248835, 2 examined (ex.), 67.4–74.1 mm SL; *Amblyceps mangois*, UMMZ 244866, 2 ex., 36.5–37.8 mm SL; *Liobagrus somjinensis*, TCWC uncat., 1 ex., 42.8 mm SL. — Amphiliidae: *Amphilius uranoscopus*, CU 93740, 2 ex., 41.8–55.8 mm SL; CU 95213, 1 ex., 41.7 mm SL. — Anchariidae: *Ancharius fuscus*, AMNH 93702, 1 ex., 88.4 mm SL. — Ariidae: *Ariopsis felis*, TCWC 19690.02, 2 ex., 61.8–80.7 mm SL; *Arius jordani*, TCWC 19740.01, 2 ex., 50.0–51.1 mm SL; *Bagre marinus*, TCWC 547.07, 1 ex., 79.7 mm SL. — Aspredinidae: *Bunocephalus* sp., TCWC 19741.01, 2 ex., 33.8–43.4 mm SL; *Pseudobunocephalus lundbergi*, ANSP 168810, 5 ex., 20.1–22.7 mm SL. — Astroblepidae: *Astroblepus* sp., CU 78735, 2 ex., 32.1–54.4 mm SL; CU 78811, 2 ex., 27.8–30.0 mm SL. — Auchenipteridae: *Tatia intermedia*, TCWC 19752.01, 4 ex., 37.6–60.8 mm SL; *Trachycorystes* sp., FMNH 85945, 3 ex., 55.7–65.8 mm SL. — Auchenoglanididae: *Auchenoglanis occidentalis*, CU 90478, 2 ex., 26.4–35.8 mm SL. — Austroglanididae: *Austroglanis gilli*, ANSP 177966, 1 ex., 71.8 mm SL — Bagridae: *Pseudomystus siamensis*, CAS 94782, 5 ex., 35.5–58.0 mm SL. — Callichthyidae: *Corydoras panda*, TCWC 19753.01, 6 ex., 8.7–18.9 mm SL; TCWC 20491.02, 1 stained for neuromast (neuro.), 32.0 mm SL. — Cetopsidae: *Helogenes marmoratus*, ANSP 175833, 1 ex., 50.7 mm SL; ANSP 177185, 4 ex., 30.9–36.7 mm SL. — Chacidae: *Chaca chaca*, UMMZ 208728, 1 ex., 156.0 mm SL. — Clariidae: *Clarias batrachus*, UMMZ 217578, 3 ex., 99.7–105.2 mm SL; *Clarias gariepinus* TCWC 15276.09, 2 ex., 62.5–71.3 mm SL. — Claroteidae: *Chrysichthys mabusi*, CU 91692, 2 ex., 58.0–80.7 mm SL. — Cranoglanididae: *Cranoglanis boudierius*, CAS-SU 69758, 1 ex., 97.0 mm SL. — Diplomystidae: *Diplomystes chilensis*, AMNH 55327, 1 ex., 64.4 mm SL; *Diplomystes papillosus*, CAS 81539, 1 ex., 118.0 mm SL. — Doradidae: *Ossanocora punctata*, TCWC 16723.16, 2 ex., 34.9–51.8 mm SL; *Platydoras armatulus*, TCWC 19754.01, 1 ex., 45.1 mm SL. — Heptateridae: *Goeldiella eques*, ANSP 177187, 2 ex., 99.2–104.5 mm SL. — Heteropneustidae: *Heteropneustes fossilis*, CAS 29627, 2 ex., 122.3–123.2 mm SL. — Horabagridae: *Horabagrus brachysoma*, TCWC 19755.01, 2 ex., 53.2–56.1 mm SL. — Ictaluridae: *Ameiurus melas* TCWC 15355.08, 1 ex., 66.0 mm SL; TCWC 20490.01, 1 neuro., 45.0 mm SL; *Ictalurus furcatus* TCWC 19756.01, 4 ex., 64.9–70.8 mm SL; *Ictalurus punctatus*, TCWC 19757.01, 7 ex., 11.7–36.2 mm SL; TCWC 20490.02, 1 neuro., 60.0 mm SL; TCWC 20491.04, 100 ex., 7.7 mm NL–44.9 mm SL; TCWC 20491.05, 45 ex., 8.6 mm NL–21.2 mm SL; TCWC 20491.06, 1 skeletal preparation (skel), 426 mm SL; TCWC 20491.07, 1 skel, 436 mm SL; TCWC 20491.08, 1 skel, 441 mm SL; TCWC 20491.03, 1 pectoral fin sectioned, 30.1 mm SL; *Noturus flavus* UAIC 14314.07, 1 ex., 73.4 mm SL; *Noturus gyrinus*, TCWC 15438.13, 1 ex., 41.5 mm SL; TCWC 19758.01, 6 ex., 8.6–36.6 mm SL; TCWC 20490.03, 2 neuro., 25.0 mm SL–27.0 mm SL; TCWC 20491.10, 120 ex., 5.4 mm SL–26.4 mm SL; TCWC 20491.11, 38 ex., 5.8 mm SL–13.1 mm SL. *Pylodictis olivaris* TCWC 7834.10, 1 ex., 61.1 mm SL; TCWC 20490.04, 1 neuro., 56.0 mm SL. — Kryptoglanidae: *Kryptoglanis shajii*, BMNH uncat., 1 ex., 60.0 mm SL — Loricariidae: *Ancistrus* sp., TCWC 19759.01, 5 ex., 5.6–16.5 mm SL;

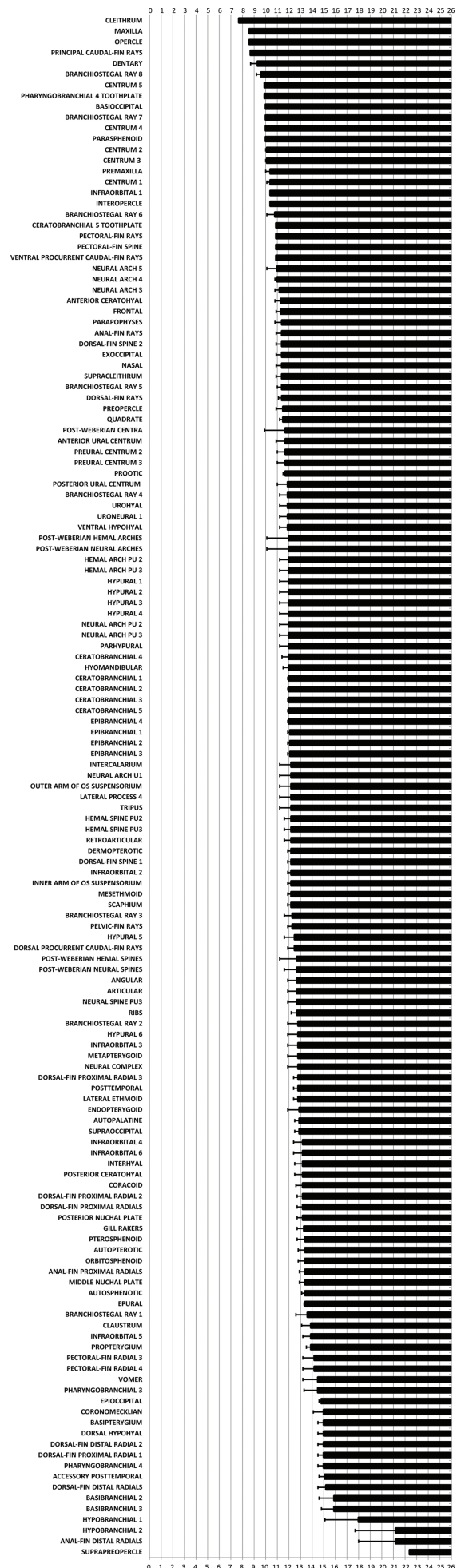
TCWC 20491.01, 2 neuro., 11.0 mm SL–11.6 mm SL; *Hemipsilichthys vestigipinnis*, USNM 314657, 3 ex., 45.2–59.8 mm SL. — Malapteruridae: *Malapterurus oguensis*, CU 92271, 1 ex., 49.9 mm SL; CU 95140, 1 ex., 56.4 mm SL. — Mochokidae: *Microsynodontis* sp., TCWC 19760.01, 1 ex., 26.2 mm SL; *Synodontis* sp., TCWC 20491.13, 2 neuro., 24.0 mm SL–25.0 mm SL. — Nematogenyidae: *Nematogenys inermis*, USNM 84343, 1 ex., 25.8 mm SL. — Pangasiidae: *Pangasius macronema*, CAS 29360, 3 ex., 50.5–66.5 mm SL; UMMZ 214029, 2 ex., 103.9–104.7 mm SL. — Pimelodidae: *Pimelodus ornatus*, LACM 41735.022; LACM 41740.015; *Pimelodus pictus*, TCWC 19761.01, 2 ex., 33.1–37.6 mm SL; TCWC 20491.12, 1 neuro., 42.0 mm SL. — Plotosidae: *Plotosus lineatus*, FMNH 110269, 5 ex., 21.0–66.7 mm SL. — Pseudopimelodidae: *Microglanis poecilus*, AMNH 54973, 2 ex., 23.1–23.9 mm SL. — Ritidae: *Rita rita*, CAS-SU 34866, 1 ex., 85.0 mm SL. — Schilbeidae: *Parailia congica*, AMNH 246178, 2 ex., 60.5–60.8; *Parailia pellucida*, USNM 229794, 3 ex., 29.9–32.3 mm SL; *Schilbe intermedius* TCWC 15286.18, 3 ex., 57.6–72.7 mm SL. — Scoloplacidae: *Scoloplax empousa*, FMNH 108610, 5 ex., 12.8–19.1 mm SL. — Siluridae: *Kryptopterus* sp., TCWC 20491.09, 1 neuro., 43.0 mm SL; *Silurus asotus*, ANSP 185139, 3 ex., 51.2–67.5 mm SL; *Silurus glanis*, BMNH 2005.7.5.944–1034, 4 ex., 17.2–85.0 mm SL; *Wallago attu*, CAS 92824, 2 ex., 69.2–71.0. — Sisoridae: *Glyptothorax sinensis*, UMMZ 246438, 1 ex., 60.7 mm SL; *Parachilognanis hodgarti*, CAS 50170; KU 29549; KU 40556; *Pseudolaguvia kapuri*, CAS 50294, 4 ex., 23.4–26.6 mm SL. — Trichomycteridae: *Henonemus* sp., TCWC 13989.19, 1 ex., 69.7 mm SL; *Trichomycterus hasemani*, ANSP 175851, 3 ex., 13.2–13.9 mm SL.

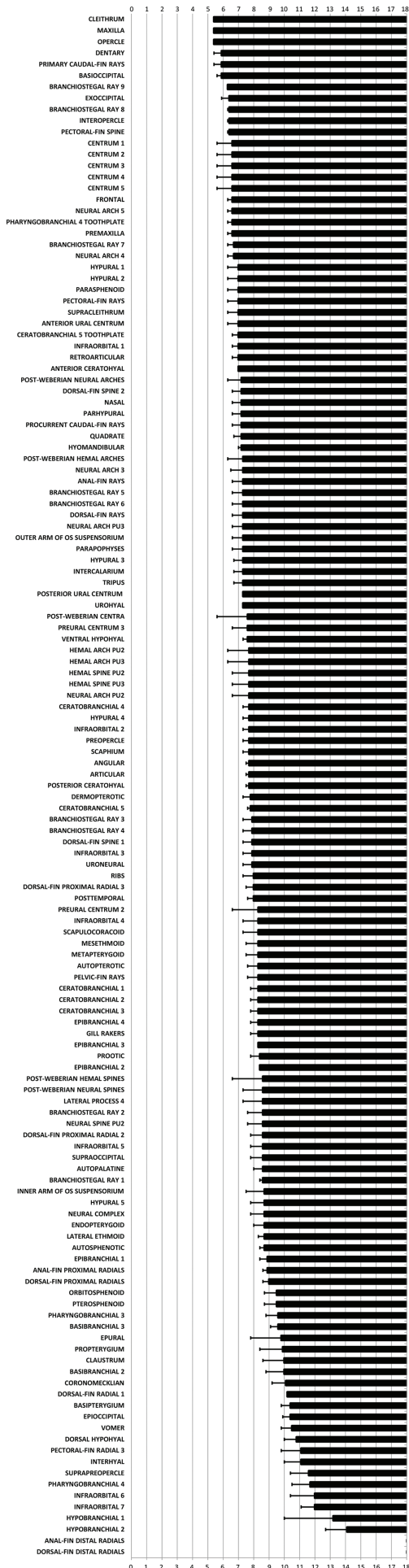
Results

Overview of skeletal development

Approximately 328 and 286 individual elements (not including individual fin rays, gill rakers, or parapophyses) are present in the skeleton of *Ictalurus punctatus* and *Noturus gyrinus*, respectively. The total number of skeletal elements considered herein was condensed to 143 elements in *I. punctatus* and 137 elements in *N. gyrinus* by treating multiple serially repetitive elements as a single element. This included branchiostegal rays, vertebral elements posterior to vertebra 5 (excluding parapophyses and ribs) and anterior to preural vertebra 3, dorsal- and anal-fin proximal and distal radials (excluding dorsal-fin proximal radials 1–3), and post-Weberian ribs. All elements of the skeleton are ossified by 22.4 mm SL in *I. punctatus* (Fig. 1) and 14.1 mm SL in *N. gyrinus* (Fig. 2). The first bone to appear in both species is the cleithrum, which is present in the smallest specimens ex-

Figure 1. Ossification sequence of 143 skeletal elements of *Ictalurus punctatus*. Black bars along horizontal axis represent the length at which a particular ossification is present in all individuals (fixed). Error bars associated with black bars indicate the length at which a particular ossification is present in some but not all individuals. Vertical axis represents length in mm NL/SL.





amined (7.7 mm NL in *I. punctatus* and 5.4 mm SL in *N. gyrinus*) with the maxilla, opercle, dentary and primary caudal-fin rays being the next elements to appear. The last bones to appear in *I. punctatus* include hypobranchial 2, the anal-fin distal radials, and the suprapreopercle. In *N. gyrinus*, the last bones to appear include hypobranchial 2, and the distal radials of the dorsal and anal fins. The dorsal- and anal-fin distal radials of *N. gyrinus* were absent from the developmental series compiled for the species but are present in larger specimens (36.6 mm SL; TCWC 19758.01).

Skeletal development of *Ictalurus punctatus*

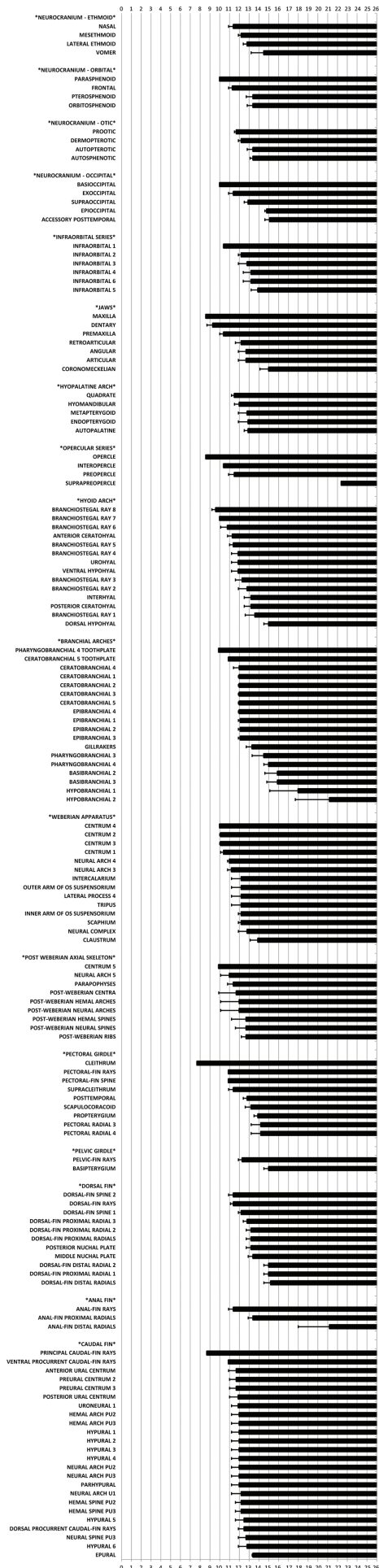
In the following sections, I provide a detailed overview of skeletal development in *Ictalurus punctatus*. A previous description of development for the post-Weberian axial skeleton in *I. punctatus* was provided by Grande and Shardo (2002); however, their descriptions were based on 18 stages determined by the presence of a single character (e.g., presence of hypural 1) and as a result information on timing of ossification in particular elements (e.g., anal-fin proximal and distal radials) was not included. Any discrepancies between our developmental series and the description of Grande and Shardo (2002) are mentioned in the description for the relevant elements. For each region of the skeleton, the sequence of ossification for the bony elements of that region is provided first, followed by a description of development for each individual element in that region. Ossification sequences are arranged based on the length (NL/SL) at which presence of each element becomes fixed. In instances where multiple elements of a region become fixed at the same length, elements are ordered based on length at first appearance (NL/SL) then alphabetically. I conclude each section with a brief overview of skeletal development in *Noturus gyrinus*, including the sequence of ossification for the bony elements of that region, and make note of any differences identified between the two species.

Neurocranium ethmoid region

The most common sequence of ossification: nasal (11.4 mm SL) – mesethmoid (12.2 mm SL) – lateral ethmoid (12.8 mm SL) – vomer (14.5 mm SL) (Figs 5–8).

Nasal. The nasal is a dermal ossification that first appears in some individuals of 10.9 mm SL (Figs 5A, 6A, 7A) as a thin lamina of bone located laterally to the sphenosphenalis commissure. As the ossification expands, it becomes

Figure 2. Ossification sequence of 137 skeletal elements of *Noturus gyrinus*. Black bars along horizontal axis represent the length at which a particular ossification is present in all individuals (fixed). Error bars associated with black bars indicate the length at which a particular ossification is present in some but not all individuals. Vertical axis represents length in mm SL.

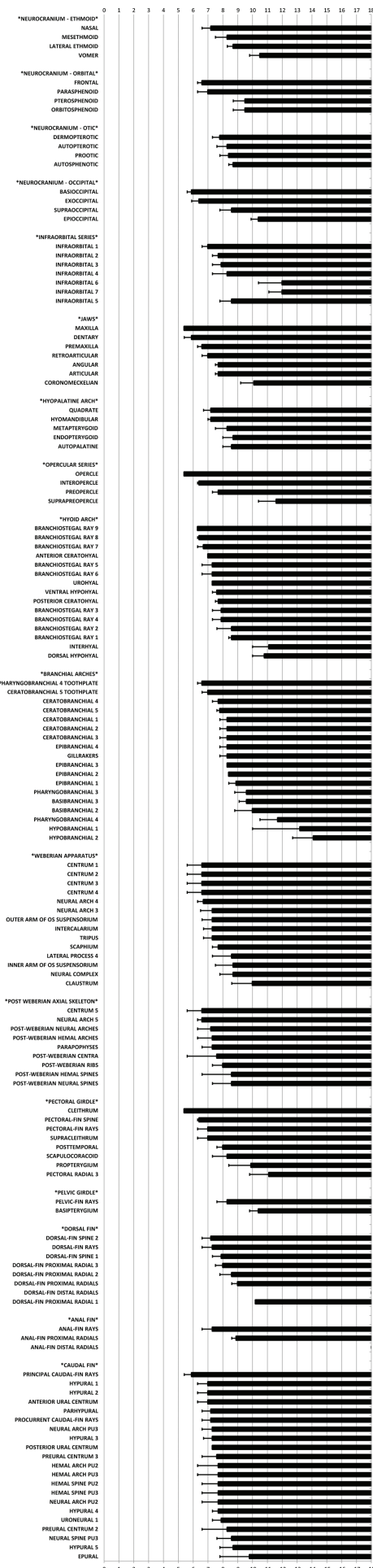


trough-like and extends from just dorsal to the lamina orbitonasalis to the anterior border of the ethmoid plate (12.2 mm SL; Figs 5B, 6B, 7B). The ossification begins to close dorsally forming a tube-like canal; however, a distinct opening in the ossification remains anterolaterally (13.3 mm SL; Fig. 5C) which will eventually become an opening for supraorbital sensory pore 2.

Mesethmoid. The mesethmoid first appears at 11.9 mm SL as a paired perichondral ossification located along the anteriodorsal edge of the ethmoid cornua of the ethmoid plate. By 13.2 mm SL (Figs 5C, 6C, 7C) the bone ossification has expanded ventrally to cover the anteroventral edge of the ethmoid cornua at the point of articulation with the premaxilla and shortly after, at 14.0 mm SL, the perichondral ossification has extended posteriorly along the ethmoid cartilage medial to the nasal capsule. The two separate ossifications continue to expand and, by 15.9 mm SL, meet each other medially over the antero-dorsal surface of the ethmoid plate and fuse. At the same size, small flanges of membrane bone have formed from the tips of the preethmoid cornua which extend towards and are connected to the premaxilla via dense connective tissue. At 18.0 mm SL (Figs 5D, 6D, 7D), the mesethmoid covers much of the ethmoid plate which has begun to ossify endochondrally. By 44.9 mm SL (Figs 5F, 6F, 7F), the mesethmoid is endochondrally ossified and has started to form sutures with the frontals and the lateral ethmoids posterodorsally; however, a large portion of ethmoid cartilage still remains between the mesethmoid and the lateral ethmoids medial to the nasal capsules. Posteroventrally, the mesethmoid extends dorsal to the anteriormost edge of the parasphenoid and the vomer. In the adult (426 mm SL; Fig. 8), the mesethmoid has expanded anteriorly along its connection with the premaxilla with the two extensions of bone almost meeting each other medially. The connection with the premaxilla has become tight and rigid and is difficult to separate. Postero-dorsally, the mesethmoid is strongly sutured to the frontals and forms the anterior most border of the anterior cranial fontanelle and ventrally has formed an additional connection with a small anterior process of the lateral ethmoids. The mesethmoid has grown in width and extends further posteriorly to rim the anteromedial portion of the foramen for the passage of the olfactory nerve (I).

Lateral Ethmoid. The paired lateral ethmoid first appears (12.4 mm SL) as a perichondral ossification of the lamina orbitonasalis at its mid-length near the orbitonasal foramen. At 13.4 mm SL the ossification has expanded on both the anterior and posterior surface of the lamina or-

Figure 3. Ossification sequence of 143 skeletal elements of *Ictalurus punctatus* separated by skeletal region. Black bars along horizontal axis represent the length at which a particular ossification is present in all individuals (fixed). Error bars associated with black bars indicate the length at which a particular ossification is present in some but not all individuals. Vertical axis represents length in mm NL/SL.



bitonasalis, which is pierced by the orbitonasal foramen, which is now completely surrounded by bone. The lateral ethmoid continues to spread towards the taenia marginalis anterior and sphenoseptalis commissure dorsally and the ethmoid plate ventrally, and extends around the lateral edge of the lamina orbitonasalis by 15.9 mm SL. By 18.0 mm SL (Figs 5D, 6D, 7D) the ossification has continued to expand around the posterior border of the olfactory foramen anteriorly and the anterior border of the preoptic fontanelle in the orbit. A thin membrane bone extension of the lateral ethmoid has formed along the anterolateral margin of the perichondral part of the bone forming an anterior rim for the orbit. By 44.9 mm SL (Figs 5F, 6F, 7F), the lateral ethmoid forms the entire anterior wall of the orbit, extending from the ventral surface of the mesethmoid and the frontal dorsally to the parasphenoid ventrally. Posteriorly it borders the orbitosphenoid, which remains separated by the preoptic fontanelle. In the adult condition (426 mm SL; Fig. 8), the lateral ethmoid has continued to expand anteriorly, now meeting the mesethmoid anteriorly and completing the ventral border of the foramen for the passage of the olfactory nerve (I). Posteriorly, the lateral ethmoid has expanded to enclose much of the preoptic fontanelle with only a small opening remaining; however, in some individuals (Fig. 8) the fontanelle remains relatively large.

Vomer. The dermal vomer first appears in some individuals as small as 13.2 mm SL (Figs 6C, 7C) as a thin inverted U-shaped bone located ventrally on the ethmoid plate just anterior to the parasphenoid. At 16.5 mm SL, the lateral edges of the vomer have extended further posteriorly on either side of the parasphenoid. Medially, the vomer has gained a posterior process that extends ventral to the parasphenoid and a shorter rounded anterior process. In adult specimens (Fig. 8), the vomer lies ventral to the overlapping parasphenoid and mesethmoid. The posterior extension of the vomer has become much longer giving the bone its characteristic T-shape and the ventral surface of the bone exhibits sculpturing posteriorly.

Comparison with *Noturus gyrinus*. The most common sequence of ossification for this region in *Noturus gyrinus* is as follows: nasal (7.2 mm SL) – mesethmoid (8.3 mm SL) – lateral ethmoid (8.7 mm SL) – vomer (10.5 mm SL).

No differences in the sequence of ossification were identified between *Noturus gyrinus* and *Ictalurus punctatus* in the ethmoid region of the neurocranium, which is similar in both species and show no major differences in adult morphology.

Figure 4. Ossification sequence of 137 skeletal elements of *Noturus gyrinus* separated by skeletal region. Black bars along horizontal axis represent the length at which a particular ossification is present in all individuals (fixed). Error bars associated with black bars indicate the length at which a particular ossification is present in some but not all individuals. Vertical axis represents length in mm SL.

Neurocranium orbital region

The most common sequence of ossification: parasphenoid (10.0 mm SL) – frontal (11.3 mm SL) – pterosphenoid and orbitosphenoid (13.4 mm SL) (Figs 5–8).

Parasphenoid. The parasphenoid first appears in individuals of 10.0 mm SL as a thin plate of bone of bone running medial to the trabeculae cranii and ventral to a portion of the hypophyseal foramen. By 11.3 mm SL, the parasphenoid has expanded anteriorly and posteriorly, now covering the entirety of the hypophyseal foramen, with both ends tapering in width giving the bone a rhomboid appearance. Posteriorly it extends across the ventral surface of the otic capsule where it stops ventral to the anterior tip of the notochord and anteriorly it reaches the point of the lamina orbitonasalis. Two small ascending processes, represented by thin laminae of bone, have formed along the lateral margin near the widest point of the bone. At 13.3 mm SL (Figs 6C, 7C), the anterior and posterior ends have widened and the posterior margin now overlays the anteroventral surface of the basioccipital, in line with the notochord. The lateral ascending processes have grown larger and are located directly ventral to the newly formed pterosphenoid. The anterior margin of the parasphenoid extends dorsal to the vomer and reaches its anterior edge. At this point, the lateral margin of the parasphenoid posterior to the lateral ascending process has expanded posterodorsally towards the anteroventral border of the prootic. The ascending process continues to expand dorsally towards the pterosphenoid, effectively separating the optico-trigemino-facial foramen into separate optic and trigemino-facial foramina by 21.2 mm SL (Figs 6E, 7E) with the posterior process forming an interdigitating suture with the pterosphenoid by 42.1 mm SL (Figs 6F, 7F).

Frontal. The dermal frontal first appears (10.9 mm SL; Figs 5A, 6A, 7A) as a thin ossification around the frontal portion of the supraorbital sensory canal. It is located medial to the taenia marginalis and extends on both sides of the epiphyseal bar and is more heavily ossified just behind the epiphyseal bar. By 12.2 mm SL (Figs 5B, 6B, 7B), the frontal runs the length of the taenia marginalis reaching the sphenoseptalis commissure anteriorly and the anterior end of the otic capsule posteriorly. The underlying bone supporting the supraorbital canal has expanded medially forming a large flat plate of bone. As the frontal continues to expand, the canal supporting the parietal branch of the supraorbital canal starts to ossify (13.2 mm SL; Figs 5D, 6D). At 15.9 mm SL, the frontals meet each other across the midline at the point of the epiphyseal bar. Posteriorly, the frontal contacts the anterior membrane bone extensions of the supraoccipital and anteriorly it almost reaches the mesethmoid. The ossification surrounding the supraorbital sensory canal are almost completely enclosed at this stage. By 21.2 mm SL (Figs 5E, 6E), the frontal has formed an interdigitating suture with the mesethmoid anteriorly and overlaps the anterior margin of the supraoccipital and autosphenotic.

By 44.9 mm SL (Fig. 5F, 6F), the frontal has started to acquire its typical surface sculpturing and expands medially, reducing the size of the cranial fontanelle. In adults (426 mm SL; Fig. 8) the cranial fontanelles are restricted to very narrow elongate gaps on the dorsal surface of the neurocranium. Additionally, the frontal has ventral extensions of bone which form interdigitating sutures with the orbitosphenoid and pterosphenoid.

Pterosphenoid. The pterosphenoid first appears at 12.7 mm SL as a paired perichondral ossification on the dorsal margin of the common foramen for the passage of the optic (II), trigeminal (V) and facial (VII) nerves, and becomes fixed in development at 13.4 mm SL. By 14.2 mm SL, the perichondral ossification has expanded in size to become semicircular in shape. Membrane bone processes extend ventrally from the perichondral ossification leaving two openings, which (by 15.9 mm SL in most specimens) become surrounded by bone forming the foramina for the passage of the ophthalmic branch of the trigeminal and facial nerves. The bone continues to expand in all directions and by 21.2 mm SL (Figs 6E, 7E) the ventral margin almost reaches the ascending process of the parasphenoid, creating separate optic and trigemino-facial foramina. At 42.1 mm SL (Figs 6F, 7F), it meets the frontal dorsally and has formed an interdigitating suture with the ascending process of the parasphenoid but still remains separate from the orbitosphenoid and autosphenotic by a strip of cartilage. In the adult neurocranium (426 mm SL; Fig. 8), the gap between the pterosphenoid and the orbitosphenoid is closed with the two bones sutured to one another and the pterosphenoid is also sutured to a ventral extension of the frontal. A bony process has formed on the lateral wall of the pterosphenoid where the anterodorsal extension of the hyomandibular firmly attaches.

Orbitosphenoid: The paired orbitosphenoid originates at 12.8 mm SL as a small perichondral ossification along the anterior margin of the common foramen for the passage of the Optic (II), Trigeminal (V) and Facial (VII) nerves, and becomes fixed in development at 13.4 mm SL. The perichondral ossification expands across the cartilage anteriorly and becomes crescentic in appearance by 14.2 mm SL. As the orbitosphenoid grows, it eventually meets its antimere ventrally and the two elements fuse into a single ossification (16.2 mm SL). At 18.0 mm SL (Fig. 6D), the orbitosphenoid has spread to the posterior margin of the preoptic fontanelle, and by 21.2 mm SL (Fig. 6F) a lamina of membrane bone extends anteriorly over part of the fontanelle. The orbitosphenoid continues to grow, replacing much of the cartilage immediately posterior to the lamina orbitonasalis. Interdigitated sutures have started to form with the lateral ethmoid anteriorly, dorsal to the preoptic fontanelle, the pterosphenoid posteriorly and the parasphenoid posteroventrally, dorsal and ventral to the optic foramen, respectively. However, much of its respective border, excluding that with the parasphenoid, remain separated by cartilage. In adults (426 mm SL; Fig. 8) the cartilage surrounding the borders of the orbitosphenoid has been mostly replaced by bone and posterodorsally the

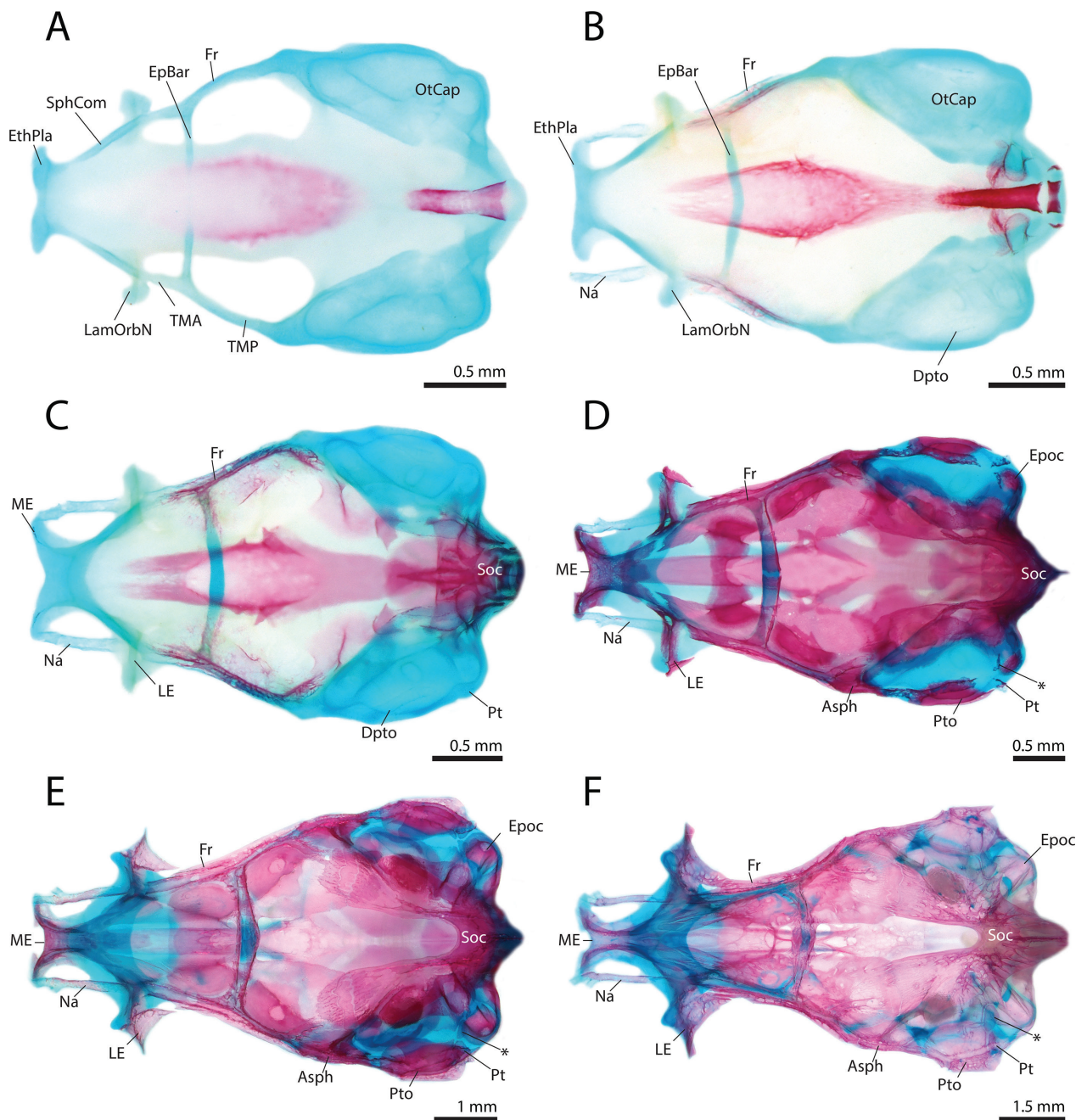


Figure 5. Ontogeny of the neurocranium of *Ictalurus punctatus* in dorsal view. **A** 10.9 mm SL. **B** 12.2 mm SL. **C** 13.3 mm SL. **D** 18.0 mm SL. **E** 21.2 mm SL. **F** 44.9 mm SL. Abbreviations: *, Accessory posttemporal; Asp, Autosphenotic; Dpto, Dermopteric; EpBar, Epiphysal bar; Epoc, Epioccipital; EthPla, Ethmoid plate; Fr, Frontal; LamOrbN, Lamina orbitonasalis; LE, Lateral ethmoid; ME, Mesethmoid; Na, Nasal; OtCap, Otic capsule; Pt, Posttemporal; Pto, Pterotic; Soc, Supraoccipital; SphCom, Sphenoseptalis commissure; TMA, Taenia marginalis anterior; TMP, Taenia marginalis posterior.

orbitosphenoid forms an interdigitated suture with a ventral extension of the vomer. The portion of the preoptic fontanelle bordered by the orbitosphenoid has been completely covered in bone; however, in some individuals a small portion of the preoptic fontanelle extends onto the area of the orbitosphenoid (Fig. 8).

Comparison with *Noturus gyrinus*: The most common sequence of ossification for this region in *Noturus gyrinus* is as follows: frontal (6.6 mm SL) – parasphenoid (7.0 mm SL) – pterosphenooid and orbitosphenoid (9.5 mm SL).

The only difference in the sequence of ossification identified between *Noturus gyrinus* and *Ictalurus punctatus* in the orbital region of the neurocranium is that the frontal appears before the parasphenoid while in *I. punctatus* it appears after the parasphenoid. The orbital region of *N. gyrinus* and *I. punctatus* are otherwise similar, and no major differences in adult morphology are observed in this region.

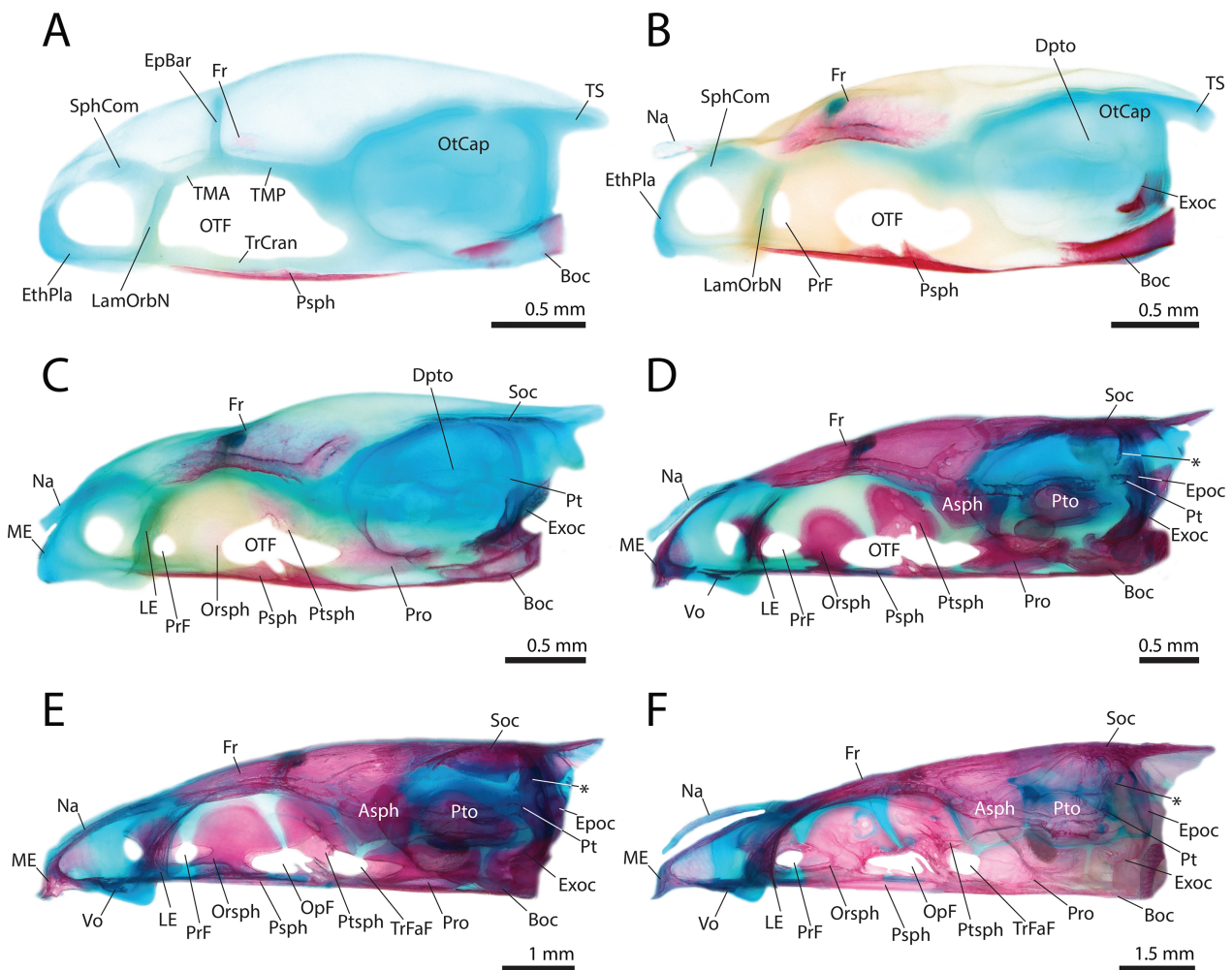


Figure 6. Ontogeny of the neurocranium of *Ictalurus punctatus* in left lateral view. **A** 10.9 mm SL. **B** 12.2 mm SL. **C** 13.3 mm SL. **D** 18.0 mm SL. **E** 21.2 mm SL. **F** 44.9 mm SL. Abbreviations: *, Accessory posttemporal; Asph, Autosphenotic; Boc, Basioccipital; Dpto, Dermopterotic; EpBar, Epiphysial bar; Epoc, Epioccipital; EthPla, Ethmoid plate; Exoc, Exoccipital; Fr, Frontal; LamOrbN, Lamina orbitonasalis; LE, Lateral ethmoid; ME, Mesethmoid; Na, Nasal; OpF, Foramen for the passage of the optic nerve (II); Orsph, Orbitosphenoid; OtCap, Otic capsule; OTF, Common foramen for the passage of the optic (II), trigeminal (V), and Facial (VII) nerves; PrF, Preoptic fontanelle; Pro, Prootic; Psph, Parasphenoid; Pt, Posttemporal; Pto, Pterotic; Ptsph, Pterosphenoid; Soc, Supraoccipital; SphCom, Sphenoseptalis commissure; TMA, Taenia marginalis anterior; TMP, Taenia marginalis posterior; TrCran, Trabecula cranii; TrFaF, Common foramen for the passage of the trigeminal (V) and facial nerves (VII); TS, Tectum synoticum; Vo, Vomer.

Neurocranium otic region

The most common sequence of ossification: prootic (11.7 mm SL) – pterotic (12.2 mm SL) – autosphenotic (13.4 mm SL) (Figs 5–8).

Prootic. The paired chondral prootic is one of the largest bones in the neurocranium. It first appears at 11.5 mm SL as a perichondral ossification on the ventrolateral surface of the otic capsule ventral to the utricular capsule, and is found in all individuals of 11.7 mm SL or larger. The prootic has started to ossify endochondrally and reaches the posterior edge of the common foramen for the passage of the optic (II), trigeminal (V) and facial (VII) nerves anteriorly (13.3 mm SL; Fig. 6C, 7C). It has also expanded to cover part of the anterior surface of the anterior vertical semicircular canal and utricular capsule, as well as the anterior portion of the saccular capsule. At 15.9 mm

SL, the bone has further expanded to contact the parasphenoid ventrally, and a membranous extension covers a posterior portion of the common foramen for the passage of the optic (II), trigeminal (V) and facial (VII) nerves. The prootic increases in size but changes little in shape and by 42.1 mm SL (Fig. 6F, 7F) the surface has become slightly sculptured. It has begun to form an interdigitated suture with the parasphenoid but still remains separate from the neighboring bones by a thin strip of cartilage. In adult specimens (426 mm SL; Fig. 8), the prootic borders the autosphenotic, pterosphenoid, basioccipital and exoccipital forming a solid floor to the braincase. However, a thin strip of cartilage still remains along its dorsal edge, separating the prootic from the pterotic.

Pterotic. The compound pterotic is composed of both chondral (autopterotic) and dermal (dermopterotic) bones. The dermopterotic is the first to appear (11.9 mm SL) on

the posterolateral surface of the otic capsule as two thin, trough shaped ossifications of the pterotic portion of the otic sensory canal. By 13.3 mm SL (Figs 5C, 6C), the autopterotic can be seen as a small perichondral ossification on the lateral surface of the otic capsule, ventral to the dermopterotic. The sensory canal ossifications of the dermopterotic continue to expand towards each other and by 14.2 mm SL they have fused into a single trough of bone leaving an opening in its ventral wall which connects the otic sensory canal to the preoperculo-mandibular sensory canal. At the same stage, the autopterotic is ovoid in appearance and has begun to endochondrally ossify. The autopterotic continues to grow and eventually meets the dermopterotic anterodorsally and the two elements fuse forming the pterotic (15.5 mm SL). Shortly after this (16.2 mm SL), a membranous lamina of bone has started to form along the lateral margin of the pterotic with a small pointed process extending posteriorly past the chondral portion of the bone. Additionally, the pterotic overlies the lateral border of the horizontal semicircular canal. Bone has started to enclose the roof of the pterotic portion of the otic sensory canal by 17.8 mm SL (Figs 5D, 6D) and by 21.2 (Figs 5E, 6E) this canal is fully enclosed. At this stage, the lamina of bone has expanded lateroventrally where it contacts the supraclathrum. Anteriorly, the pterotic has just reached the border of the autosphenotic, although much of the border remains cartilaginous. The sensory canal meets the autosphenotic portion of the otic canal anteriorly, and posteriorly it ends just anterior to the posttemporal. At 42.1 mm SL (Figs 5F, 6F, 7F), the pterotic forms a suture with the supraoccipital dorsally. Posteriorly it meets the posttemporal and lies ventral to a portion of the accessory posttemporal. The pterotic remains separated by cartilage from the epioccipital posteriorly and the exoccipital and the prootic ventrally. The medial surface of the bone forms the lateral surface of the utricular canal and the lateral surface has become slightly sculptured. In the adult condition (426 mm SL; Fig. 8), the prootic forms tight sutures with all of its surrounding bones on the dorsal surface of the neurocranium including the posttemporal, accessory posttemporal and epioccipital; however, a thin strip of cartilage remains between the pterotic and the autosphenotic, prootic, exoccipital and epioccipital along its ventral margin.

Autosphenotic. The autosphenotic first appears at 13.1 mm SL as a perichondral ossification at the junction of the taenia marginalis and the otic capsule. By 14.2 mm SL, the autosphenotic has started to endochondrally ossify and by 15.4 mm SL it covers the anteroventral border of the anterior vertical semicircular canal and has expanded dorsally to the anterodorsal edge of the otic capsule where it meets the frontal. At this stage, a trough shaped ossification of membrane bone arises from the autosphenotic along the sphenotic portion of the otic sensory canal. The roof of the sensory canal has started to form in bone by 17.8 mm SL (Fig. 6D) and is fully enclosed by 21.2 mm SL (Fig. 6E). By 42.1 mm SL (Figs 5F, 6F, 7F), the sphenotic has extended posteriorly and contacts the supraoccipital and the pterotic. Anteriorly the sphenotic

portion of the otic sensory canal ossification joins the infraorbital and supraorbital sensory canals at the border of the sphenotic and the frontal. In the adult neurocranium (426 mm SL; Fig. 8) the autosphenotic contacts and is sutured to the prootic and the pterosphenoid ventrally but otherwise remains mostly unchanged in shape.

Comparison with *Noturus gyrinus*. The most common sequence of ossification for this region in *Noturus gyrinus* is as follows: prootic (8.4 mm SL) – pterotic (7.8 mm SL) – autosphenotic (8.7 mm SL).

No differences in the sequence of ossification were identified between *Noturus gyrinus* and *Ictalurus punctatus* in the otic region of the neurocranium, which is similar in both species and show no major differences in adult morphology.

Neurocranium occipital region

The most common sequence of ossification: basioccipital (10.0 mm SL) – exoccipital (11.4 mm SL) – posttemporal (12.8 mm SL) – supraoccipital (12.9 mm SL) – epioccipital (14.8 mm SL) – accessory posttemporal (15.1 mm SL) (Figs 5–8).

Basioccipital. The basioccipital originates as a perichordal ossification around the anterior tip of the notochord at the base of the cranium (10.0 mm NL). By 12.0 mm SL (Figs 6B, 7B), the entire cranial portion of the notochord is surrounded by a thin ossification. The basioccipital extends lateroventrally from the notochord as a perichondral ossification on the ventral surface of the otic capsule and a small membranous lamina of bone has started to form on the dorsal surface of the perichordal ossification. At 14.2 mm SL, the membranous lamina has expanded anteriorly forming a flat sheet and posteriorly it has formed into a pointed process on either side of the notochord that extends dorsally towards the exoccipital forming part of the posterodorsal wall of the lagenar capsule. Ventrally, the perichondral part of the basioccipital has expanded to form a circular ossification that extends from the back of the cranium to the anteriormost tip of the notochord, forming most of the ventral surface of the saccular capsule and the entirety of the ventral surface of the lagenar capsule. The anterior membranous extension has expanded anterolaterally towards the posteroventral margin of the prootic giving it a triangular appearance (15.4 mm SL). The basioccipital changes little in appearance and shape as it continues to grow, becoming slightly larger and having a sculptured surface (42.1 mm SL; Figs 5F, 6F, 7F). In the adult, it is bordered posterodorsally by the exoccipital and anteriorly by the prootic and parasphenoid.

Exoccipital. The paired exoccipital first appears at 10.9 mm SL (Figs 6A, 7A) and is fixed in development at 11.4 mm SL. It starts as a perichondral ossification around the occipital arches dorsolateral to the notochord. The ossification continues to spread over the occipital arch and by 12.2 mm SL (Figs 6B, 7B) it possesses a lamina of

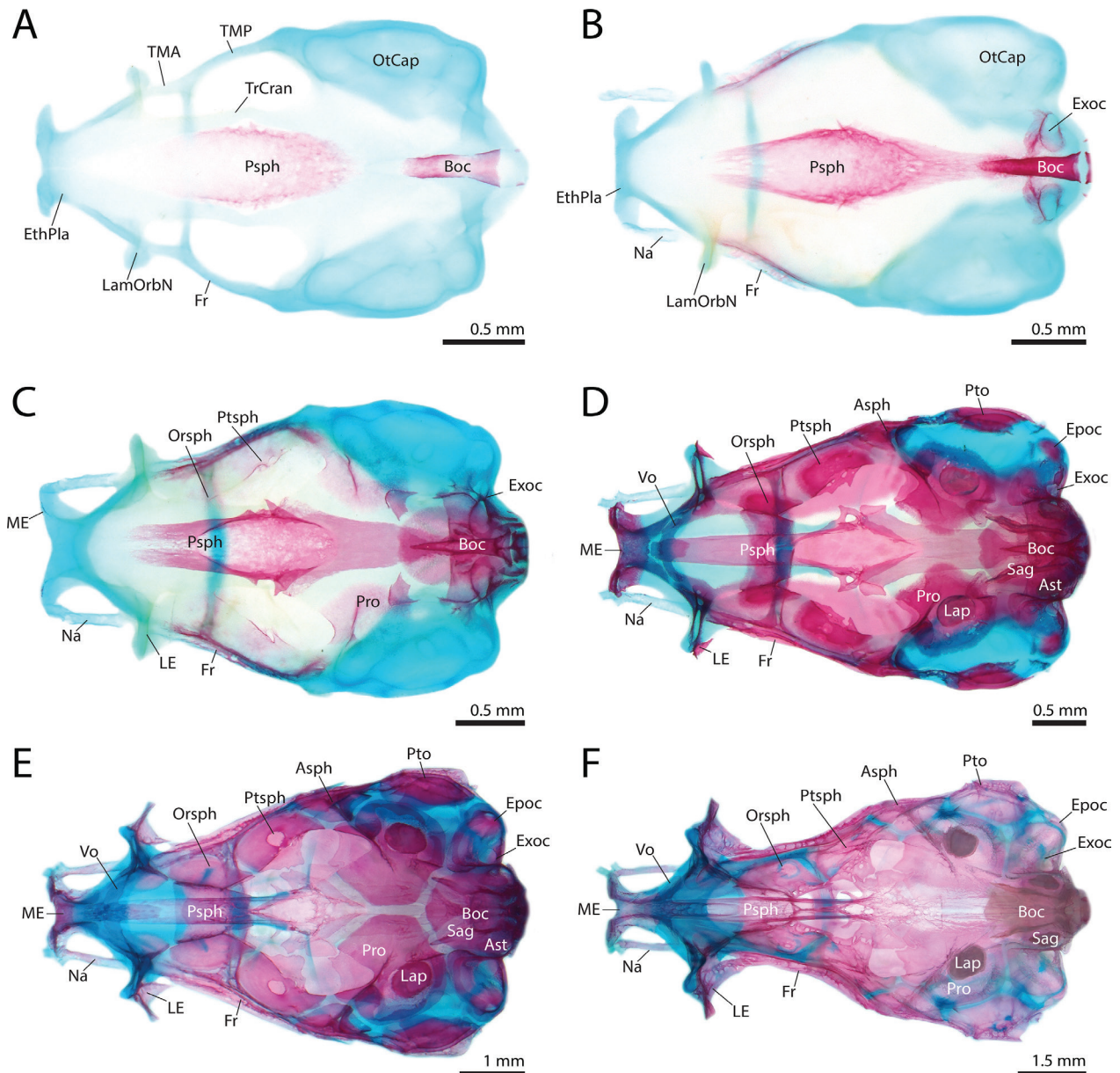


Figure 7. Ontogeny of the neurocranium of *Ictalurus punctatus* in ventral view. **A** 10.9 mm SL. **B** 12.2 mm SL. **C** 13.3 mm SL. **D** 18.0 mm SL. **E** 21.2 mm SL. **F** 44.9 mm SL. Asph, Autosphenotic; Ast, Asteriscus; Boc, Basioccipital; Epoc, Epioccipital; EthPla, Ethmoid plate; Exoc, Exoccipital; Fr, Frontal; LamOrbN, Lamina orbitonasalis; Lap, Lapillus; LE, Lateral ethmoid; ME, Mesethmoid; Na, Nasal; Orsph, Orbitosphenoid; OtCap, Otic capsule; Pro, Prootic; Psph, Parasphenoid; Pto, Pterotic; Ptsph, Pterosphenoid; Sag, Sagitta; Soc, TMA, Taenia marginalis anterior; TMP, Taenia marginalis posterior; TrCran, Trabecula cranii; Vo, Vomer.

membrane bone anteriorly that forms a portion of the roof of the saccular and lagenar capsules. By 13.4 mm SL (Figs 6C, 7C), the exoccipital covers most of the occipital arch forming the lateral margin of the foramen magnum. The posterior margin of the foramen for the passage of the glossopharyngeal (IX) nerve and the entire rim of the foramen for the passage of the vagus (X) nerve are perichondrally ossified. A small membranous extension has formed on the dorsoposterior margin of the exoccipital directly anterior to the *concha* of the *scaphium*. At 15.4 mm SL, the foramina for the glossopharyngeal (IX) and vagal (X) nerves are completely surrounded by the exoccipital. A ventral extension of the lamina of membrane bone along the posterior margin of the exoccipital meets a

similar dorsally directed process of membrane bone from the posteroventral margin of the exoccipital, creating the foramen for an occipital spinal nerve (16.2 mm SL). As the bone continues to expand it forms the lateral wall of the lagenar capsule (18.0 mm SL; Figs 6D, 7D) and at 44.9 mm SL (Figs 6F, 7F) it remains separated from all of the surrounding elements by a strip of cartilage. In adult specimens (426 mm SL; Fig. 8), the exoccipital has met, and formed sutures with, the epioccipital dorsolaterally, prootic anteroventrally and basioccipital ventrally but remains separated from the supraoccipital and pterotic by cartilage. The posterior membranous extension of the exoccipital now contacts the anterior margin of the *claus-trum*.

Posttemporal. The posttemporal can first be observed in 12.4 mm SL individuals as a small weakly ossified trough of bone around the lateral line sensory canal anterior to the supracleithrum and in line with the posterior margin of the chondrocranium. By 16.2 mm SL, the roof of the sensory canal has begun to close with bone and by 21.2 mm SL (Figs 5E, 6E) a small flange of bone has started to form its anterodorsal margin. At 42.1 mm SL (Figs 5F, 6F), the posttemporal is bordered by the pterotic anteriorly, the supracleithrum posteriorly and the accessory posttemporal dorsally. The sensory canal ossification is completely enclosed, forming a tube, but still only weakly ossified. A flange of the posttemporal extends dorsally over the posterior edge of the pterotic towards the accessory posttemporal. In adults (426 mm SL; Fig. 8), the posttemporal has expanded into rhomboid plate of bone. It overlies and forms a suture with the pterotic along its anterior and lateral border and is also sutured to the accessory posttemporal medially, effectively becoming a part of the dorsal surface of the neurocranium.

Supraoccipital. Whether this element is of compound origin (parietal+supraoccipital) or not has been a contentious subject in the past. Herein I refer to the element as the supraoccipital and further discuss the homology of this bone in the discussion. The supraoccipital originates as a pair of perichondral ossifications in the tectum synoticum on either side of the posterior cranial fontanelle (12.5 mm SL first appearance, 12.9 mm SL fixed length). Soon after (13.3 mm SL; Figs 5C, 6C), the paired elements have expanded and are endochondrally ossifying. A small ridge of membrane bone extends laterally from the perichondral ossification over a groove in the otic capsule, which carries an accessory ramus of the facial nerve (VII). This membranous ridge of bone runs the length of the supraoccipital and extends anteriorly beyond the margin of the otic capsule. By 14.1 mm SL, the paired ossifications have met and fused into a single U-shaped bone around the posterior margin of the posterior cranial fontanelle. The ridges of membrane bone on either side of the fontanelle extend posteromedially and meet to form a point at the posterior tip of the tectum synoticum. The anterior membranous extensions have expanded to meet the frontals (15.9 mm SL) with the anterior most margin extending under the posterior edge of the frontals. At this size, the supraoccipital starts to expand around the anterodorsal and posterodorsal margin of the anterior and posterior semicircular canals respectively. The groove for the passage of the accessory ramus of the facial nerve (VII) is completely enclosed in bone leaving a pair of foramina at the back of the cranium through which the nerve passes prior to extending along either side of the body. The posteromedial extensions of membrane bone completely cover the dorsal surface of the tectum synoticum giving the posterior margin of the bone a triangular point which, by 18.0 mm SL, extends beyond the posterior margin of the tectum synoticum and possesses a small vertical extension of membrane bone forming the supraoccipital crest. By 21.2 mm SL (Figs 5E, 6E), the bone still retains the same relative shape but has grown in size,

just meeting the epioccipital posterolaterally. The supraoccipital crest has continued to expand ventrally forming a triangular vertical lamina of bone that extends to the posterior tip of the tectum synoticum. At 42.1 mm SL (Figs 5F, 6F), the supraoccipital forms the posterior third of the cranial roof. It has a strong interdigitating suture with the frontal and now meets the autosphenotic at its anterolateral most corner and the pterotic along most of its lateral border. Posterolaterally, the supraoccipital also contacts the accessory posttemporal and the anterodorsal tip of the supracleithrum, and posteroventrally it still remains separated from the exoccipital by a thin strip of cartilage. Posteriorly the supraoccipital crest forms a connection with the first proximal radial of the dorsal-fin and ventral to this, two anterolateral projections of the neural complex of the Weberian apparatus contact the posterior surface of the supraoccipital. In the adult condition (426 mm SL; Fig. 8), little has changed in its relative shape and size. The supraoccipital now forms an interdigitated suture with the accessory posttemporal and the dorsal surface of the supraoccipital crest has become heavily sculptured.

Epioccipital. The paired chondral epioccipital first appears at 14.6 mm SL in some individuals as a small circular perichondral ossification of the posterior otic capsule just ventral to the tip of the anterior arm of the supracleithrum. It has started to endochondrally ossify by 15.6 mm SL and it continues to increase in size and extends ventrally, becoming more ovoid and covering the posteroventral portion of the posterior vertical semicircular canal of the inner ear (21.2 mm SL; Figs 5E, 6E). By 44.9 mm SL (Figs 5F, 6F, 7F), it has increased in size but changed little in shape and remains separated from all surrounding bones by a thin strip of cartilage except for the supraoccipital which it meets anterodorsally. In adult individuals (426 mm SL; Fig. 8), the epioccipital is now sutured to the exoccipital ventrally and the pterotic laterally. It also forms the ventral surface of a fossa which receives the tip of the dorsal arm of the supraoccipital.

Accessory posttemporal. The homology of this element located on the dorsolateral surface of the cranium in some ictalurids has been contentious in the past (see Lundberg 1975; Fink and Fink 1981; Arratia and Gayet 1995; Slobodian and Pastana 2018). Herein I refer to this element as the accessory posttemporal and further discuss the homology of this element in the discussion. The accessory posttemporal is a small dermal plate-like ossification that first appears at 14.6 mm SL as a small splint of bone anterior to the dorsal tip of the supracleithrum. At 21.2 mm SL (Figs 5E, 6E) it has started to expand anteroventrally and by 42.1 mm SL (Figs 5F, 6F) it forms a plate of bone overlying the anterolateral portion of the border between the supraoccipital and epioccipital. It tapers ventrally to meet the posterodorsal tip of the pterotic and the dorsal margin of the posttemporal. In adults (426 mm SL; Fig. 8) the accessory posttemporal has become a part of the dorsal-surface of the neurocranium and is sutured to the posttemporal laterally, the pterotic anteriorly

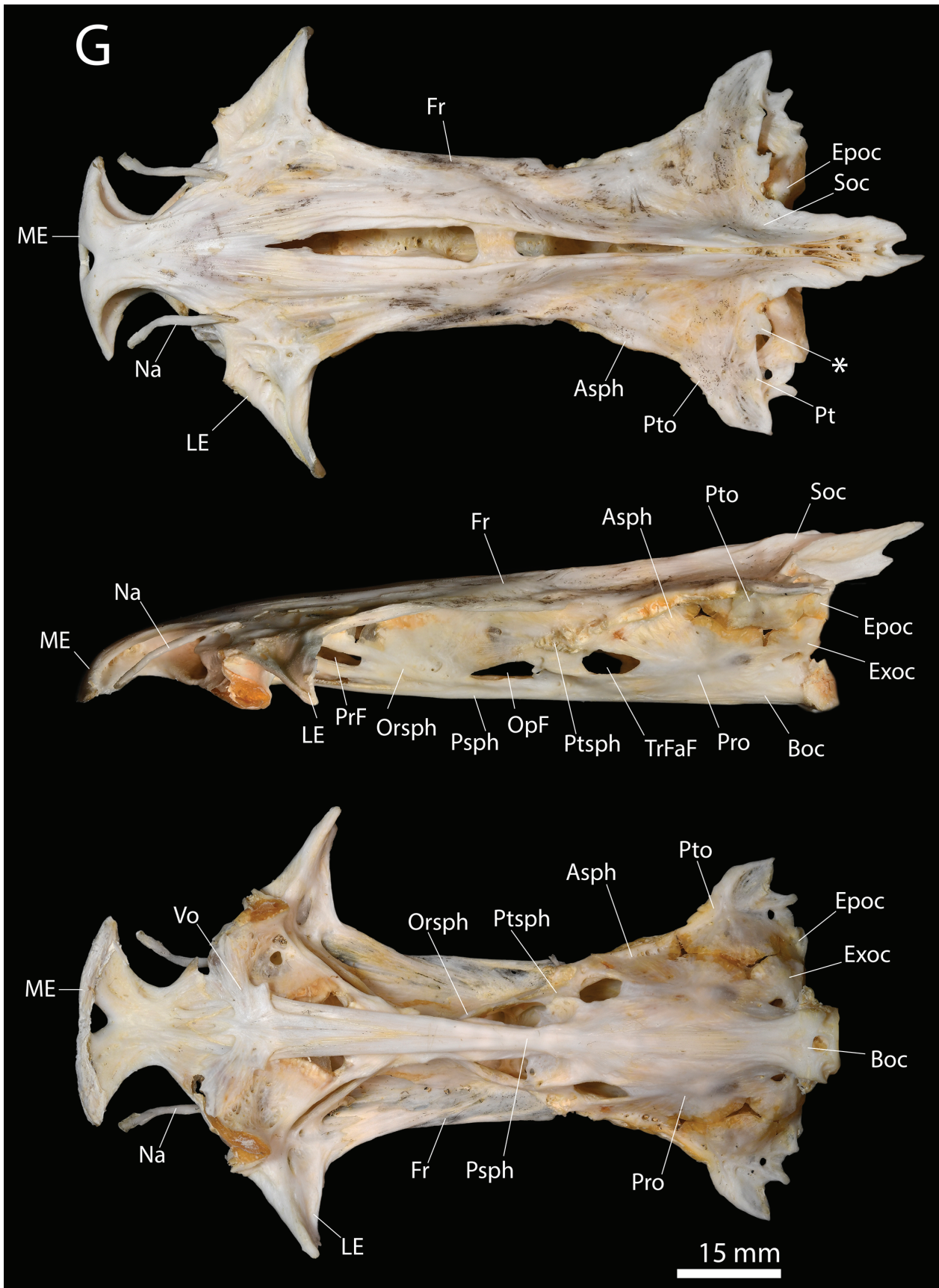


Figure 8. *Ictalurus punctatus*, Neurocranium of specimen TCWC 20491.06, 426 mm SL, in dorsal **A**, lateral **B** and ventral view **C**. Abbreviations: *, Accessory posttemporal; Asph, Autosphenotic; Boc, Basioccipital; Epoc, Epioccipital; Exoc, Exoccipital; Fr, Frontal; LE, Lateral ethmoid; ME, Mesethmoid; Na, Nasal; OpF, Foramen for the passage of the optic nerve (II); Orsph, Orbito-sphenoid; PrF, Preoptic fontanelle; Pro, Prootic; Psph, Parasphenoid; Pt, Posttemporal; Pto, Pterotic; Ptsph, Pterosphenoid; Soc, Supraoccipital; TrFaF, Common foramen for the passage of the trigeminal (V) and facial nerves (VII); Vo, Vomer.

and the supraoccipital medially. It forms the dorsal roof of a fossa which receives the tip of the dorsal arm of the supracleithrum.

Comparison with *Noturus gyrinus*. The most common sequence of ossification for this region in *Noturus gyrinus* is as follows: basioccipital (5.9 mm SL) – exoccipital (6.4 mm SL) – posttemporal (8.0 mm SL) – supraoccipital (8.6 mm SL) – epioccipital (10.4 mm SL).

No differences in the sequence of ossification were identified between *Noturus gyrinus* and *Ictalurus punctatus* in the occipital region of the neurocranium. The occipital region of *N. gyrinus* differs slightly from that of *I. punctatus* in that the accessory posttemporal is absent and the posttemporal consists of only a canal ossification with no laminar portion.

Jaws

The most common sequence of ossification: maxilla (8.6 mm NL) – dentary (9.3 mm NL) – premaxilla (10.4 mm SL) – retroarticular (12.2 mm SL) – anguloarticular (12.7 mm SL) – coronomeckelian (15 mm SL) (Fig. 9).

Maxilla. The paired maxilla is one of the first three elements to ossify in the skeleton of *Ictalurus punctatus* (8.6 mm NL). It starts off as a slightly curved lamina located anteriorly to the *pars autopalatina* that extends laterally to cover the anteroproximal tip of the maxillary barbel cartilage. By 11.3 mm SL (Fig. 9A), the maxilla has become more heavily ossified but overall maintains the same shape. The medial edge is slightly concave and wraps around the lateroventral edge of an anterior process of the *pars autopalatina* while the lateral edge cups the anterior half of the base of the maxillary barbel. Around 17.8 mm SL (Fig., 9D), the dorsalmost and ventralmost points of articulation with the *pars autopalatina* form small extensions of bone, each capped in cartilage, that increase the area of contact for articulation between the two elements. In adults, the maxilla covers the anterior half of the proximal 1/12th of the maxillary barbel cartilage and the lateral most tip ends in a narrow, pointed process.

Dentary. The dentary originates early in development, appearing in specimens as small as 8.7 mm NL as a dermal lamina of bone lateral to Meckel's cartilage. The first few teeth can be seen in specimens of 10.4 mm SL at which point the dentary extends across the length of Meckel's cartilage up to the coronoid process. Shortly after this (11.2 mm SL; Fig. 9A), dermal bone of the mandibular portion of the preoperculo-mandibular sensory canal starts to form as a ventral extension at the mid-length of the dentary. By 12.0 mm SL (Fig. 9B), there are four conical teeth ankylosed to the dentary with several more teeth under development in the adjacent gum tissue (extraosseus). Posteriorly, the dentary has begun to expand towards the coronoid process of Meckel's cartilage dorsally, while ventrally it extends farther, below the anterior edge of the articular surface of the cartilage. The mandibular portion of the preoperculo-mandibular canal

is a trough of bone that spans much of the ventral edge of the dentary before it begins to curve medially. At 14.1 mm SL, bone has started to enclose the roof of the sensory canal and the dentary possesses two distinct rows of conical teeth. The coronoid process of the dentary is fully formed by 17.7 mm SL (Fig. 9D) and the dentary now overlaps the anteriormost portion of the anguloarticular. The mandibular portion of the preoperculo-mandibular sensory canal is fully enclosed by 21.2 mm SL (Fig. 9E), except for four circular openings associated with the preoperculo-mandibular sensory canal pores 2–5. Multiple rows of conical teeth are present on the dentary by 44.9 mm SL (Fig. 9F) and there is minor sculpturing on the coronoid process, closely resembling the adult condition.

Premaxilla. The paired premaxilla originates as small splint of bone located ventral to the tips of the ethmoid cornua (10.1–10.4 mm SL) with the first teeth appearing shortly after this (11.5 mm SL). By 12.4 mm SL (Fig. 9B) the premaxilla has become a wider lamina of bone extending close to the midline of the ethmoid plate and supports 6 conical teeth with additional teeth observed under development. By 14.1 mm SL, there are two distinctive rows of conical teeth present with a third beginning to develop behind them. Although a clear gap is still present between the premaxillae, they are already connected via dense connective tissue. At 15.9 mm SL, these paired bones have become rectangular in shape, support three irregular rows of conical teeth and together span the distance between the medial edges of the *pars autopalatina*. Dorsally, they have a small process that extends towards membranous extensions of the mesethmoid to which they are strongly attached via a dense connective tissue. As the specimens continue to grow, additional rows of teeth are added to the premaxillae, becoming almost brush-like in appearance and the symphysis becomes mostly obscured by the overlying teeth (44.9 mm SL; Fig. 9F). Little changes other than an increase in size in adult individuals (441 mm SL; Fig. 10A) and the premaxilla now forms a tight, rigid connection with its antimeric and the mesethmoid which is very difficult to separate.

Retroarticular. The retroarticular is first observed in specimens of 11.6 mm SL as a perichondral ossification at the point of attachment of the interoperculo-retroarticular ligament on the posteroventral-most tip of Meckel's cartilage. The retroarticular becomes more heavily ossified around the posterior tip of Meckel's cartilage and around 13.0 mm SL (Fig. 9C) it meets and fuses with the anguloarticular to become a compound element. It can still be readily distinguished as a highly ossified cap on the posterior edge of the anguloarticular up to 17.7 mm SL; however, it becomes less apparent in larger sizes until it is no longer distinguishable (21.5 mm SL; Fig. 9E).

Anguloarticular. The anguloarticular is a compound element composed of the dermal angular and the endoskeletal articular, although the two bones were not observed as separate ossifications. The element first appears as an ossification on the dorsal edge of Meckel's cartilage pos-

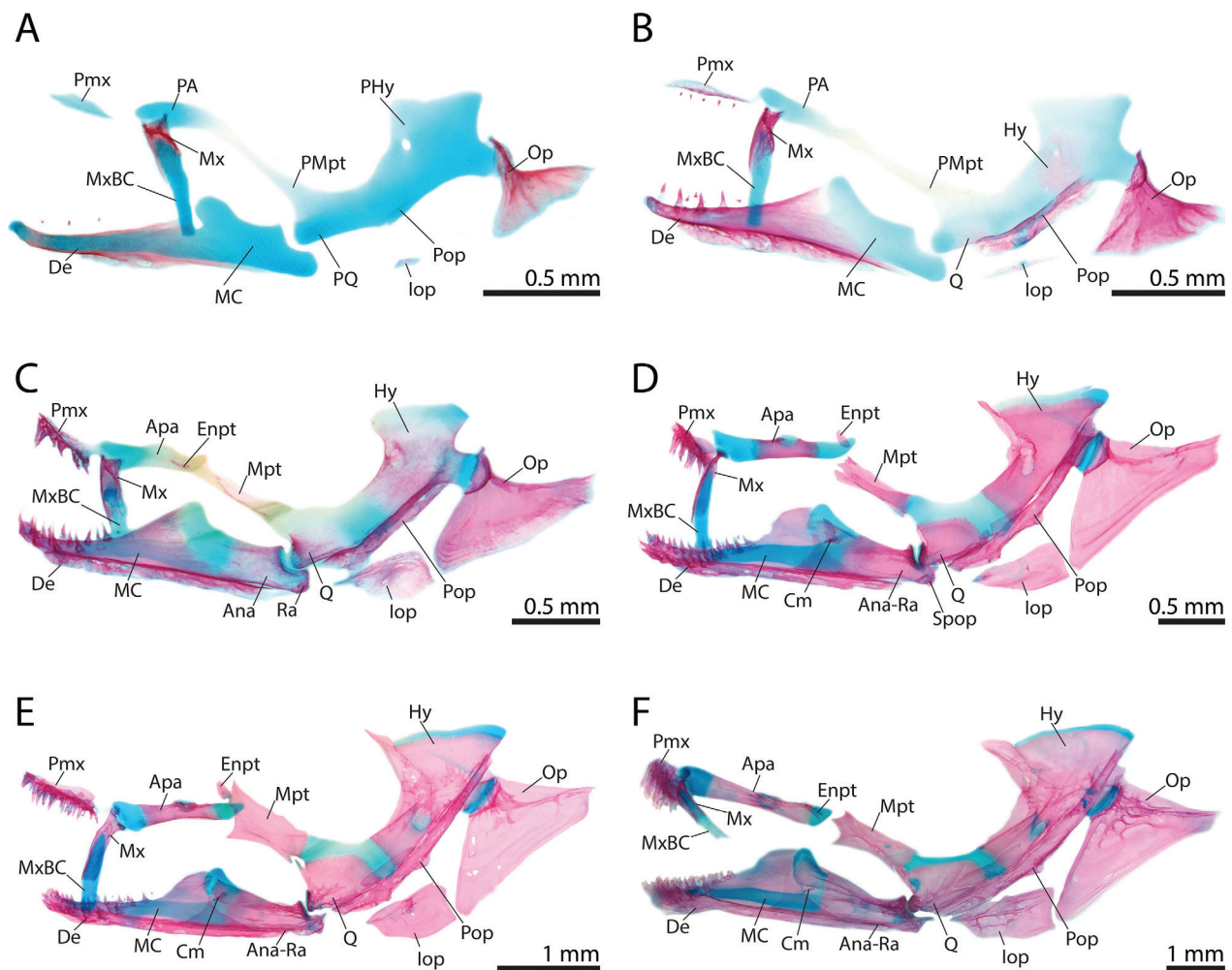


Figure 9. Ontogeny of the hyopalatine arch, jaws and opercular series of *Ictalurus punctatus*. **A** 11.2 mm SL. **B** 12.2 mm SL. **C** 13.3 mm SL. **D** 18.0 mm SL. **E** 21.5 mm SL. **F** Suprapreopercle not shown, 44.9 mm SL. Abbreviations: Ana, Anguloarticular; Ana-Ra, Anguloarticular+retroarticular; Apa, Autopalatine; Cm, Coronomeckelian; De, Dentary; Enpt, Endopterygoid; Hy, Hyomandibular; lop, Interopercle; MC, Meckel's cartilage; Mpt, Metapterygoid; Mx, Maxilla; MxBC, Mandibular barbel cartilage; Op, Opercle; PA, *Pars autopalatina*; PHy, *Pars hyomandibularis*; PMpt, *Pars metapterygoidea*; Pmx, Premaxilla; Pop, Preopercle; PQ, *Pars quadrata*; Q, Quadrate; Ra, Retroarticular; Sop, Subopercle; Spop, Subpreopercular bone.

terior to the coronoid process (11.9 mm SL). The anguloarticular ossifies in a dorsoventral direction becoming saddle-shaped in appearance at 12.5 mm SL. At 13.0 mm SL the bone completely encompasses the posterior end of Meckel's cartilage (Fig. 9C). Anteriorly, it lies dorsal to the dentary and posteriorly it has expanded to meet and fuse with the retroarticular. At 15.9 mm SL the posterior end of Meckel's cartilage is endochondrally ossifying with only a small portion of cartilage remaining at the point of articulation with the quadrate. The angular portion of the anguloarticular extends anteriorly where it lies medial to the posterior end of the dentary and posteriorly, a tiny recurved process can be seen on the posterodorsal tip of the bone. A subpreopercular bone (*sensu* Egge 2007) forms around the mandibular portion of the preoperculo-mandibular sensory canal (17.7 mm SL) laterally to the anguloarticular and fuses with the underlying bone by 21.2 mm SL (Fig. 9E). By 44.9 mm SL (Fig. 9F) the anguloarticular completely covers the posterior remnant of Meckel's cartilage, meeting the coronoid process of the dentary anterodorsally. The surface of the bone

that articulates with the quadrate has become enlarged and more posteriorly directed and the lateral surface of the bone is now slightly sculptured, resembling the adult condition.

Coronomeckelian. The coronomeckelian is a small dermal bone that is first observed as a tiny ossification located medially to the coronal process of Meckel's cartilage at the tendinous insertion of the A3 adductor mandibulae (15.0 mm SL). It becomes triangular in shape shortly after ossifying (16.2 mm SL) and maintains this shape and position during its early ontogeny, only increasing in size (44.9 mm SL; Fig. 9F). In adults (441 mm SL; Fig. 10C), the coronomeckelian is no longer a triangular plate of bone and wraps laterodorsally around Meckel's cartilage and has a firm connection with the dentary laterally and the anguloarticular posteriorly.

Comparison with *Noturus gyrinus*. The most common sequence of ossification for this region in *Noturus gyrinus* is as follows: maxilla (5.4 mm NL)– dentary (5.9 mm

NL) – premaxilla (6.6 mm SL) – retroarticular (7.0 mm SL) – anguloarticular (7.7 mm SL) – coronomeckelian (10.1 mm SL).

No differences in the sequence of ossification between *Noturus gyrinus* and *Ictalurus punctatus* were identified in the jaws. The jaws of *N. gyrinus* and *I. punctatus* are similar, and no major differences in adult morphology are observed in this region.

Hyopalatine arch

The most common sequence of ossification: quadrate (11.5 mm SL) – hyomandibular (12.0 mm SL) – metapterygoid (12.8 mm SL) – endopterygoid and autopalatine (12.9 mm SL) (Fig. 9).

Quadrate. the quadrate is an endoskeletal bone that first appears in some individuals of 11.2 mm SL (Fig. 9A) as a perichondral ossification along the ventral edge of the *pars quadrata* of the quadratometapterygoid portion of the palatoquadrate cartilage, which in catfishes is continuous with the hyosymplectic cartilage and separate from the *pars autopalatina*. The perichondral ossification extends dorsally to encircle the anteroventral portion of the *pars quadrata* that articulates with the lower jaw and the quadrate has begun to endochondrally ossify (12.2 mm SL; Fig. 9B). By 14.0 mm SL, the quadrate has expanded into a triangular bone and the posteroventral process of the quadrate (*sensu* Arratia and Schultze 1991) runs along the dorsal edge of the preopercle. A strip of membrane bone forms medial to the ventral portion of the preopercle (15.9 mm SL) and is joined with the posteroventral process anteriorly forming a shallow trough in which the dorsal margin of the overlapping preopercle rests. The quadrate has also become more heavily ossified near the connection with the lower jaw but remains cartilaginous at the joint. At 18.0 mm SL (Fig. 9D), the point of connection with the lower jaw is now restricted to an anteriorly directed articular facet and a thin lamina of membrane bone has formed along the anterior edge of the quadrate above the facet. By 21.5 mm SL (Fig. 9E) the anterior lamina possesses an anterodorsal spine-like process extending towards the posteroventral corner of the metapterygoid. The medial surface of the quadrate possesses some sculpturing near the articular facet. In individuals up to 44.9 mm SL (Fig. 9F), the quadrate has changed little and still remains separated from the hyomandibular and most of the metapterygoid by cartilage. The anterodorsal process now sits tightly between a similar posteroventral process and the chondral portion of the metapterygoid forming a rigid connection between the two. The quadrate forms a more rigid connection with the preopercle posteriorly. In the adult condition (441 mm SL; Fig. 10A), the quadrate is now strongly sutured to the metapterygoid along their shared medial border but remains separated from the hyomandibular by cartilage. Posteriorly the quadrate is overlain by and strongly sutured to the expanded preopercle.

Hyomandibular. The hyomandibular originates as a perichondral ossification around the *pars hyomandibu-*

laris near the foramen for the passage of the hyomandibular branch of the facial nerve (VII) and may appear as early as 11.5 mm SL. By 13.2 mm SL (Fig. 9C) the bone has spread to cover most of the *pars hyomandibularis* excluding the dorsal and posterior articular heads, which articulate with the neurocranium and opercle respectively, and the ventral arm that joins the *pars quadratometapterygoid*. At 15.9 mm SL, two small flanges of membrane bone flank the shaft of the hyomandibular, one anterior to the foramen for the passage of the hyomandibular branch of the facial nerve (VII) and one posterior, directly above the posterior articular head. Additionally, a thin splint of membrane bone extends from the anterodorsal most corner of the hyomandibular towards the pterosphenoid. A flange of membrane bone has formed on the posterior margin of the hyomandibular below the posterior articular head by 18.0 mm SL (Fig. 9D) and the cartilage is beginning to be fully replaced by bone near the foramen. By 21.2 mm SL (Fig. 9E), the anterodorsal extension of membrane bone forms a tight connection with a similar process on the pterosphenoid. The membrane bone along the posterior margin has formed a shelf for the medial surface of the preopercle as it runs the length of the hyomandibular. At 44.9 mm SL (Fig. 9F), the cartilage has been completely replaced by bone in the middle of the hyomandibular shaft with cartilage still remaining in the dorsal head and ventral arm. The surface of the bone has become lightly sculptured where only bone remains and the connection between the hyomandibular and the preopercle has become firmer. In adult specimens (441 mm SL; Fig. 10A), the hyomandibular possesses an anteroventral flange of bone that forms a strong interdigitated suture with the greatly expanded metapterygoid and has formed a strong suture with the preopercle posteriorly. Posterodorsally, a small flange of bone extends from the hyomandibular reaching and underlying the suprapreopercle of the preoperculo-mandibular canal.

Metapterygoid. The metapterygoid starts off as a perichondral ossification around the middle of the anterior process of the *pars metapterygoid* (11.9 mm SL), which in catfishes has rotated and shifted anteriorly towards the *pars autopalatina*. By 13.3 mm SL (Fig. 9C), the entire anterior process is covered in perichondral bone and a small membranous projection has appeared on the tip of the process supporting a ligamentous connection to the autopalatine and neurocranium in which the endopterygoid has ossified. The metapterygoid is endochondrally ossifying at 15.9 mm SL and a continuous vertical lamina of membrane bone extends along the entire ventral length of the bone up and around to the middle of the dorsal edge. By 18.0 mm SL the lamina of bone extends the length of the dorsal margin of the main body of the metapterygoid and has expanded to take on a somewhat rectangular shape (Fig. 9D) and by 21.0 mm SL (Fig. 9E) possesses anterior and posterior ventral processes, the latter extending towards a similar process of the quadrate. By 44.9 mm SL (Fig. 9F), the metapterygoid has increased in size and the posteroventral process attaches to the anterodorsal projection of the quadrate. The anterior

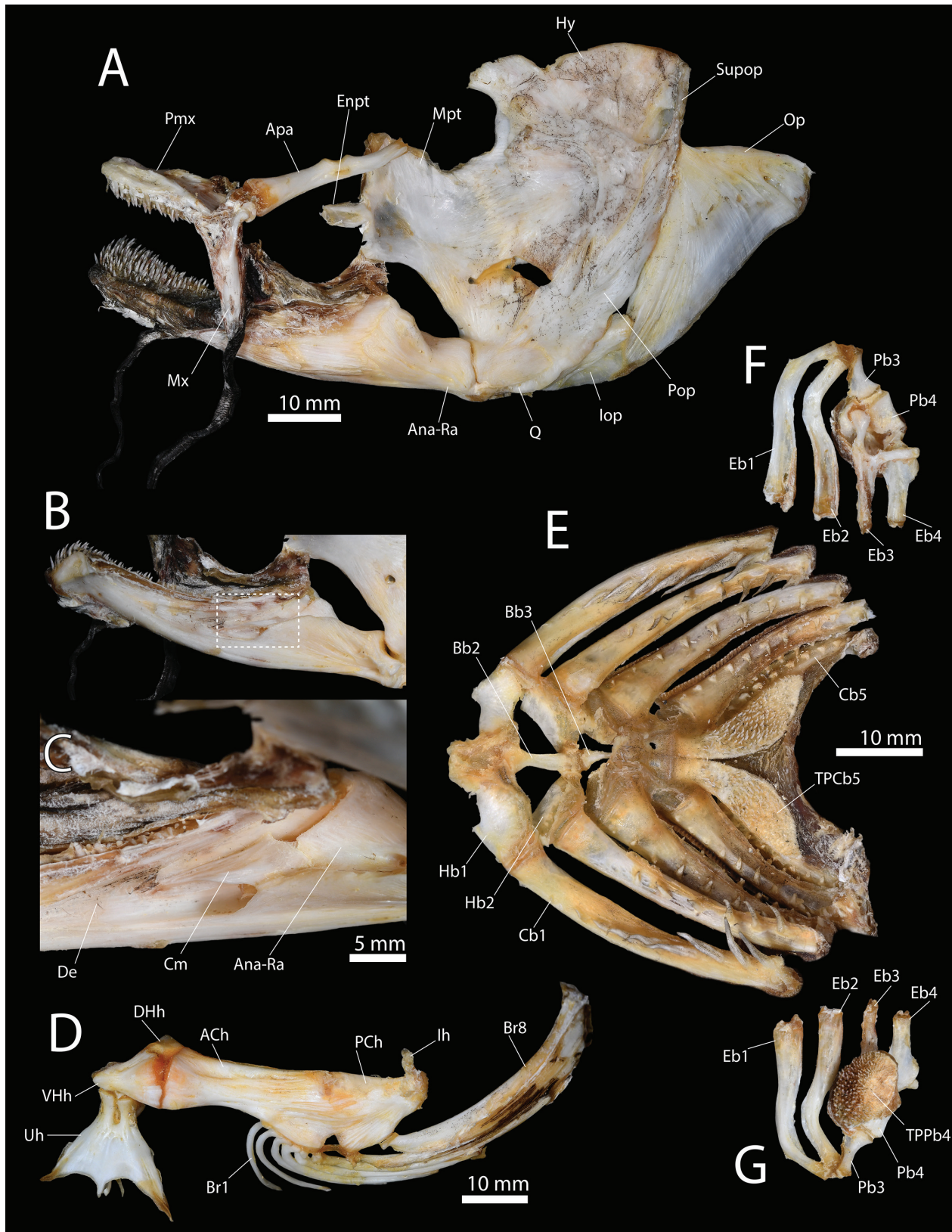


Figure 10. *Ictalurus punctatus*, specimen TCWC 20491.08, 441 mm SL (A), (B), (C), (E), and TCWC 20491.07, 436 mm SL (D). **A** Hyopalatine arch, jaws and opercular series in lateral view. **B** Lower jaw in medial view. Area outline by white box indicates location of (C). **C** Coronomeckelian on medial surface of the lower jaw. **D** Hyoid bar in lateral view. **E** Ventral gill arches in dorsal view. **F** Dorsal gill arches in dorsal view. **G** Dorsal gill arches in ventral view. Abbreviations: ACh, Anterior ceratohyal; Ana-Ra, Anguloarticular+retroarticular; Apa, Autopalatine; Bb, Basibranchial; Br, Branchiostegal ray; Cb, Ceratobranchial; Cm, Coronomeckelian; De, Dentary; DHh, Dorsal hypohyal; Eb, Epibranchial; Enpt, Endopterygoid; Hb, Hypobranchial; Hy, Hyomandibular; lh, Interhyal; lop, Interopercle; Mpt, Metapterygoid; Mx, Maxilla; Op, Opercle; Pb, Pharyngobranchial; PCh, Posterior ceratohyal; Pmx, Premaxilla; Pop, Preopercle; Q, Quadrate; Sop, Subopercle; Supop, Suprapreopercle; TPCb, Toothplate of ceratobranchial; TPPb, Toothplate of pharyngobranchial; Uh, Urohyal; VHh, Ventral hypohyal.

edge has three distinct tips, the dorsal of which supports a ligamentous connection to the ventrolateral margin of the orbitosphenoid, the middle supports a ligamentous connection to the endopterygoid and the ventral most supports a ligamentous connection to the lateral edge of the autopalatine. In adult individuals (441 mm SL; Fig. 10A), the metapterygoid has greatly expanded dorsally and is almost rectangular in shape. Posteriorly it forms a strong interdigitated suture with the hyomandibular and ventrally forms a strong connection with the quadrate medially, although a small remnant of cartilage remains between the two laterally. The three distinct tips along the anterior edge of the metapterygoid can no longer be distinguished and it now reaches the plate-like endopterygoid with both bones separated by only a short ligament.

Endopterygoid. The endopterygoid first appears as a thin splint of bone in the ligamentous connection between the metapterygoid, autopalatine and neurocranium in individuals as small as 11.9 mm SL. The bone expands into a thin lamina of bone (14.1 mm SL) and by 15.6 mm SL it has become large enough to replace the portion of the ligament in which it has formed resulting in three ligamentous connections to the metapterygoid posteriorly, the autopalatine laterally and the vomer anteriorly. An additional, second ligament connecting the endopterygoid to the vomer was previously reported (Arratia 1992) although this connection was not observed in our largest C&S specimen (44.9 mm SL). The endopterygoid eventually expands into a small rectangular plate of bone, representing the adult condition (441 mm SL; Fig. 10A), which abuts the metapterygoid posteriorly and sits medial to the posterior tip of the autopalatine retaining only a short ligamentous connection to both.

Autopalatine. The autopalatine starts as a perichondral ossification (12.5 mm SL) around the middle of the cylindrical *pars autopalatina*, which originates as an independent cartilage separate from the rest of the palatoquadrate. By 13.9 mm SL it has expanded into a cylindrical ossification around the middle third of the *pars autopalatina* except for a dorsomedial facet for the articulation with the lateral ethmoid. Anteriorly, the cartilaginous head of the autopalatine possesses a ventrolateral groove for the articulation of the maxilla. The *pars autopalatina* has increased in size with the posterior tip extending almost to the metapterygoid by 18.0 mm SL (Fig. 9D) and by 21.2 mm SL (Fig. 9E) the autopalatine has started to endochondrally ossify. Light sculpturing is present around the articular facet for the lateral ethmoid and a lateral and medial flange of membrane bone has formed on the posterior half of the bone. By 44.9 mm SL (Fig. 9F), the autopalatine has become more elongate and is completely ossified, except for the anterior and posterior tips as well as the dorsomedial articular facet for the lateral ethmoid, and the middle of the bone is more heavily sculptured, resembling the adult condition (441 mm SL; Fig. 10A).

Comparison with *Noturus gyrinus*. The most common sequence of ossification for this region in *Noturus gyri-*

nus is as follows: quadrate and hyomandibular (7.2 mm SL) – metapterygoid (8.3 mm SL) – autopalatine (8.6 mm SL) – endopterygoid (8.7 mm SL).

The sequence of ossification in the hyopalatine arch differs between *Noturus gyrinus* and *Ictalurus punctatus* in that the quadrate appears before the hyomandibular in *I. punctatus* while in *N. gyrinus* they are fixed in development at the same size. However, the quadrate does appear before the hyomandibular in some individuals of *N. gyrinus*. Additionally, the autopalatine appears before the endopterygoid while in *I. punctatus*, despite being fixed in development at the same size, the endopterygoid is present before the autopalatine in some individuals. The hyopalatine arch of *N. gyrinus* and *I. punctatus* are similar, and no major differences in adult morphology are observed in this region.

Opercular series

The most common sequence of ossification: opercle (8.6 mm NL) – interopercle (10.4 mm SL) – preopercle (11.5 mm SL) – suprapreopercle (22.4 mm SL) (Fig. 9).

Opercle. The dermal opercle is one of the first skeletal elements to appear in *Ictalurus punctatus* (8.6 mm NL) and was first observed as a thin dermal ossification extending posteroventrally from the posterior condyle of the *pars hyomandibularis* of the hyosymplectic cartilage. At 9.6 mm NL, the posterior end of the ossification begins to widen and by 10.8 mm SL the opercle has become fan-shaped with a concave anterior and dorsal edge, the latter of which is more heavily ossified. As the opercle continues to expand, its anteroventral margin becomes more rounded as it gets closer to the posterior margin of the interopercle while its posterior dorsal tip ends in a sharp point (13.0 mm SL; Fig. 9C). The cup-shaped articular surface of the opercle completely surrounds the posterior condyle of the *pars hyomandibularis*. A thin lamina of bone begins to form along the dorsal edge by 15.0 mm SL and by 21.5 mm SL (Fig. 9E) extends to the posterior most tip of the opercle resulting in a straight dorsal margin. In adult specimens, the lateral surface has become sculptured proximally while the distal edge remains smooth.

Interopercle. The dermal interopercle first appears at 10.4 mm SL as a small splint of bone lateral to the connection between the ceratohyal and interhyal cartilages. By 13.3 mm SL (Fig. 9C), the interopercle has grown in length, almost meeting the anterior edge of the opercle. The bone has widened posteriorly while anteriorly it terminates in a fine point, which accommodates the posterior end of the interoperculo-retroarticular ligament. The interopercle takes on a rhomboid shape as the bone continues to grow (18.6 mm SL) and the posterior edge becomes curved around the margin of the opercle where the two bones border each other (21.5 mm SL; Fig. 9E). In adult specimens, the lateral surface has become sculptured but the overall shape has changed little from the earlier stages.

Preopercle. The preopercle forms as a splint of bone (10.9 mm SL) along the posterior margin of the hyosymplectic and *pars quadrata* cartilages at the point of contact with the interhyal cartilage. At 12.2 mm SL (Fig. 9B), the ossification has expanded dorsally to cover the posterior margin of the *pars hyomandibularis* up to the posterior condyle and has formed into a trough-shaped canal, the preopercular portion of the preoperculo-mandibular sensory canal, with three small foramina associated with the innervation of neuromasts. The walls of the canal begin expanding to cover the canal (14.1 mm SL) which becomes completely enclosed by 15.9 mm SL except for two openings for the preoperculo-mandibular sensory canal pores 8 and 9, the first located lateral to the interhyal cartilage and the second opening posterior in line with the border of the opercle and interopercle. Additionally, a ventral lamina of bone is present between the anterior opening of the canal and the posterior of the two pores and a dorsal lamina is forming at the junction of the hyomandibular and the quadrate. At 44.9 mm SL (Fig. 9F), the preopercle extends almost the entire length of the posterior margin of the quadrate and hyomandibular. The ventral lamina of bone has expanded and runs almost the entire length of the bone and is heavily sculptured while the dorsal lamina has only expanded slightly. In adults (441 mm SL; Fig. 10A), the preopercle has expanded to laterally cover the posterior and posteroventral portion of the opercle and hyomandibular, respectively, and is now strongly sutured to both.

Suprapreopercle. The suprapreopercle is the last element to appear in the entire skeleton of *Ictalurus punctatus* (22.4 mm SL) and is first observed as a small ossification located between the preopercle and the pterotic. At 44.9 mm SL (Fig. 9F) it is a weakly ossified trough-shaped bone that forms around the preoperculo-mandibular canal in the gap between the pterotic and preopercle just after it branches off of the otic canal. In the adult stage (441 mm SL; Fig. 10A), the suprapreopercle has become a tube-shaped ossification and overlies a posterodorsal process of the hyomandibular and almost contacts the dorsal-most tip of the preopercle ventrally.

Comparison with *Noturus gyrinus*. The most common sequence of ossification for this region in *Noturus gyrinus* is as follows: opercle (5.4 mm NL) – interopercle (6.4 mm SL) – preopercle (7.7 mm SL) – suprapreopercle (11.6 mm SL).

No differences in the sequence of ossification were identified between *Noturus gyrinus* and *Ictalurus punctatus* in the opercular series, which is similar in both species and show no major differences in adult morphology

Infraorbitals

The most common sequence of ossification: lacrimal (10.4 mm SL) – infraorbital 2 (12.2 mm SL) – infraorbital 3 (12.8 mm SL) – infraorbital 4 and 6 (13.2 mm SL) – infraorbital 5 (13.9 mm SL) (Fig. 11).

Lacrimal. The lacrimal first appears at 10.4 mm SL as a small dermal bone located dorsal to the articulation between the maxilla and *pars autopalatina* and anterior to the lamina orbitonasalis (Fig. 11A). By 11.5 mm SL it expands dorsally and ventrally giving the bone a distinct L shape. The anterior and posterior edges of the dorsal process have just started to form roughly the shape of a trough. At 12.5 mm SL (Fig. 11B), the roof of the infraorbital sensory canal has begun to close in the dorsal portion of the lacrimal. The anterior process has become triangular ending in a distinct tip and a small posteriorly directed process has just formed. By 14.1 mm SL, the dorsal portion of the bone is represented solely by a fully enclosed canal ossification and the posterior process extends to the lamina orbitonasalis resulting in a roughly rhomboid lamina of bone ventral to the canal ossification. The lacrimal increases in size and changes little until 21.2 mm SL, at which point the ventral lamina of bone expands dorsally on either side of the ventral third of the canal ossification. The posterior projection continues to widen, becoming ovoid, and is closely associated with the remnant of the lamina orbitonasalis and the lateral ethmoid posteriorly.

Infraorbital 2. Infraorbital 2 first appears as small trough-shaped bone just posterior to the lacrimal at 11.9 mm SL. A single foramen for innervation of neuromasts in the infraorbital sensory canal is present in the center of the ossification. At 13.2 mm SL (Fig. 11C), bone starts to cover the roof of the canal and by 14.0 mm SL the canal bone becomes enclosed and sits directly medial to the posterior process of the lacrimal. By 44.9 mm SL (Fig. 11E), infraorbital 2 is closely associated with, yet separate from, the posterior process of the lacrimal.

Infraorbital 3. Infraorbital 3 first appears (11.9 mm SL, Fig. 11B) as a small dermal bone surrounding a foramen for innervation of neuromasts in the infraorbital sensory canal. It is located just posterior to infraorbital 2 and in line with the posterior margin of the lamina orbitonasalis. By 14.1 mm SL, the bone completely encloses the infraorbital sensory canal and has started to lengthen. By 44.9 mm SL (Fig. 11E), infraorbital 3 resembles the adult condition and extends over the posterior limit of the lacrimal and almost reaches the anterior rim of the orbit.

Infraorbital 4. Infraorbital 4 first appears (in some individuals as small as 12.4 mm SL) as a small lamina of bone around a foramen for the innervation of neuromasts ventral to the anterior quarter of the eye. It becomes trough shaped shortly after this (13.1 mm SL; Fig. 11C) and by 14.1 mm SL the canal has become completely enclosed by bone. By 44.9 mm SL (Fig. 11E), it resembles the adult condition and sits ventral to the anterior half of the eye.

Infraorbital 6. Infraorbital 6 is the largest infraorbital in the series. It appears directly ventral to the junction of the supraorbital, infraorbital and otic sensory canals near the vertical midline of the eye and at approximately the same

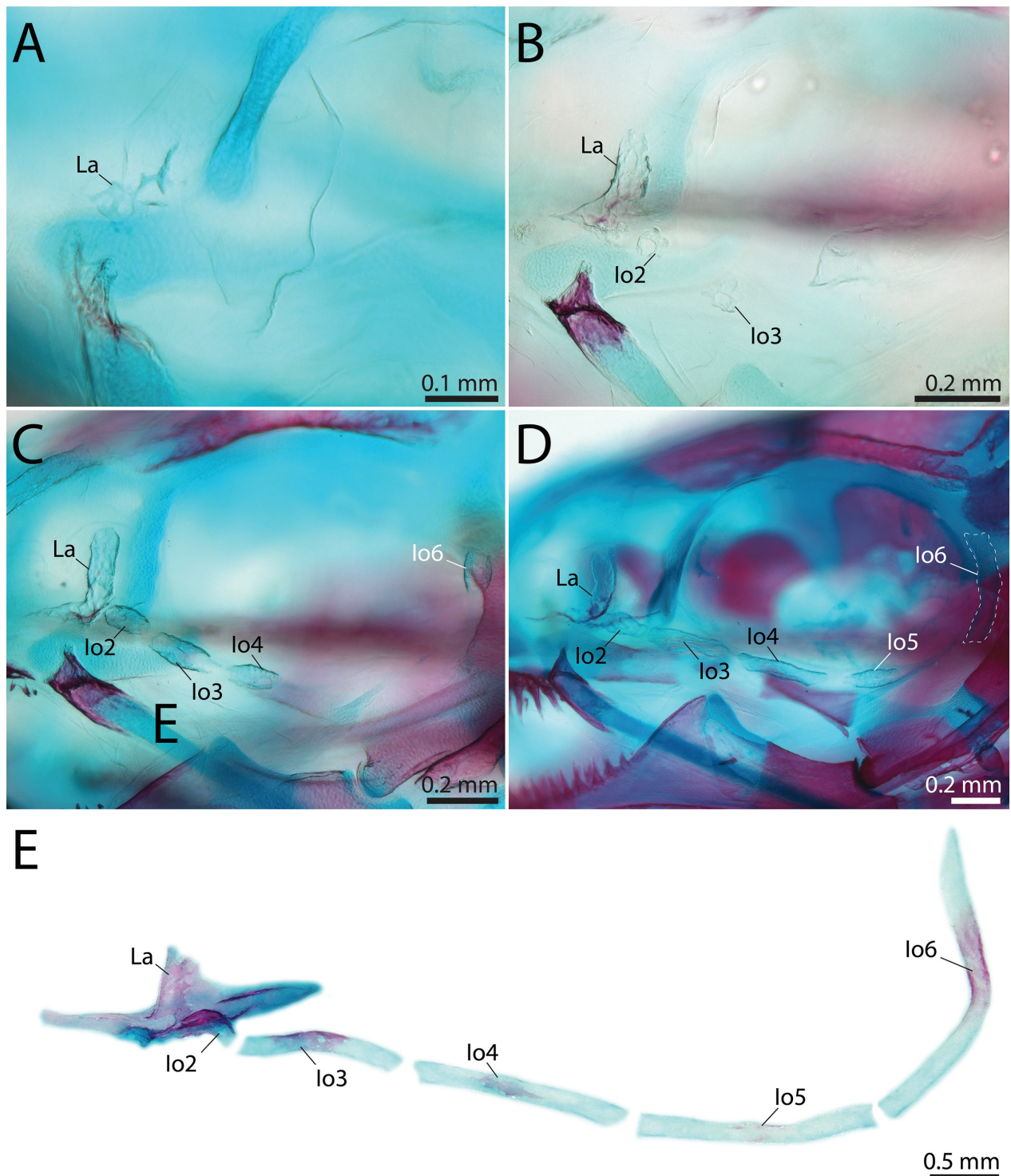


Figure 11. Ontogeny of the infraorbitals of *Ictalurus punctatus*. **A** 11.2 mm SL. **B** 12.7 mm SL. **C** 13.2 mm SL. **D** 15.0 mm SL. **E** 44.9 mm SL. Abbreviations: Io, Infraorbital; La, Lacrimal.

time as infraorbital 4 (12.4 mm SL). The canal becomes enclosed in bone by 14.1 mm SL and the bone continues to increase in length. By 44.9 mm SL (Fig. 11E), it expands from just below the frontal down to the posteroventral extent of the eye forming the posterior rim of the orbit resembling the adult condition.

Infraorbital 5. Infraorbital 5 forms around a foramen for the innervation of neuromasts in individuals as small as 13.2 mm SL (Fig. 11C) in line with the posterior quarter

of the eye. The canal ossification is closed by 14.6 mm SL (Fig. 11D) and the bone continues to lengthen until it spans the posterior half of the eye forming the ventral border of the orbital rim along with infraorbital 4, thus resembling the adult condition (44.9 mm SL; Fig. 11E).

Comparison with *Noturus gyrinus*. The most common sequence of ossification for this region in *Noturus gyrinus* is as follows: lacrimal (7.0 mm SL) – infraorbital 2 (7.7 mm SL) – infraorbital 3 (7.9 mm SL) – infraorbital 4

(8.3 mm SL) – infraorbital 5 (8.6 mm SL) – infraorbital 6 and 7 (12 mm SL).

The only difference observed in the sequence of ossification between *Noturus gyrinus* and *Ictalurus punctatus* in the infraorbital series is that infraorbital 5 appears before infraorbital 6 in *N. gyrinus* while it appears after infraorbital 6 in *I. punctatus*. The infraorbitals of *N. gyrinus* and *I. punctatus* are generally similar except for *N. gyrinus* possessing an additional element, infraorbital 7. The only difference noted is the shape of the lacrimal in *N. gyrinus* in which the anterior process is more elongate and the posterior process is a narrow splint that does not reach the lamina orbitonasalis.

Hyoid bar

The most common sequence of ossification: branchiostegal ray 8 (9.6 mm NL) – branchiostegal ray 7 (10.0 mm SL) – branchiostegal ray 6 (10.8 mm SL) – anterior ceratohyal (11.3 mm SL) – branchiostegal ray 5 (11.4 mm SL) – branchiostegal ray 4, urohyal and ventral hypohyal (11.9 mm SL) – branchiostegal ray 3 (12.3 mm SL) – branchiostegal ray 2 (12.8 mm SL) – interhyal and posterior ceratohyal (13.2 mm SL) – branchiostegal ray 1 (13.6 mm SL) – dorsal hypohyal (15.0 mm SL) (Fig. 12).

Branchiostegal Rays. The branchiostegal rays appear as thin dermal ossifications extending posteroventrally from the hyoid bar. The first branchiostegal ray to develop is the posteriormost, branchiostegal ray 8 (9.2 mm NL), along the posteroventral margin of the deepest portion of the ceratohyal cartilage. The next three branchiostegal rays to appear are branchiostegal rays 7 (10.0 mm SL; Fig. 12A), 6 (10.1 mm SL), and 5 (11.2 mm SL), which are associated with the ventral edge of the deepest portion of the ceratohyal cartilage. By the appearance of branchiostegal ray 5, branchiostegal ray 8 now reaches the midline of the opercle but remains a thin splint of bone. The branchiostegal rays continue to develop in a postero-anterior direction with the last, branchiostegal ray 1, appearing by 12.6 mm SL. At this point branchiostegal ray 8 has started to widen posteriorly and now reaches the posterior point of and connects to the opercle via dense connective tissue. By 15.9 mm SL, all of the branchiostegal rays are recurved posteriorly with branchiostegal rays 5–8 now widened into thin sheets of bone. By 21.2 mm SL, all eight branchiostegal rays are at a stage resembling the adult condition. Branchiostegal rays 1–5 articulate with the medioventral edge of the anterior ceratohyal, branchiostegal rays 6 and 7 articulate with the ventral margin of the remaining ceratohyal cartilage, between the anterior and posterior ceratohyal, and branchiostegal ray 8 articulates with the lateral surface of the posterior ceratohyal. The last two branchiostegal rays, 7 and 8, are closely associated with the opercular series, forming a close connection with the posterior margin of the opercle.

Anterior Ceratohyal. The anterior ceratohyal develops (10.8 mm SL) as a perichondral ossification around the middle of the slender anterior portion of the ceratohyal

cartilage. The cylindrical ossification extends anteriorly and posteriorly until it covers the middle third of the ceratohyal cartilage (12.5 mm SL; Fig. 12B). A thin lamina of membrane bone appears along the dorsal edge of the anterior ceratohyal where it is narrowest (14.0 mm SL), and by 16.2 mm SL a similar extension of membrane bone flanks the ventral margin. At this stage, the ossification has started to spread onto the deeper portion of the ceratohyal cartilage posteriorly giving the bone a more hourglass shape. By 17.7 mm SL, the anterior ceratohyal almost covers the entirety of the anterior half of the deepest portion of the ceratohyal cartilage, of which only a thin strip remains between the anterior and posterior ceratohyals. The middle of the anterior ceratohyal is now endochondrally ossified and the medial surface has become lightly sculptured. By 44.9 mm SL (Fig. 12E), the anterior ceratohyal sutures with the posterior ceratohyal across the medial surface of the ceratohyal cartilage remnant and anteriorly remains separated from the ventral hypohyal by a thin strip of cartilage. The surface of the bone has become more heavily sculptured. In adult individuals (436 mm SL; Fig. 10D), the anterior ceratohyal is strongly sutured with the posterior ceratohyal laterally; however, a thin strip of the ceratohyal cartilage remains internally and can be seen dorsal and ventral to the suture.

Urohyal. The urohyal originates as a pair of ossifications in the posterior portion of the sternohyoideus tendons that insert on the medial surface of the anterior most point of the ceratohyal cartilage (11.2 mm SL). The two ossifications expand in a fan-like direction posteriorly and fuse by 12.2 mm SL, forming a sheet of bone ventrally. By 13.2 mm SL (Fig. 12C), a ‘Y’ shaped dorsal extension of bone has appeared medially running the length of the body of the urohyal and its lateral margins also extend posteriorly giving the bone three distinct tips along the posterior edge. The two anterior tips in the dorsal flange of bone have started to expand laterodorsally and medioventrally forming two angled surfaces of bone (16.2 mm SL). By 21.5 mm SL, the aforementioned flanges have joined medially forming a slightly anterior facing cup-like process. At 44.9 mm SL (Fig. 12E), the posterior edge of the cup-like process sits ventral to the anterior tip of the anterior basibranchial copula and in adults, the basibranchial copula articulates with this cup-like process. However, no ‘chondroid bone’ was observed to be fused to the dorsal portion of the urohyal as has been reported previously in adults ictalurids (Arratia and Schultze 1990).

Ventral Hypohyal. The paired, chondral, ventral hypohyal develops (11.2 mm SL) ventrally on the medioventral process of the anterior head of the ceratohyal cartilage that supports the insertion of the sternohyoideus tendons. At 12.5 mm SL (Fig. 12B), the ossification has spread anteriorly to cover the entire ventral surface of the anteromedial process while posteriorly it has started to expand along the medial edge of the ceratohyal cartilage. Just dorsal to the middle of the bone, a foramen for the afferent hyoidean artery has formed in the cartilage. The bone has started to spread dorsally, cupping the ventral

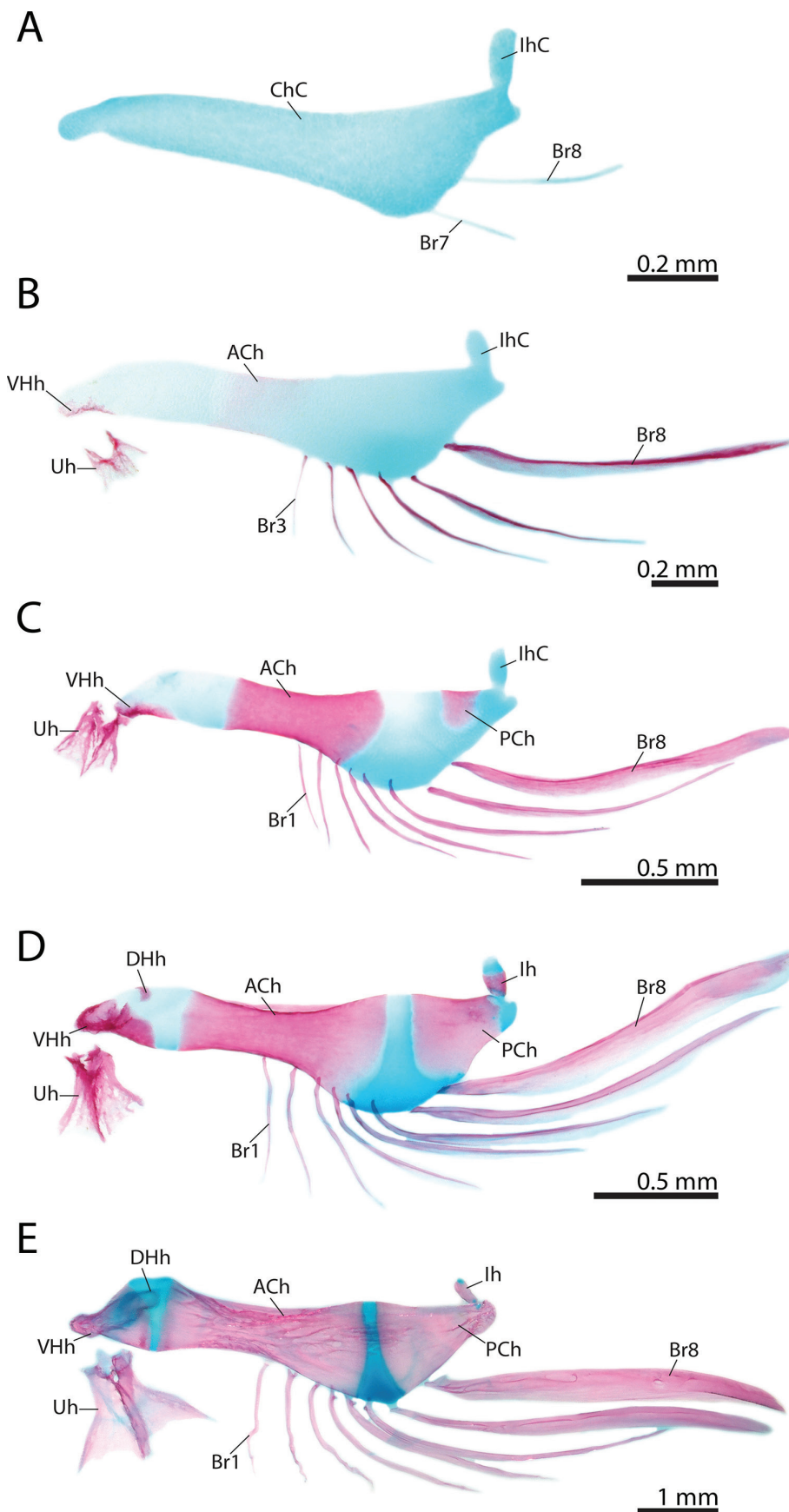


Figure 12. Ontogeny of the hyoid bar of *Ictalurus punctatus*. **A** 10 mm NL. **B** 12.5 mm SL. **C** 13.3 mm SL. **D** 15.0 mm SL. **E** 44.9 mm SL. Abbreviations: ACh, Anterior ceratohyal; Br, Branchiostegal ray; DHh, Dorsal hypohyal; Dh, Dorsal hypohyal; Ih, Interthyral; IhC, Interthyral cartilage; PCh, Posterior ceratohyal; Uh, Urohyal; VHH, Ventral hypohyal.

edge of the anteromedial process (14.0 mm SL) and by 15.9 mm SL it covers the anterolateral tips of the cartilage and even expands onto the dorsal surface of the anteromedial process by 15.9 mm SL. At this stage, the

ventral hypohyal continues to spread posteriorly covering much of the anterior head of the ceratohyal cartilage ventrally. The foramen for the afferent hyoidean artery has become dorsoventrally elongated with the ventral

hypohyal forming the border of the ventral half of the opening. By 18.0 mm SL, the ventral hypohyal covers the ventral half of the anterior head of the ceratohyal cartilage and the opening for the afferent hyoidean artery has expanded further dorsally where it forms a circular opening in the cartilage above the ventral hypohyal. By 21.5 mm SL, the bone has endochondrally ossified anteroventrally and forms a tight connection with its antimeres across the midline. The ventral elongate portion of the opening for the afferent hyoidean artery has begun to fill with bone and by 44.9 mm SL (Fig. 12E) only the dorsal rounded portion of the foramen located in the cartilage above the ventral hypohyal remains. The bone is lightly sculptured anteroventrally and still remains separated by cartilage from the dorsal hypohyal and the anterior ceratohyal, a condition similar to that of adults (436 mm SL; Fig. 10D).

Interhyal. The small interhyal cartilage forms a connection between, and is continuous with, the ceratohyal and the *pars quadrata-hyomandibularis* cartilages. The interhyal first appears as perichondral ossification around the interhyal cartilage in some individuals as small as 12.5 mm SL, shortly after the cartilaginous connections with the ceratohyal and *pars quadrata-hyomandibularis* cartilage begins to regress. By 14.0 mm SL, the perichondral ossification covers most of the interhyal cartilage which is now an independent cartilage with connective tissue replacing its previously cartilaginous dorsal and ventral connections. It continues to become more heavily ossified (21.2 mm SL) and by 44.9 mm SL (Fig. 12E) it has become slightly more elongate, started to endochondrally ossify, yet retains cartilage at its dorsal and ventral tips. A small ridge of membrane bone has started to form along the anterior edge. In adult individuals (436 mm SL; Fig. 10D) the interhyal is a small rod shaped bone that has changed little from earlier stages other than being more heavily ossified.

Posterior Ceratohyal. The posterior ceratohyal develops in individuals as small as 12.5 mm SL as an ossification on the lateral surface of the ceratohyal cartilage just anterior to its ligamentous connection with the interopercle. Shortly after (13.1 mm SL; Fig. 12C), it expands into a saddle shaped ossification in the dorsal half of the cartilage and by 15.9 mm SL the perichondral ossification has expanded around the entire posterior end of the ceratohyal cartilage excluding the point of articulation with the interhyal. At 21.5 mm SL, the posterior ceratohyal is endochondrally ossifying and a ridge of membrane bone has formed on the posteroventral margin of the bone. Anteriorly it remains separated from the anterior ceratohyal by a thin strip of cartilage. On the medial surface, a superficial process of the posterior ceratohyal has started to extend across this cartilage and by 44.9 mm SL (Fig. 12E), it forms an interdigitating suture with the anterior ceratohyal medially. The ridge of membrane bone has become curved and the posterior tip of the bone is now sculptured. Little has changed in adults (436 mm SL; Fig. 10D), other than the posterior ceratohyal also forming

laterally an interdigitating suture with the anterior ceratohyal.

Dorsal Hypohyal. the dorsal hypohyal originates as a perichondral ossification medially on the posterodorsal process of the anterior head of the ceratohyal cartilage (14.5 mm SL). The bone is saddle shaped (15.9 mm SL) and slowly expands to incorporate the entire medial corner of the posterodorsal process (21.5 mm SL). By 44.9 mm SL, the dorsal hypohyal has changed little in shape but has expanded ventrally towards the ventral hypohyal, from which it remains separated by cartilage. In adult individuals (436 mm SL), the dorsal hypohyal covers the entire posterodorsal process which now ends in a distinct point giving the bone a conical appearance.

Comparison with *Noturus gyrinus*. The most common sequence of ossification for this region in *Noturus gyrinus* is as follows: branchiostegal ray 9 (6.3 mm NL) – branchiostegal ray 8 (6.4 mm NL) – branchiostegal ray 7 (6.7 mm SL) – anterior ceratohyal (7.0 mm SL) – branchiostegal ray 5 and 6 (7.3 mm SL) – urohyal (7.3 mm SL) – ventral hypohyal (7.6 mm SL) – posterior ceratohyal (7.7 mm SL) – branchiostegal ray 3 and 4 (7.9 mm SL) – branchiostegal ray 2 and 1 (8.6 mm SL) – dorsal hypohyal (10.8 mm SL) – interhyal (11.1 mm SL).

The sequence of ossification in the hyoid bar differs between *Noturus gyrinus* and *Ictalurus punctatus* in that the interhyal is the last element to appear in *N. gyrinus* while in *I. punctatus* it appears before the dorsal hypohyal at the same time as the posterior ceratohyal. The hyoid bar of *N. gyrinus* and *I. punctatus* differ in the total number of branchiostegal rays (9 in *N. gyrinus* vs. 8 in *I. punctatus*). Although development of the branchiostegal rays also occurs in a posterior to anterior direction, the precise sequence of appearance was not as well resolved in *N. gyrinus*.

Branchial skeleton

The most common sequence of ossification: pharyngobranchial 4 toothplate (9.9 mm NL) – ceratobranchial 5 toothplate (10.9 mm SL) – ceratobranchial 1, 2, 3, 4, 5 and epibranchial 4 (12.0 mm SL) – epibranchial 1, 2 and 3 (12.1 mm SL) – gill rakers (13.3 mm SL) – pharyngobranchial 3 (14.5 mm SL) – pharyngobranchial 4 (15.0 mm SL) – basibranchial 2 and 3 (15.9 mm SL) – hypobranchial 1 (18.0 mm SL) – hypobranchial 2 (21.2 mm SL) (Fig. 13).

Ceratobranchials. The ceratobranchials start as perichondral ossifications around the middle of their respective cartilages. The first to ossify is ceratobranchial 4 (11.4 mm SL) with the remaining ceratobranchials ossifying shortly after (11.8 mm SL). The perichondral ossification expands towards the tips of the cartilages and the teeth associated with the lower pharyngeal jaws are ankylosed to ceratobranchial 5 toothplate which has already fused with ceratobranchial 5 (12.9 mm SL; Fig. 13B). By 14.1 mm SL, ceratobranchials 1–5 are completely ossified

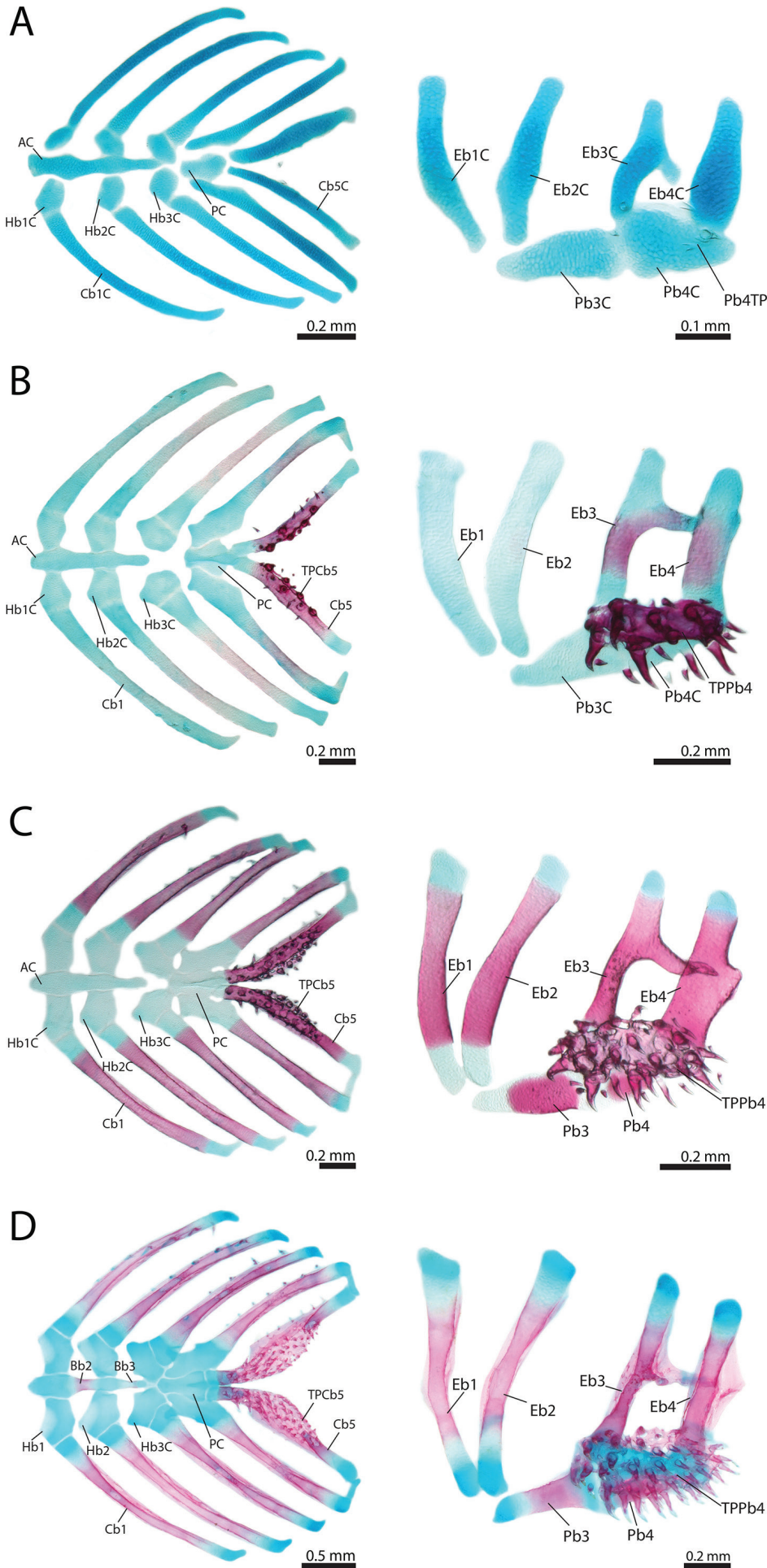


Figure 13. Ontogeny of the branchial skeleton of *Ictalurus punctatus*. Ventral and dorsal gill arches shown in left and right column respectively. **A** 10.9 mm SL. **B** 12.9 mm SL. **C** 15.0 mm SL. **D** 20.6 mm SL. Abbreviations: AC, Anterior copula; Bb, Basibranchial; BbC, Basibranchial cartilage; Cb, Ceratobranchial; CbC, Ceratobranchial cartilage; Eb, Epibranchial; EbC, Epibranchial cartilage; Hb, Hypobranchial; HbC, Hypobranchial cartilage; Pb, Pharyngobranchial; PbC, Pharyngobranchial cartilage; PC, Posterior copula; TPCb, Toothplate of ceratobranchial; TPPb, Toothplate of pharyngobranchial.

perichondrally except for the tips and at 15.0 mm SL (Fig. 13C), flanges of membrane bone have appeared on the anterior and posterior edges of the ceratobranchials. By 20.6 mm SL (Fig. 13D), the ceratobranchials are endochondrally ossifying at the center and by 44.9 mm SL, they are fully ossified and resemble the adult condition (Fig. 10E).

Epibranchials. Epibranchials 1–4 ossify perichondrally around the midline of the epibranchial cartilages and, like in the ceratobranchials, ossification proceeds to spread across the entirety of the cartilages, excluding the tips which remain cartilaginous. The epibranchials ossify rapidly with all of them first appearing in individuals as small as 11.9 mm SL with epibranchial 4 being the first to become fixed in development at 12.0 mm SL. Additionally a posterior to anterior sequence of epibranchial ossification is suggested by a single specimen (11.9 mm SL) in which only epibranchials 3 and 4 are present. By 15.0 mm SL (Fig. 13C), all four epibranchials are completely perichondrally ossified including the uncinat process of epibranchial 3 which is connected to the anterodorsal surface of epibranchial 4 via connective tissue, and possesses a pointed flange of membrane bone at its tip. By 20.6 mm SL (Fig. 13D), all four epibranchials have begun to endochondrally ossify and possess flanges of membrane bone along their anterior and posterior margins. By 44.9 mm SL, the posterior flange of epibranchial 4 has expanded posterodorsally forming a large sheet of bone and the epibranchials closely resemble the adult condition (Fig. 10E). In adult individuals (441 mm SL; Fig. 10F,G) the flanges of membrane bone have expanded, flattening the epibranchials. Epibranchials 1 and 2 are slightly recurved and their medial tips articulate with the anterior tip of pharyngobranchial 3. Epibranchials 3 and 4 have changed little in shape and their medial tips are ventrally curved to support pharyngobranchial 4 toothplate in addition to articulating with pharyngobranchials 3 and 4 respectively.

Gill Rakers. The gill rakers first appear on ceratobranchial 1 in individuals as small as 12.7 mm SL and by 13.3 mm SL, at least one gill raker is associated with each of the five ceratobranchials. By 15.9 mm SL, 5–6 gill rakers are present on each ceratobranchial and a single gill raker is associated with epibranchials 1 and 2. At 20.6 mm SL (Fig. 13D), the gill rakers along the anterior margin of ceratobranchial 1 have become more elongate, an additional gill raker is associated with epibranchials 1 and 2 and a single gill raker has formed on epibranchial 3. At 44.9 mm SL, 6–8 gill rakers are present on the anterior margin of all five ceratobranchials and the posterior edge of ceratobranchials 3 and 4. Epibranchials 1 and 2 possess four gill rakers and epibranchials 3 and 4 possess only one each. In adult individuals (441 mm SL), ceratobranchials 1–5 possess a total of 8–9 gill rakers while the number of gill rakers on the epibranchials remain unchanged. The anterior row of gill rakers associated with the pharyngeal arches decrease in length in an anteroposterior direction with the longest gill rakers located on the first arch and the shortest on the fifth arch.

Pharyngobranchials. Only two pharyngobranchial cartilages, those of arches 3 and 4, are present in *Ictalurus punctatus*. Teeth associated with pharyngobranchial 4 toothplate can be seen in individuals as small as 9.9 mm SL ventral to the pharyngobranchial 4 cartilage (Fig. 13A). Pharyngobranchial 3 is the first of the two to ossify in individuals as small as 13.3 mm SL with pharyngobranchial 4 first appearing at 14.5 mm SL. Both start as perichondral ossifications around the medial edge of the middle of the pharyngobranchial cartilages. By 16.2 mm SL, pharyngobranchial 3 completely encircles the middle of pharyngobranchial 3 cartilage and by 20.6 mm SL (Fig. 13D) a small flange of membrane bone has started to form on its lateral margin. At the same size, pharyngobranchial 4 has expanded into a larger semicircular perichondral ossification but remains cartilaginous laterally. A flange of membrane bone is present on its medial margin as well. By 44.9 mm SL, flanges of membrane bone border the length of pharyngobranchial 3 on the lateral and medial faces and pharyngobranchial 4 remains relatively unchanged. In adults (441 mm SL; Fig. 10F,G), the membrane bone associated with pharyngobranchial 3 has expanded to make the posterior end of the bone about twice as wide as the anterior tip.

Basibranchials. Only two basibranchials, basibranchial 2 and 3, are present in *Ictalurus punctatus*. These form as perichondral bands of bone around the middle and posterior end of the anterior basibranchial copula. Both ossifications appear at approximately the same time with basibranchial 2 appearing slightly earlier (basibranchial 2, 14.6 mm SL; basibranchial 3, 14.8 mm SL). The basibranchials become more elongate (20.6 mm SL; Fig. 4D) and by 44.9 mm SL they have increased in size but changed little in shape. The dorsal surface of basibranchial 2 is lightly sculptured at this size and both basibranchials have reached a condition similar to that found in adults (441 mm SL; Fig. 10E). The posterior basibranchial copula remains cartilaginous and articulates closely with the medial tips of ceratobranchials 4 and 5.

Hypobranchials. The hypobranchials are some of the last bones to ossify in *Ictalurus punctatus*. Hypobranchial 1 first appears at 15.1 mm SL and hypobranchial 2 at 17.7 mm SL. Both start as perichondral ossifications at the anterolateral tips of hypobranchial cartilages 1 and 2. By 20.6 mm SL (Fig. 4D), the perichondral ossifications have expanded medially and are now semicircular in shape and the anterolateral tips are more heavily ossified. By 44.9 mm SL, the hypobranchials have grown posteriorly but still only cover the anterior two-thirds of the cartilages and the anterolateral tips have become more heavily ossified, resembling the adult condition (Fig. 10E). Though hypobranchial 3 cartilage is present in *I. punctatus*, hypobranchial 3 does not ossify and is absent even in the adult stage.

Comparison with *Noturus gyrinus*. The most common sequence of ossification for this region in *Noturus gyrinus* is as follows: pharyngobranchial 4 toothplate (6.6 mm

NL) – ceratobranchial 5 toothplate (7.0 mm SL) – ceratobranchial 4 (7.7 mm SL) – ceratobranchial 5 (7.8 mm SL) – ceratobranchial 1, 2 and 3, epibranchial 4 and 3, and gill rakers (8.3 mm SL) – epibranchial 2 (8.4 mm SL) – epibranchial 1 (8.9 mm SL), pharyngobranchial 3 and basibranchial 3 (9.6 mm SL) – basibranchial 2 (10.0 mm SL) – pharyngobranchial 4 (11.7 mm SL) – hypobranchial 1 (13.2 mm SL) – hypobranchial 2 (14.1 mm SL).

The sequence of ossification in the branchial skeleton differs between *Noturus gyrinus* and *Ictalurus punctatus* in that the gill rakers appear before epibranchials 1 and 2 in *N. gyrinus* and pharyngobranchial 4 appears after basibranchials 3 and 2. The sequence of ossification was better resolved in *N. gyrinus* with a general posterior to anterior direction of development in the ceratobranchials and epibranchials. Although this could not be determined in *I. punctatus* based on initial ossification, the same pattern could be derived from how well ossified the bones were in the earliest stages of appearance. The branchial skeleton of *N. gyrinus* and *I. punctatus* are similar, and the only difference was in the size of the gill rakers which were relatively much larger in *N. gyrinus*.

Weberian apparatus and associated centra

The most common sequence of ossification: centrum 4 (10.0 mm SL) – centrum 2 and 3 (10.1 mm SL) – centrum 1 (10.4 mm SL) – neural arch 4 (11.0 mm SL) – neural arch 3 (11.2 mm SL) – *intercalarium*, outer arm of the *os suspensorium*, *tripus*, inner arm of the *os suspensorium* and *scaphium* (12.2 mm SL) – *claustrum* (13.9 mm SL) (Figs 14–16).

Centra 1–4. Although the first four centra appear in a posterior to anterior direction starting with centrum 4, all four centra were present in some individuals of 10.0 mm SL, the smallest size in which centra were observed. All four centra originate as a pair of perichordal ossifications on the lateroventral margin of the notochord which proceed to expand and meet at the dorsal and ventral midlines. At 10.6 mm SL (Fig. 14A), a lateral extension of bone arising from the fourth centrum, the lateral process of the fourth vertebra (*sensu* Ichiyanagi et al., 1997) is present between basidorsal 4 and basiventral 4 and by 11.8 mm SL, a small process representing the rudiment of the lateral process of the third vertebra (*sensu* Ichiyanagi et al., 1997) is present on the dorsolateral surface of the third centrum ventral to basidorsal 3. At 12.2 mm SL (Figs 14B, 15A, 16A), the fourth centrum is the longest of the anterior four centra, being slightly longer than post Weberian centra, followed by centrum 3 and centra 1 and 2 which are approximately half the width of a regular centrum. By 12.7 mm SL (Figs 14C, 15B, 16B), the lateral process of vertebra 4 has expanded laterally and is in the process of fusing to the *os suspensorium*. The lateral process of centrum 3 spans the length of the centrum and possesses an anterior process which extends out past the transformator process of the *tripus*. Centra 3 and 4 both possess a pair of ventral bony ridges that extend the length

of the centra where they contact the swimbladder. By 13.1 mm SL, centra 2–4 have started to fuse ventrally and the anterior projection of the lateral process of the third vertebra has met and fused to the transformator process of the *tripus* (Figs 15C, 16C). At 15.0 mm SL (Fig. 14E), centra 2–4 are completely fused forming a compound centrum which possesses two prominent ventral ridges of bone at the point of attachment to the swimbladder. Posteriorly, these ridges are closely associated with similar ventrolateral ridges of bone on centrum 5. Centrum 1 is significantly shorter than other centra in the vertebral column. It remains separate from centra 2–4 but possesses two ventrolateral processes that project towards the anterior-most tip of the ridges associated with the fused centra. In the adult condition (426 mm SL; Fig. 17), the compound centrum is a solid element with no indication of its fused nature. The ventrolateral ridges associated with the compound centrum now form sutured connections to the ventrolateral processes of centra 1 and 5.

Neural Arches 3 and 4. The neural arches of vertebrae 3 and 4 first appear (10.8 mm SL) as perichondral ossification of the pair of basidorsal cartilages of centrum 3 and 4. By 12.2 mm SL (Fig. 14B), neural arch 4 has expanded to cover basidorsals 4, except for the dorsal end which is confluent with the neural complex cartilage. Neural arch 3 is almost completely perichondrally ossified around basidorsals 3, and possesses a small dorsal process of membrane bone. The neural complex cartilage extends anteriorly from basidorsal 4 above, but not contacting, neural arch 3, and then medially where it meets its counterpart, forming a ‘U’-shaped cartilage. A dorsomedial extension of cartilage arises from the anterior midline of the neural complex cartilage towards the *tectum synoticum*. At 12.7 mm SL (Fig. 14C), membranous processes extend from the dorsal tips of neural arch 4 on either side of the ventral tip of the dorsal-fin proximal radial 2 and a small lamina of membrane bone is forming on the anterior edge of neural arch 4. The ossification from neural arch 4 has begun to spread anteriorly onto the neural complex and the dorsal tips of neural arch 3 now contact the neural complex cartilage medially. The ossification of the neural complex spans the gap between the tips of neural arches 3 and 4 by 13.3 mm SL (Fig. 14D), and the anteromedial process of the neural complex cartilage is directed more dorsally. The posterodorsal membranous tips of neural arch 4 have expanded to become triangular in shape and the anterior lamina of membrane bone meets and joins with an anterodorsal process of the lateral process of vertebra 4. The perichondral ossification of the neural complex spreads medially over the posterior half of the cartilage and by 15.0 mm SL (Fig. 14E), meets and fuses with its counterpart across the midline. The posterodorsal processes of neural arch 4 have extended dorsally with the tips reaching lateral to the middle nuchal process of dorsal-fin proximal radial 2. A pair of anterodorsal processes dorsal to neural arch 3 is extending towards the back of the cranium on either side of the anterodorsal process of the neural complex cartilage. A median crest of bone has appeared on the dorsal surface

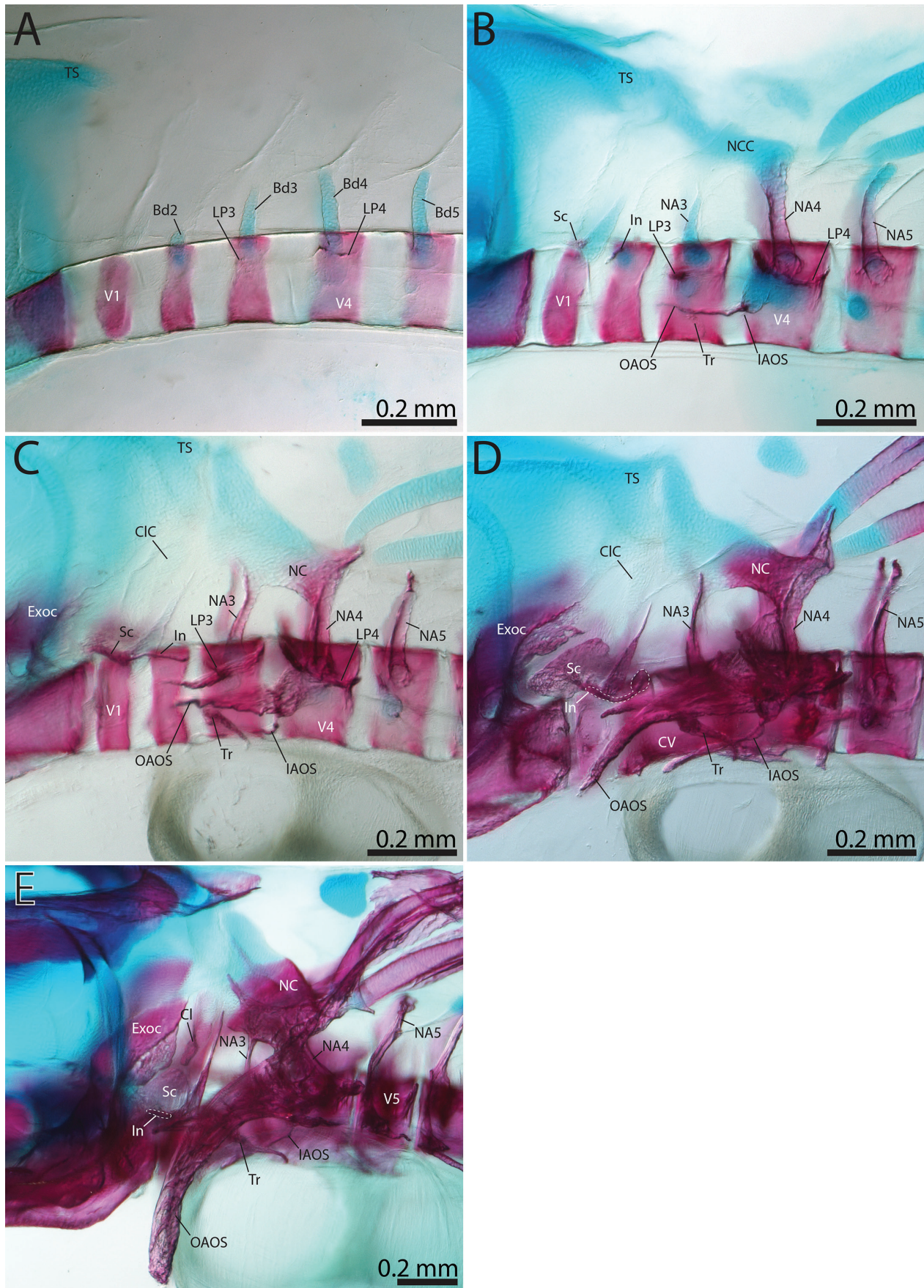


Figure 14. Ontogeny of the Weberian apparatus of *Ictalurus punctatus* in lateral view. **A** 10.6 mm SL. **B** 12.2 mm SL. **C** 12.7 mm SL. **D** 13.3 mm SL. **E** 15.0 mm SL. Abbreviations: Bd, Basidorsal; Cl, Claustrium; CIC, Claustrium cartilage; Exoc, Exoccipital; In, Intercalarium; NA, Neural arch; NC, Neural complex; NCC, Neural complex cartilage; IAOS, Inner arm of *Os suspensorium*; LP, Lateral Process; OAOS, Outer arm of *Os suspensorium*; Sc, Scaphium; Tr, Tripus; TS, Tectum synoticum; V, Vertebra.

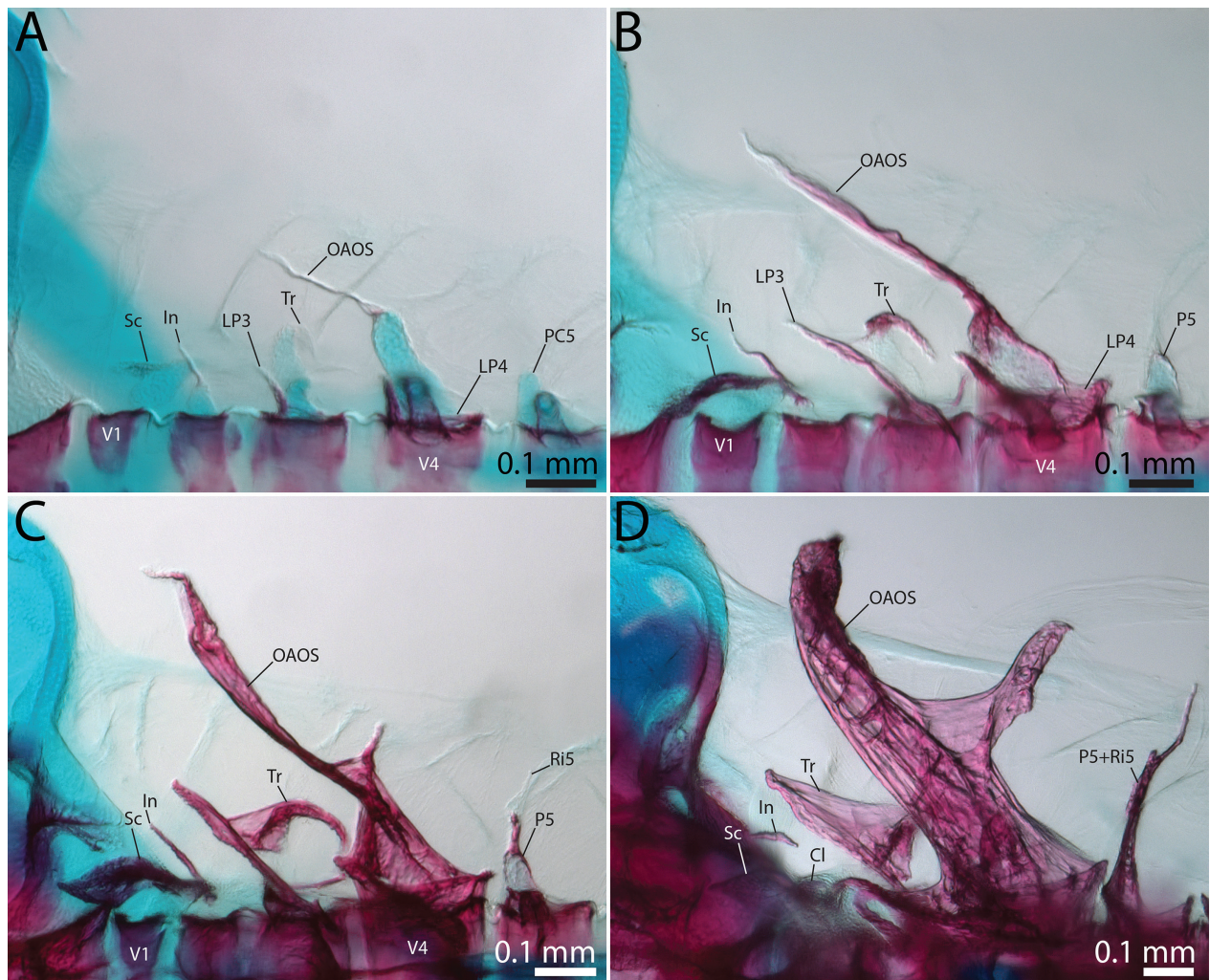


Figure 15. Ontogeny of the Weberian apparatus of *Ictalurus punctatus* in dorsal view. **A** 12.2 mm SL. **B** 12.7 mm SL. **C** 13.3 mm SL. **D** 15.0 mm SL. Abbreviations: Cl, *Clastrum*; In, *Intercalarium*; LP, *Lateral Process*; OAOS, *Outer arm of Os suspensorium*; P, *Parapophysis*; Ri, *Rib*; Sc, *Scaphium*; Tr, *Tripus*; V, *Vertebra*.

of the neural complex ossification (17.8 mm SL) and by 21.2 mm SL has expanded to reach across the length of the bone, branching posteriorly to meet the posterodorsal processes on either side of dorsal-fin proximal radial 2. These posterodorsal processes form a close connection with the middle nuchal plate via dense connective tissue. The lateral gap between neural arches 3 and 4 has completely been filled in with bone and the whole structure forms a tunnel around the spinal cord. By 44.9 mm SL, a stage resembling the adult condition (Fig. 17), the tips of the anterodorsal processes dorsal to neural arch 3 contact and firmly attach to the posterior surface of the supraoccipital. The whole neural complex has become heavily sculptured. A separate supraneural 3 cartilage was reported by Grande and Shardo (2002) to appear anterior to and fuse to neural arch 3, becoming part of the neural complex; however, the neural complex cartilage of *Ictalurus punctatus* does not originate as an independent element in the material examined here.

Intercalarium. The *intercalarium* first appears as perichondral ossification around the basidorsal of vertebra 2 in individuals as small as 11.2 mm SL. At 12.2 mm SL

(Figs 14B, 15A, 16A), an anterolateral process, the *manubrium*, has formed from the perichondral ossification and by 12.7 mm SL (Figs 14C, 15B, 16B) it extends laterally to the *scaphium*. The perichondral ossifications of the *intercalarium* and the basidorsal become reduced and were no longer observed by 13.3 mm SL (Figs 14D, 15C, 16C), leaving only the *manubrium* of the *intercalarium*, the tip of which lies in the interossicular ligament. By 15.0 mm SL (Figs 14E, 15D, 16D), the *manubrium* starts to reduce in size and begins to break down, except for the tip which remains in the interossicular ligament between the *tripus* and the *scaphium*. By 17.7 mm SL, the tip of the *manubrium* is all that remains and in the adult condition (426 mm SL; Fig. 17), this nodule of bone has grown in size to fill the gap between the anterior tip of the *tripus* and the *concha* of the *scaphium*, remaining separated from these two elements by short interossicular ligaments.

Os suspensorium. The *os suspensorium* first appears as a perichondral ossification around the tip of basiventral 4 (11.2 mm SL) in which the outer arm is already present as a thin anteriorly directed process. By 12.2 mm SL (Figs 14B, 15A, 16A), the outer arm has extended lateral to

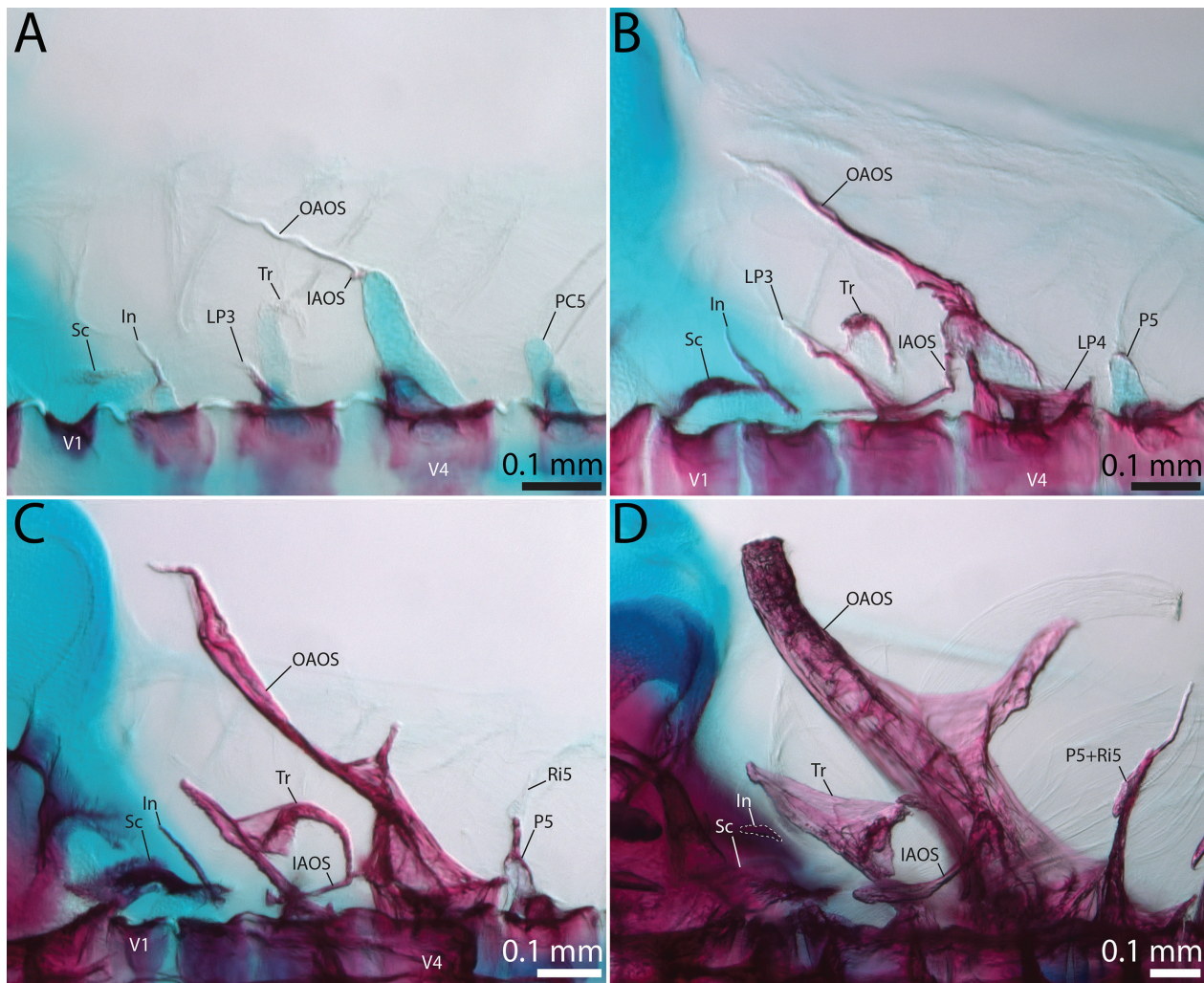


Figure 16. Ontogeny of the Weberian apparatus of *Ictalurus punctatus* in ventral view. **A** 12.2 mm SL. **B** 12.7 mm SL. **C** 13.3 mm SL. **D** 15.0 mm SL. Abbreviations: In, *Intercalarium*; IAOS, *Inner arm of Os suspensorium*; LP, *Lateral Process*; OAOS, *Outer arm of Os suspensorium*; P, *Parapophysis*; Ri, *Rib*; Sc, *Scaphium*; Tr, *Tripus*; V, *Vertebra*.

the anterior margin of vertebra 3 and an additional small process, the inner arm, is present on the tip of basiventral 4 ventromedial to the outer arm. The outer arm of the *os suspensorium* extends anterolaterally towards the pectoral girdle while the inner arm has expanded anteromedially towards the vertebral column where it curves anteriorly and lies parallel to the dorsal surface of the swimbladder and medial to the transformator process of the *tripus*. The perichondral ossification of the *os suspensorium* expands medially covering much of the basiventral cartilage and in some individuals of this size, meets and begins to fuse with the lateral process of vertebra 4 posteriorly. This fusion is complete by 13.3 mm SL (Figs 14D, 15C, 16C), with laminar expansions of bone forming anteriorly and posteriorly from the perichondral ossification of the *os suspensorium*. At 15.0 mm SL (Figs 14E, 15D, 16D), the outer arm has become more robust and its surface is now sculptured. The distal tip of the outer arm (equivalent to the Müllerian process of Tavolga, 1962) forms a close association with the medial surface of the cleithrum and cleithral cartilage (Fig. 18). A posterolateral process has formed along the posterior margin of the outer arm at this size and by 17.8 mm SL, bone has formed between this

process and the posterior margin of the centrum creating a large sheet of bone. The outer arm has formed a firm connection with the medial arm of the supracleithrum as well as a ligamentous connection which extends dorsally to the cleithrum and cleithral cartilage and joins the ventrolateral process of the supracleithrum (Fig. 18). By 44.9 mm SL, a stage resembling the adult condition (Fig. 17), the laminar sheets of bone forming from the outer arm of the *os suspensorium* have grown in size and now appear as large wing-shaped expansions, covering much of vertebral column just posterior to the cranium. The inner arm has expanded in width but remains otherwise unchanged.

Tripus. The *tripus* originates as a perichondral ossification around the tip of basiventral 3 with a small membranous process directed posteriorly, the transformator process (11.2 mm SL). As the transformator process grows it curves ventromedially (12.7 mm SL; Figs 14C, 15B, 16B) and by 13.3 mm SL (Figs 14D, 15C, 16C) the tip of the process reaches towards the inner arm of the *os suspensorium* and sits dorsal to the swimbladder. At this size, an anteriorly directed process extending from the lateral process of centrum 3 begins to fuse to the base of

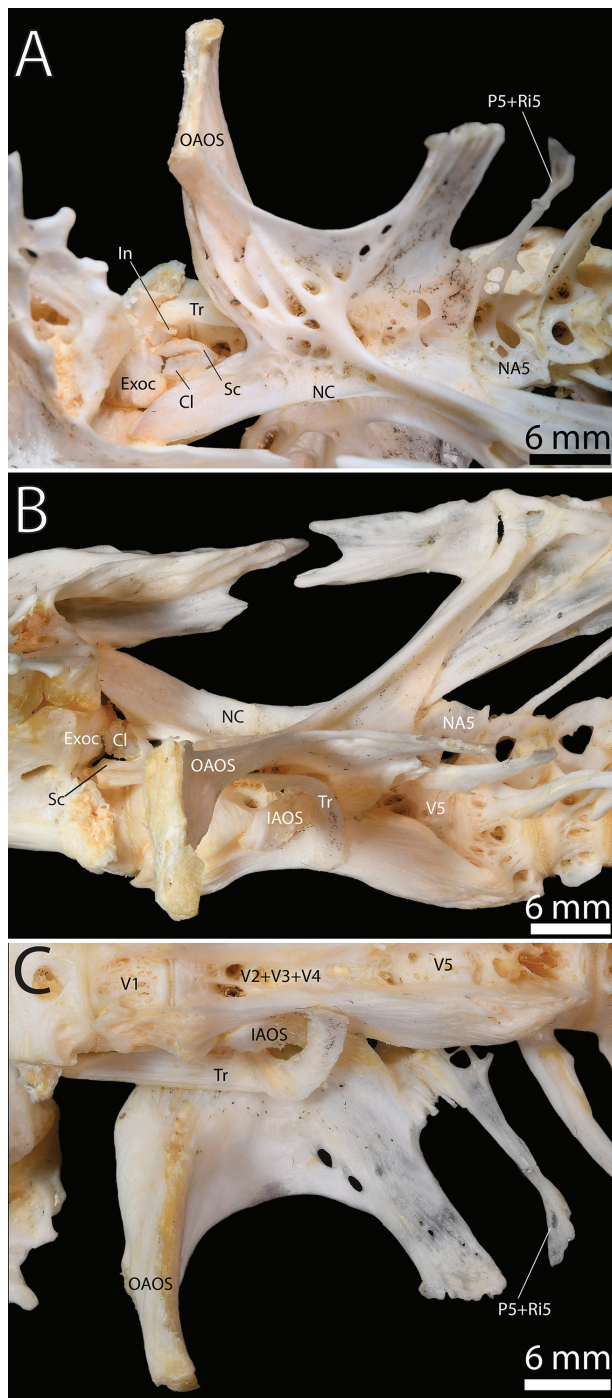


Figure 17. *Ictalurus punctatus*, Weberian apparatus of specimen TCWC 20491.06, 426 mm SL, in dorsal **A**, lateral **B** and ventral view **C**. Abbreviations: Cl, *Claustrum*; Exoc, Exoccipital; In, *Intercalarium*; NC, Neural complex; IAOS, Inner arm of *Os suspensorium*; OAOS, Outer arm of *Os suspensorium*; Sc, *Scaphium*; Tr, *Tripus*; V, Vertebra.

the *tripus* at the tip of the basiventral process and forms the anteriormost extent of the *tripus*. By 14.1 mm SL, a thin lamina of bone has formed lateral from this point of fusion filling the gap between the anteriormost tip of the *tripus* and the lateralmost extent of the transformator process, giving the anterior half a distinct triangular shape. The transformator process is now semicircular in shape extending posteriorly to the inner arm of the *os suspensorium*

and rests on the dorsal surface of the swimbladder. By 15.0 mm SL (Figs 14E, 15D, 16D), the anteriormost tip of the *tripus* reaches lateral to and is connected via an interossicular ligament to the anterior tip of the *manubrium* of the *intercalarium*. The *tripus* continues to grow but changes little in shape or size and in the adults the interossicular ligament connecting it to the *intercalarium* has decreased in relative size with the two bones almost touching (426 mm SL; Fig. 17).

Scaphium. The *scaphium* appears in individuals as small as 11.9 mm SL as a perichondral ossification around the dorsal half of basidorsal 1 and a small membrane bone process can be seen extending anteriorly from the middle of the basidorsal cartilage by 12.2 mm SL (Figs 14B, 15A, 16A). The perichondral ossification covers the entirety of the dorsal half of basidorsal 1 by 12.7 mm SL (Figs 14C, 15B, 16B) and possesses a thin process of membrane bone from its dorsal tip, forming the ascending process of the *scaphium*. At this size, the anterior process is more robust, extends almost to the back of the cranium and a thin lamina of bone has started to form at the anterior tip of the process. By 13.3 mm SL (Figs 14D, 15C, 16C), this lamina has expanded into a large disc, the *concha scaphium*, but still remains separate from the ascending process. The *concha* posteriorly meets and joins with the ascending process (14.1 mm SL) and by 15.0 mm SL (Figs 14E, 15D, 16D) the *concha* abuts the back of the cranium almost contacting the posterior membranous extension of the exoccipital, resembling the adult condition (426 mm SL; Fig. 17).

Claustrum. The *claustrum* is a chondral bone located between the ascending process of the *scaphium* and the back of the cranium. It first appears as a perichondral ossification on the anteroventral edge of the claustral cartilage, a homologue of the supradorsal cartilage of vertebra 1 (Britz and Hoffman 2006), from which a membrane bone process extends towards the *concha* of the *scaphium* (13.1 mm SL). By 15.0 mm SL (Figs 14E, 15D), the *claustrum* expands dorsally to cover the ventral half of the supradorsal cartilage and by 44.9 mm SL, the ossification has expanded to fill most of the gap between the ascending process of the *scaphium* and the back of the cranium, although at this stage the dorsal third of the supradorsal cartilage remains unossified.

Comparison with *Noturus gyrinus*. The most common sequence of ossification for this region in *Noturus gyrinus* is as follows: centrum 1, 2, 3 and 4 (6.6. mm SL) – neural arch 4 (6.7 mm SL) – neural arch 3, outer arm of the *os suspensorium*, *intercalarium*, and *tripus* (7.3 mm SL) – *scaphium* (7.7 mm SL) – inner arm of the *os suspensorium* (8.7 mm SL) – *claustrum* (10.0 mm SL).

No differences in the sequence of ossification were identified between *Noturus gyrinus* and *Ictalurus punctatus* in the Weberian apparatus. The Weberian apparatus of *N. gyrinus* and *I. punctatus* are similar, and no major differences in adult morphology are observed in this region.

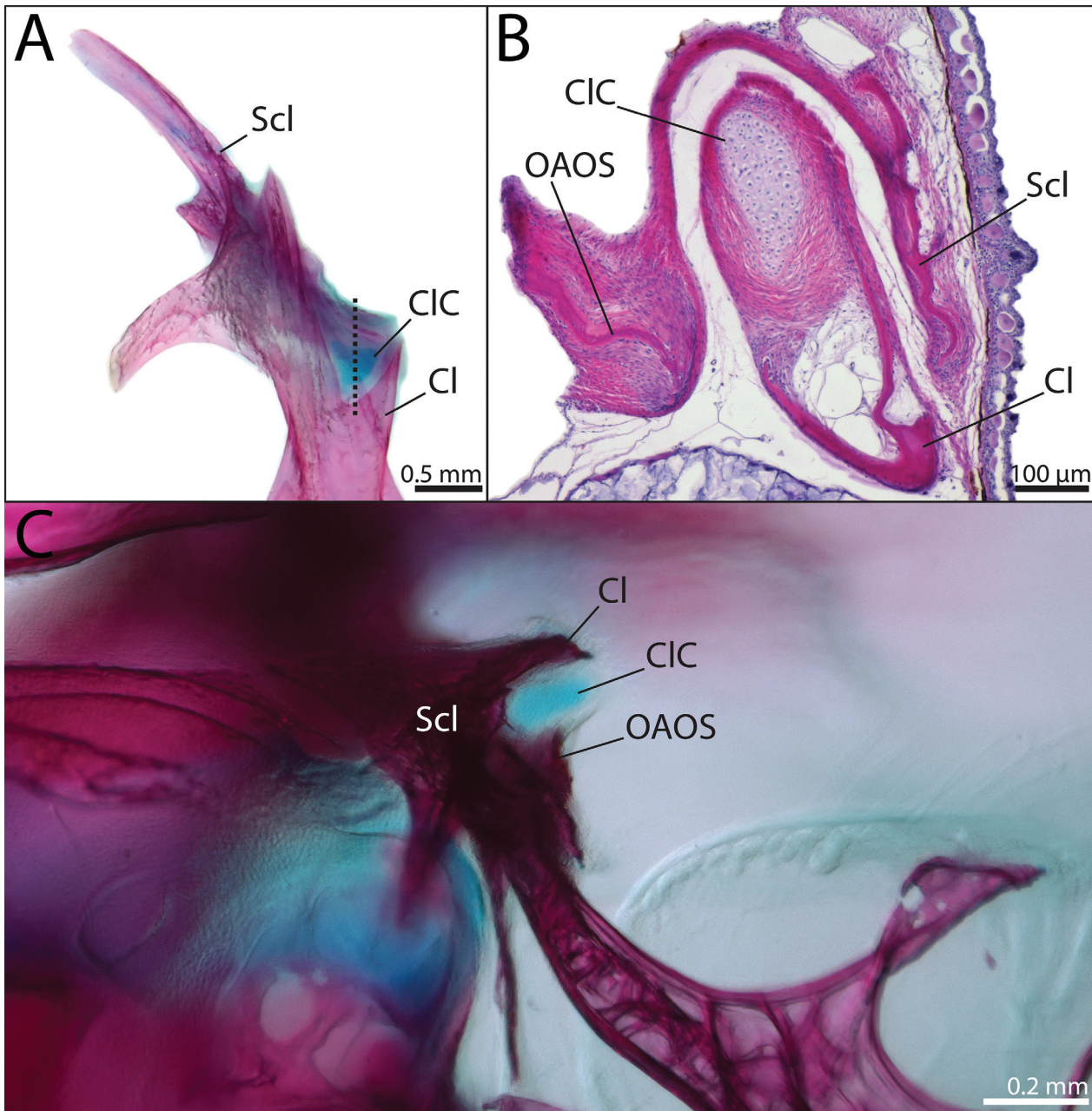


Figure 18. Cleithral cartilage of *Ictalurus punctatus* (a and c, TCWC 20491.04; b, TCWC 20491.03). **A** Medial view of upper pectoral girdle with dotted line representing approximate location of transverse section in b; 44.9 mm SL. **B** Transverse section through the upper shoulder girdle; 29.0 mm SL. **C** Dorsal view of cleithral cartilage in situ; 16.1 mm SL. Abbreviations: Cl, Cleithrum; CIC, Cleithral cartilage; OAOS, Outer arm of *Os suspensorium*; Scl, Supracleithrum.

Post-Weberian axial skeleton

The most common sequence of ossification: centrum 5 (9.9 mm SL) – neural arch 5 (11 mm SL) – parapophyses (11.4 mm SL) – post-Weberian centra (11.7 mm SL) – post-Weberian hemal arches and post-Weberian neural arches (12 mm SL) – post-Weberian hemal spines, post-Weberian neural spines and post-Weberian ribs (12.7 mm SL) (Figs 19, 20).

Centra. The centra originate as perichordal ossifications around the notochord. Centra 5–8 are the first to ossify in the entire vertebral column in individuals as small as 9.9 mm SL. Development of the vertebral column continues

anteriorly with centra 1–4 of the Weberian apparatus (see above) and posteriorly with centra 5–16 mineralized by 10.1 mm SL (Fig. 19A). These anterior abdominal centra originate as paired lateral perichordal ossifications which expand and join each other across the ventral midline and subsequently the dorsal midline. Centra 17–32 are present by 10.9 mm SL (Figs 19B, 20B) and appear to originate as four perichordal ossifications associated with the bases of the basidorsals and basiventrals. The dorsal and ventral ossifications on each side of the notochord expand toward each other until they meet forming paired perichordal ossifications on either side of the notochord. The paired ossifications then follow the pattern of the more anterior centra, joining first across the ventral and then

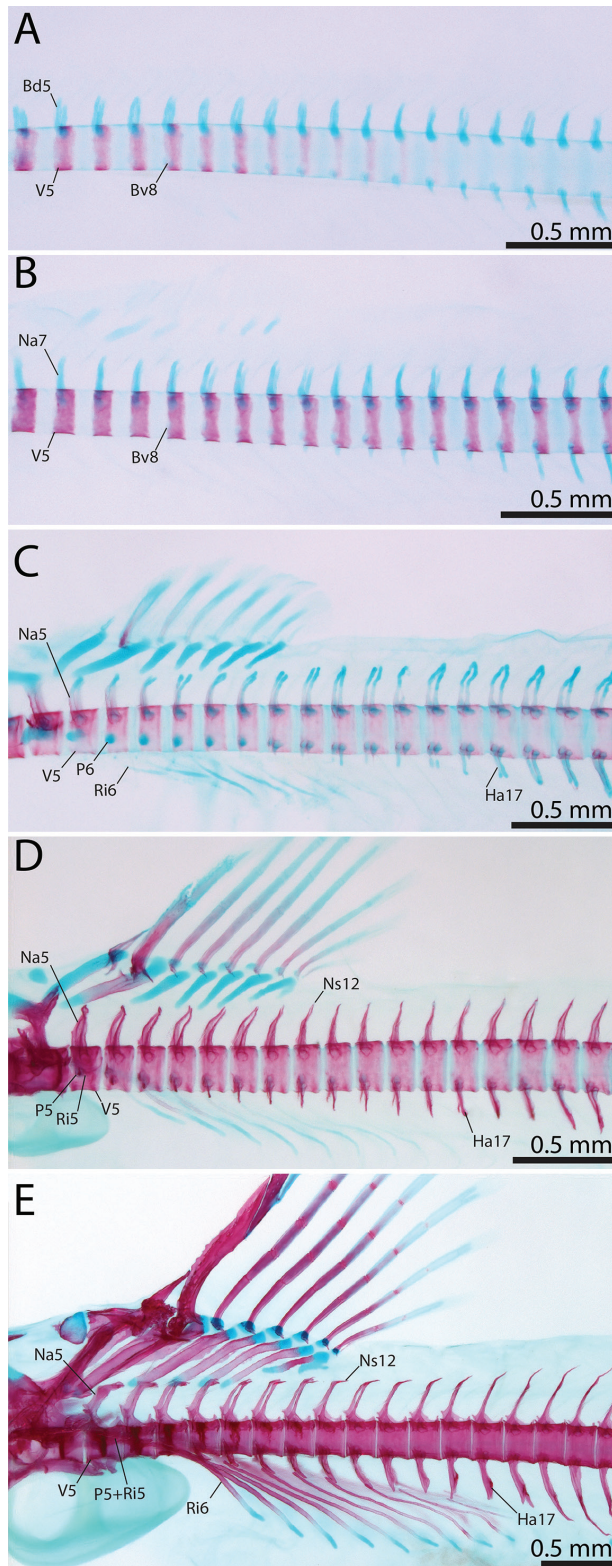


Figure 19. Ontogeny of the abdominal region of the axial skeleton in *Ictalurus punctatus*. **A** 10.1 mm SL. **B** 10.9 mm SL. **C** 12.2 mm SL. **D** 13.2 mm SL. **E** 15.5 mm SL. Abbreviations: Bd, Basidorsal; Bv, Basiventral; Ha, Hemal arch; Na, Neural arch; Ns; Neural spine; P, Parapophysis; Ri, Rib; V, Vertebra.

the dorsal midline. All of the centra, excluding preural centra 2 and 3, can be found in individuals of 11.7 mm SL or larger (Figs 19C, 20C) and by 13.2 mm SL (Figs 19D, 20D) they are completely mineralized around the

notochord. The dorsal postzygapophyses are starting to form on centra 5–26 as tiny bumps on the posterolateral edge of the centra. At 14.0 mm SL, all of the centra possess developing dorsal pre- and postzygapophyses. The dorsal prezygapophyses originate as pointed projections from a thin lamina of bone extending from the anteroventral edge of the neural arches. By 15.0 mm SL, two ventrally directed laminae of bone have formed on centrum 5 and are closely associated with the posterior tips of the ventral ridges of the compound centrum. At this stage the ventral pre- and postzygapophyses have appeared and at 15.5 mm SL (Figs 19E, 20E) a thin ridge of membrane bone has formed along the length of the centra connecting the postzygapophyses to the posterior end of the neural arches. The pre- and postzygapophyses from adjacent centra are almost in contact with one another at this point. The centra begin to take on the characteristic hourglass shape found in adults at 17.8 mm SL and by 20.1 mm SL, the centra resemble the adult condition. In adults (Fig. 20), the postzygapophyses of centra 5–10 have extended dorsally and now contact the posteriorly directed distal tip of the neural arches. The ventrolateral lamina of bone on centrum 5 is now sutured with the ventral ridges of the compound centrum. The total vertebral count most commonly observed was 51 and was comprised of 20 abdominal centra (including the four Weberian centra) and 31 caudal centra. Caudal centra counts begin with the first centrum to possess a median hemal spine and include the two ural centra.

Neural arches. The neural begin as paired basidorsal cartilages along the dorsal surface of the notochord. All of the basidorsal cartilages are present by the time the first few centra are ossified. The neural arches originate as perichondral ossifications around the base of the paired basidorsal cartilages. The first neural arches originate anteriorly with basidorsals 7–14 ossifying in an individual of 10.1 mm SL. Development of the neural arches proceed bidirectionally and by 10.9 mm SL (Figs 19B, 20B), neural arches 5–32 have formed. All of the neural arches are perichondrally ossified in individuals of 12.0 mm SL and by 12.2 mm SL (Figs 19C, 20C) most of the basidorsal cartilages are covered in perichondral bone. At this size, the paired basidorsal cartilages 16–49 have met and fused to their antimere across the dorsal midline. The neural arches are completely perichondrally ossified and have begun to endochondrally ossify by 13.2 mm SL (Figs 19D, 20D). At this point in development, left and right halves of neural arches 12–15 have fused across the dorsal midline while those of neural arches 5–11 extend towards each other distally but remain separate. By 15.5 mm SL (Figs 19E, 20E), all the neural arches are completely endochondrally ossified and neural arches 5–11 are joined across the midline, but instead of tapering and forming a neural spine, they are joined distally by a sheet of membrane bone which is associated with the posteroventral edge of proximal-middle radials 3–8. At this stage, the neural arches are connected via membrane bone ridges to the dorsal pre- and postzygapophyses. The distal tips of neural arches 5–10 continue to grow posterodorsally,

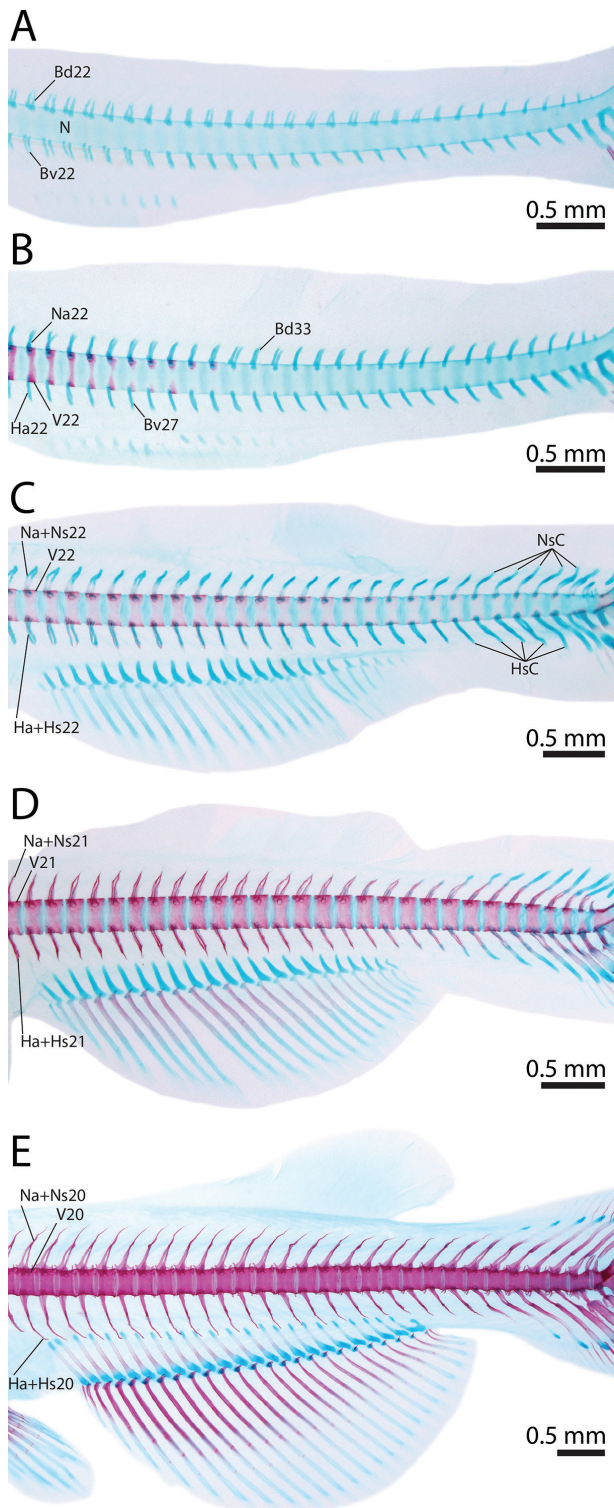


Figure 20. Ontogeny of the caudal region of the axial skeleton in *Ictalurus punctatus*. **A** 10.1 mm SL. **B** 10.9 mm SL. **C** 12.2 mm SL. **D** 13.2 mm SL. **E** 15.5 mm SL. Abbreviations: Bd, Basidorsal; Bv, Basiventral; Ha, Hemal arch; Hs, Hemal spine; Na, Neural arch; Ns; Neural spine; P, Parapophysis; Ri, Rib; V, Vertebra.

and at 20.1 mm SL these posterodorsal extensions border the ventral tips of the dorsal-fin proximal-middle radials on either side. In adults (Fig. 20), the distal tips of neural arches 5–11 have widened extensively along the rostral-caudal axis and posteroventrally they join the distal

tips of the dorsal postzygapophyses resulting in a small circular opening on the side of the vertebrae.

Parapophyses. The parapophyses are chondral bones that originate from basiventral cartilages on the lateroventral surface of the abdominal centra (Fig. 19A), excluding the transitional abdominal vertebrae which possess a complete hemal canal but lack a median hemal spine. Development of the parapophyses occurs in a posterior to anterior direction with the posteriormost basiventral cartilage, typically basiventral 16, perichondrally ossifying in some individuals as small as 10.9 mm SL. By 12.2 mm SL (Fig. 19C), all of the parapophyses are perichondrally ossifying except for that of centrum 5 which ossifies shortly after at 12.5 mm SL. At this point, small splints of membrane bone have formed at the distal tip of all of the parapophyses which serve as points of articulation for the developing ribs. The basiventral cartilages are completely covered by perichondral bone by 13.2 mm SL (Fig. 19D) and the parapophyses are endochondrally ossified by 14.0 mm SL. A thin dorsal lamina of membrane bone has also formed along the length of the parapophyses at this size. By 15.0 mm SL, the parapophyses have increased significantly in size becoming more triangular in shape and the small splint-like rib 5 has started to fuse with parapophysis 5 (Figs 15D, 16D). The fusion between the rib and parapophysis of vertebra 5 is complete at 15.5 mm SL (Fig. 19E) and the remaining parapophyses have become longer and slightly recurved. The fused parapophysis and rib of vertebra 5 extend laterally until the distal tip reaches the side of the body and the remaining parapophyses continue to expand laterally and become sickle-shaped (17.8 mm SL). In the adult (Fig. 21), the fused parapophysis and rib of vertebra 5 are now much wider and the two components have become impossible to distinguish from each other.

Hemal arches. The hemal arches are chondral bones that mineralize in the paired basiventral cartilages of the transitional abdominal and caudal vertebrae. Similar to the basidorsal cartilages, the basiventrols are all present by the time the earliest centra begin to ossify. They are uniform in size except for the four most posterior basiventrols which are thicker and more elongate than the preceding cartilages. The first hemal arches begin ossifying on centra 21–24, typically the first four caudal vertebrae, in individuals as small as 10.1 mm SL. Development proceeds anteriorly to the basiventrols of the transitional abdominal vertebrae which do not develop hemal spines but will meet each other across the ventral midline forming a hemal canal, and posteriorly until all of the hemal arches are perichondrally ossified (12.0 mm SL, Fig. 20C). At this stage, all of the basiventrols, except those of the transitional abdominal vertebrae have joined their counterpart distally across the midline forming the hemal canal. The basiventrols are completely covered in perichondral bone by 13.2 mm SL and hemal arches 18–20 form complete arches with the hemal arches 18 and 19 being joined to their counterparts by a bridge of membrane bone extending between the distal tips (Figs 19D, 20D). At 14.0 mm

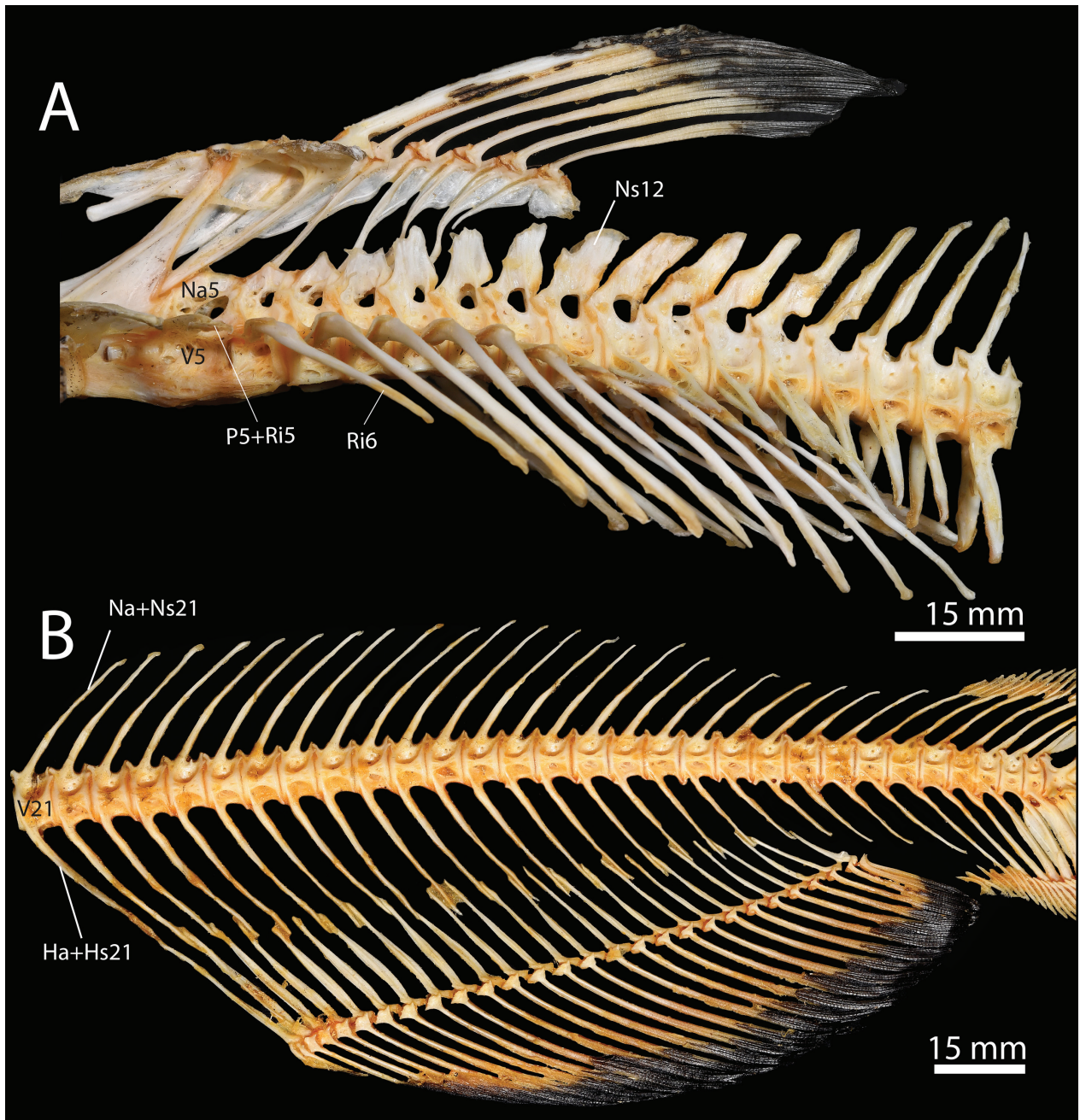


Figure 21. *Ictalurus punctatus*, specimen TCWC 20491.07, 436 mm SL (A) and TCWC 20491.08, 441 mm SL (B). **A** Abdominal region of the axial skeleton. **B** Caudal region of the axial skeleton. Abbreviations: Ha, Hemal arch; Hs, Hemal spine; Na, Neural arch; Ns; Neural spine; P, Parapophysis; Ri, Rib; V, Vertebra.

SL, the hemal arches begin to endochondrally ossify and by 15.0 mm SL, hemal arch 17 forms a complete arch with the two chondral bones connected by a thin strip of membrane bone (Figs 19E, 20E). In larger individuals (20.1 mm SL) the hemal arches are joined to the ventral pre- and postzygapophyses via membrane bone ridges. In adult individuals (Fig. 21) the hemal arches have changed little other than increasing in size and length.

Hemal spines. The hemal spines originate as membrane bone except those of preural vertebrae 2–9 which are preformed in cartilage. Hemal spines were first observed ossifying anteriorly on caudal vertebrae 25–32 as small splints of membrane bone extending from the dorsal mar-

gin of the hemal arch in an individual of 11.2 mm SL. The formation of hemal spines proceeds anteriorly towards the first caudal vertebra, typically vertebra 21, and posteriorly towards the caudal skeleton with hemal spines 21–35 ossifying by 12.2 mm SL (Fig. 20C). The ossification of all hemal spines is underway by 12.7 mm SL, with hemal spines 40–47 perichondrally ossifying around the base of their cartilage precursors. Ontogenetically, these ossifications expand dorsally along the cartilages and the membranous hemal spines grow longer but remain thin and needle-like (13.1 mm SL; Fig. 20D). By 14.0 mm SL, the hemal spines 41–42 are completely ossified and 43–47 are almost completely covered by perichondral bone except for the distalmost tip which remains carti-

luginous. The hemal spines continue to elongate and by 15.5 mm SL (Fig. 20E) they extend ventrally between the proximal-middle radials of the anal-fin. At 44.9 mm SL, the hemal spines have changed relatively little other than getting more elongate, and hemal spines 45–47 retain cartilaginous tips and serve as support for the ventral procurrent fin rays resembling the condition in adults (Fig. 20B).

Neural spines. The neural spines first appear as membrane bone ossifications on the dorsal margin of the neural arches at the middle of the vertebral column (vertebrae 27–31) in individuals as small as 11.6 mm SL. Neural spines continue to develop bidirectionally with the last to ossify being those associated with preural vertebrae 2–9, whose neural spines are preformed in cartilage (Fig. 20C). By 12.7 mm SL, the neural spines of these vertebrae are perichondrally ossifying around the base of the neural spine cartilages (Fig. 20D) and continue to progress dorsally until they cover all but the distal tips of these cartilages (14.0 mm SL). The neural spines continue to become more elongate and remain relatively thin except for neural spines 44–47 which remain cartilaginous at their distal tips and articulate with the dorsal procurrent caudal-fin rays (Fig. 19E, s20E). In adults (436 mm SL; Fig. 21A), neural spines 12–15 have widened extensively along the rostral-caudal axis and posteroventrally they join the distal tips of the dorsal postzygapophyses resulting in a small circular opening on the side of the vertebrae. No distinct neural spines ever develop on vertebrae 5–11. Grande and Shardo (2002) reported that cartilaginous median elements associated with preural centra 6–3 appeared independently of and subsequently fused to the neural spines of their respective centra. Based on the material examined herein, the median cartilaginous elements of Grande and Shardo (2002) originate from the dorsal surface of the basidorsal cartilages once a complete arch has been formed similarly to the neural spine cartilages of other otophysans (e.g., *Salminus brasiliensis*; Mattox et al. 2014).

Ribs. The first ribs to ossify are ribs 6–8 in individuals as small as 12.2 mm SL (Fig. 19C) and their presence is fixed in development at 12.7 mm SL. They originate as perichondral ossifications lateroventral to the developing parapophyses. Ossification continues distally along the rib cartilages which curve posteroventrally dorsal to the peritoneal cavity and by 12.9 mm SL ribs associated with vertebrae 9 and 10 are ossifying. A small splint like rib located lateral to the tip of the parapophysis of vertebra 5 ossifies by 13.1 mm SL (Figs 15C, 16C) around the same time as ribs 11 and 12. By 15.0 mm SL, ribs are associated with vertebra 5–15 and are fully ossified except for their distal most tips which remain cartilaginous. At this size, rib 5, which remains much shorter than the remaining ribs, begins to fuse to the parapophysis of vertebra 5 (Figs 15D, 16D) and is completely fused into a compound structure by 15.5 mm SL (Fig. 19E). The rib associated with vertebra 16 can be seen in some individuals of this size and larger; however, presence of this rib is vari-

able in *Ictalurus punctatus*. Ribs 6–15 continue to extend posteroventrally until they overlie the upper half of the peritoneal cavity (20.1 mm SL). The compound element composed of rib and parapophysis 5 remains straight and extends laterally towards the body wall. The ribs change little in the adult (Fig. 21) other than increasing in length and width.

Comparison with *Noturus gyrinus*. The most common sequence of ossification for this region in *Noturus gyrinus* is as follows: centrum 5 and neural arch 5 (6.6 mm SL) – post-Weberian neural arches (7.2 mm SL) – post-Weberian hemal arches and parapophyses (7.3 mm SL) – post-weberian centra (7.6 mm SL) – post-Weberian ribs (8 mm SL) – post-Weberian hemal spines and post-Weberian neural spines (8.6 mm SL).

The sequence of ossification in the post-Weberian axial skeleton differs between *Noturus gyrinus* and *Ictalurus punctatus* in that the parapophyses and the post-Weberian centra complete development in *N. gyrinus* after the neural and hemal arches while in *I. punctatus* they complete development before the neural and hemal arches. The post-Weberian axial skeleton of *N. gyrinus* and *I. punctatus* are very similar, and only differ in the number of abdominal and caudal vertebrae and associated elements (typically 13 abdominal vertebrae and 28 caudal vertebrae in *N. gyrinus* vs. 20 abdominal vertebrae and 31 caudal vertebrae in *I. punctatus*).

Dorsal fin

The most common sequence of ossification: dorsal-fin spine 2 and dorsal-fin rays (11.4 mm SL) – dorsal-fin spine 1 (12.2 mm SL) – dorsal-fin proximal-middle radial 3 (12.8 mm SL) – dorsal-fin proximal-middle radial 2 and dorsal-fin proximal-middle radials (13.2 mm SL) – dorsal-fin proximal-middle radial 1 (15.0 mm SL) – dorsal-fin distal radials (15.2 mm SL). (Fig. 22)

Dorsal-fin rays and spines. The dorsal fin, along with the anal fin, begins development after the pectoral fin. The dermal dorsal-fin rays first appear in the larval-fin fold by 11.4 mm SL. The second dorsal-fin ray, which will become dorsal-fin spine 2, is the first to appear in some individuals as small as 10.9 mm SL followed shortly by the third dorsal-fin ray (11.1 mm SL at first appearance). Development continues to proceed in a posterior direction until there is one fin ray in serial association with proximal-middle radials 2–8. At approximately the same time (12.2 mm SL; Fig. 22A), the first dorsal-fin ray, which will become the first dorsal-fin spine, appears dorsal to proximal-middle radial 2 and the second dorsal-fin ray begins to become more heavily ossified near its proximal base. By 12.7 mm SL, a full complement of dorsal-fin rays (ii.7) is present with the formation of dorsal-fin ray 9. Dorsal-fin rays 2–6 are segmented and have increased in length giving the dorsal-fin a rounded shape. The second-dorsal fin ray has grown to twice the width of the rest of the dorsal-fin rays and a distal ramus (*sensu* Kubicek et al. 2019) has started to form on the anterodistal tip of

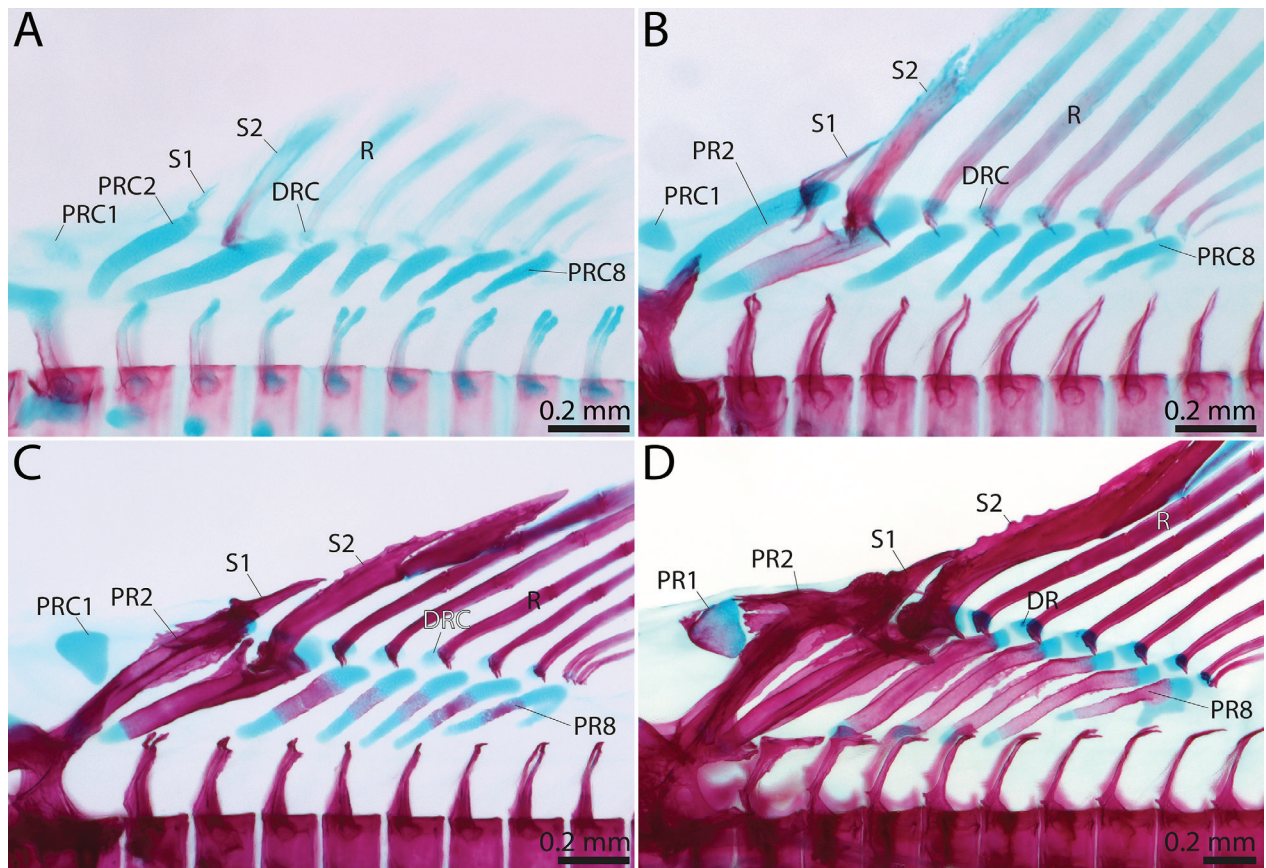


Figure 22. Ontogeny of the dorsal fin skeleton in *Ictalurus punctatus*. **A** 12.2 mm SL. **B** 13.2 mm SL. **C** 14.0 mm SL. **D** 15.5 mm SL. Abbreviations: DR, Distal radial; DRC, Distal radial cartilage; PR, Proximal-middle radial; PRC, Proximal-middle radial cartilage; R, Dorsal-fin ray; S, Dorsal-fin spine.

the proximal most segment. The anterior edge of the first segment of dorsal-fin spine 2 has fused across the midline along its distal half forming the spine proper (13.2 mm SL; Fig. 22B). Additionally, two medial projections have formed on the anteroproximal base of each hemitrichium in dorsal-fin spine 2 above a small concavity in the dorsal surface of dorsal-fin proximal radial 3. The hemitrichia of the first dorsal-fin ray have fused across the midline at the distal tip forming dorsal-fin spine 1. By this point, it has grown to approximately half the size of the first segment of dorsal-fin spine 2 with the distal-tip of dorsal-fin spine 1 reaching the ventral margin of the fused anterior edge in the former. At 14.0 mm SL (Fig. 22C), left and right halves of dorsal-fin spine 1 has completely fused across its anterior midline and although it has grown wider it has not increased in height. Dorsal-fin spine 1 possesses ventral projections which extends toward the middle nuchal plate (i.e., lateral extensions of membrane bone that form on proximal-middle radial 2 and form part of the spine locking mechanism). At the same stage, the second segment of dorsal-fin spine has begun to fuse to the proximalmost segment and the formation of two additional distal segments is underway. The left and right medial projections of the base of dorsal-fin spine 2 have met and fused across the midline of the body forming an opening in the spine between it and the ventralmost point of fusion across the anterior midline. Additionally, anteroventral projections of the base of dorsal-fin spine 2 extend towards and al-

most contact the posterior nuchal plate (i.e., lateral extensions of membrane bone that form on proximal-middle radial 3 and form part of the spine locking mechanism). Dorsal-fin rays 3–9 have continued to increase in length and are all segmented and by 15.5 mm SL (Fig. 22D) fin rays 3–6 have started to branch. At this stage, the distal tip of the first dorsal-fin spine is firmly connected to the anterior surface of the second dorsal-fin spine and both are closely associated and articulating with the middle and posterior nuchal plates respectively, allowing dorsal-fin spine 2 to be locked into an erect position. The opening in the base of dorsal-fin spine 2 has become smaller and now serves as a foramen through which a ring-like process of bone arising from dorsal proximal-middle radial 3 passes, restricting the movement of the spine to an anterior and posterior direction and creating the “chain-link” articulation (*sensu* Bridge 1896) characteristic of the second dorsal-fin spine in catfishes. A third segment is now fused to the spine proper and denticuli have started to form on the anterior edge of the proximal most segment. At 20.1 mm SL, all but the last fin-ray are branched and the dorsal-fin resembles the adult condition.

Dorsal-fin proximal-middle radials 1, 2 and 3. Dorsal-fin proximal-middle radials 2 and 3 start off as cartilaginous rods that appear dorsal to centra 5–7 (Fig. 19B). By 12.2 mm SL (Fig. 22A), proximal-middle radials 2 and 3 are approximately twice the length of the

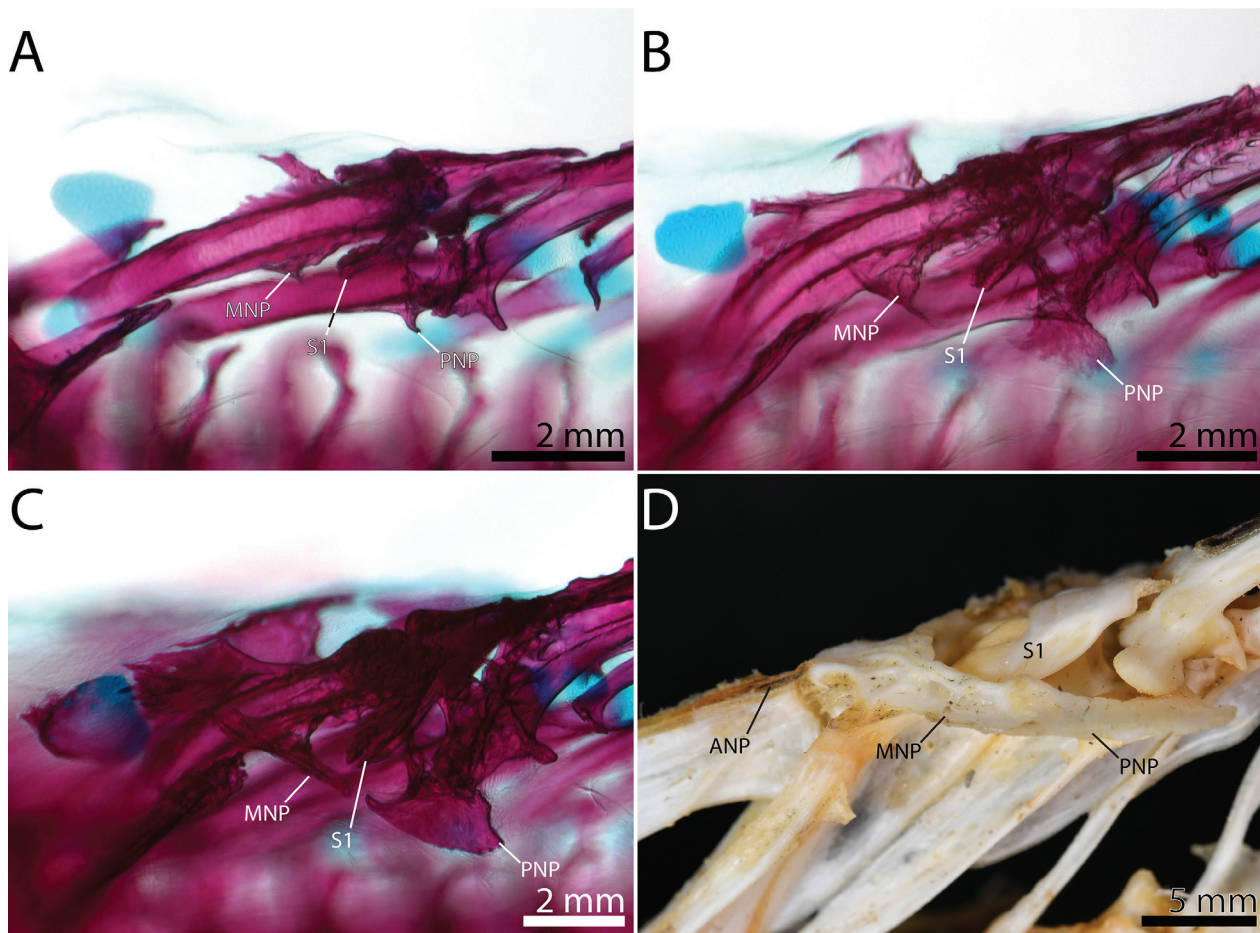


Figure 23. Ontogeny of the nuchal plates in *Ictalurus punctatus*. **A** 13.5 mm SL **B** 14.3 mm SL **C** 15.3 mm SL **D** 436 mm SL. Abbreviations: ANP, Anterior nuchal plate; MNP, Middle nuchal plate; PNP, Posterior nuchal plate; S1, 1st dorsal-fin spine.

more posterior proximal-middle radial cartilages, with the proximal tip of the latter sitting just dorsal to neural arch 5. Dorsal-fin proximal-middle radial 1 is present at this stage as a round cartilage located anterodorsally to the ventral tip of the proximal-middle radial 2. Proximal-middle radial 3 is the first to ossify (12.8 mm SL) as a perichondral ossification around the middle portion of the cartilage followed shortly by proximal-middle radial 2 at 13.2 mm SL (Fig. 22B). At this stage, proximal-middle radial 2 extends ventrally between the posterodorsal processes of neural arch 4 and the proximal tip of proximal-middle radial 3 has extended anterior to neural arch 5 and now reaches just posterior to these posterodorsal processes. The perichondral proximal-middle radial 3 extends over a large portion of the cartilage and small ridges of membrane bone, representing the early stages of the posterior nuchal plate of the spine locking mechanism, can be seen forming on the lateral edges of the bone. Additionally, a small extension of membrane bone projects dorsally from the anterior midline of the distal third of proximal-middle radial 3. Just posterior to this membranous extension, the cartilaginous distal tip has become slightly concave on its anterodorsal surface below the articulation with dorsal-fin spine 2 and a small anterior extension of cartilage can be seen extending from the tip of proximal-middle radial 3 anteriorly between the hemitrichia of dorsal-fin spine 2. By 13.5 mm SL (Fig.

23A), proximal-middle radial 2 extends over much of the cartilage and membranous ridges, the earliest stages of the middle nuchal plate of the spine locking mechanism, have formed on the lateral edges of the bone. At the same size, the posterior nuchal plate has expanded to form laterally directed rod-like extensions. In specimens of approximately 14.0 mm SL (Fig. 22C, Fig. 23B), the middle nuchal plate has extended laterally into larger flanges of membrane bone with two wing-like processes dorsally extending anteroventrally to the base of dorsal-fin spine 1. Additionally, a flange of membrane bone has started to form along the anterior and posterior midline of the bone. The rod-like extensions of the posterior nuchal plate extend ventrally to and almost contact the base of dorsal-fin spine 2. The membranous process on the anterior midline of proximal-middle radial 3 has expanded anteriorly to almost meet the posterior edge of the preceding radial and is now recurved with the tip directed towards the foramen in the base of dorsal-fin spine 2. At 15.0 mm SL, proximal-middle radial 1 is perichondrally ossified around the ventral half of the cartilage and proximal-middle radial 2 is completely ossified with the only remaining cartilage located at the proximal tip. The flange of bone on the anterior midline extends towards proximal-middle radial 1 cartilage. The membranous process on the anterior midline of proximal-middle radial 3 now abuts and forms a strong connection to the posterior edge of prox-

imal-middle radial 2 anteriorly. The recurved tip of this process contacts the perichondrally ossifying anterior extension of cartilage, which extends through the foramen in the base of dorsal-fin spine 2 forming a solid ring of bone, creating the “chain-link” articulation (*sensu* Bridge 1896) characteristic of the second dorsal-fin spine of catfishes. The middle and posterior nuchal plates have both expanded laterally forming a shelf on either side of proximal-middle radial 2 and 3 (Fig. 23C) and by 15.5 mm SL (Fig. 22D) have formed processes lateral to and enclosing the proximal base of dorsal-fin spine 1 completing the spine locking mechanism of the dorsal fin. At this stage, the middle nuchal plate has also formed a close connection with the posterodorsal processes of neural arch 4 and a membrane bone extension has formed anteriorly from proximal-middle radial 1 towards the supraoccipital crest of the neurocranium. By 17.1 mm SL, proximal-middle radial 2 forms a tight connection with proximal-middle radial 3 posteriorly and has started to form an interdigitated suture with proximal-middle radial 1 anteriorly. At this size, proximal-middle radial 1 is ossified endochondrally and is surrounded by a lamina of membrane bone, giving the radial a rhomboid shape. Anteriorly, the dorsal tip of proximal-middle radial 1 almost reaches the tip of the supraoccipital and two small pointed projections have also started to form on the anteroventral edge of the bone extending towards the back of the neurocranium. By 20.1 mm SL, the middle and posterior nuchal plates meet and begin to form an interdigitated suture. The anterodorsal tip of proximal-middle radial 1 reaches and is connected to the tip of the supraoccipital crest via dense connective tissue. In the adult, (436 mm SL; Fig. 23D, Fig. 24A), proximal-middle radials 2 and 3 are completely connected along their border, as well as with proximal-middle radials 1 and 4, and form a close connection ventrally with the posterodorsal processes of neural arch 4. Proximal-middle radial 1 is more elongate and triangular in shape and the dorsal surface of the bone has expanded slightly forming a narrow triangular-shaped anterior nuchal plate. The middle nuchal plate forms a tight suture anteriorly with the narrow anterior nuchal plate and posteriorly with the posterior nuchal plate.

Dorsal-fin proximal-middle radials 4–8. The dorsal-fin proximal-middle radials originate as small cartilages in individuals as small as 10.9 mm SL (Fig. 19B). By 12.2 mm SL (Fig. 22A) all of the proximal-middle radial cartilages are present and have become elongated and rod-shaped. The proximal-middle radial cartilages originate as perichondral bone around the middle section of the proximal-radial cartilages starting with proximal-middle radial 4 at 12.8 mm SL. The ossification of the proximal-middle proceeds posteriorly and by 14.0 mm SL (Fig. 22C) radials 4–8 are perichondrally ossified. By this stage, the dorsal-fin stay (*sensu* Weitzman 1962) has formed as a ventrally directed cartilage flange on proximal-middle radial 8. The ossifications continue to spread across the proximal-radial cartilages until all but the distal and proximal tips are covered in bone (15.0 mm SL)

and shortly after (15.5 mm SL; Fig. 22D), proximal-middle radials 4–7 start to form flanges of membrane bone along their anterior and posterior midline. At this point, the ventral tips of the radials 4–8 overlie the fused neural arches of centra 6–10. By 17.8 mm SL, the anterior and posterior flanges of membrane bone, of which one has also formed on the anterior edge of radial 8, have continued to expand, decreasing the gaps between radials. Thin laminae of membrane bone now extend laterally from the anterodorsal edge of proximal-middle radials forming a shelf directly ventral to the cartilaginous distal tip of the preceding radial. The dorsal-fin stay of proximal-middle radial 8 is ossified except for the ventral and dorsal tips and a posterior extension of cartilage has formed on the posterodorsal tip of the cartilage. In adult specimens (436 mm SL; Fig. 24A), the flanges of membrane bone completely close the gap between the radials and they are all firmly connected together via dense connective tissue.

Dorsal-fin distal radials. The dorsal-fin distal radials are chondral bones whose precursors originate as small nodules of cartilage between the proximal ends of the hemitrichia of the dorsal-fin rays (12.2 mm SL; Fig. 22A) and are serially associated with proximal-middle radials 3–8. The distal radials first appear as small lateral perichondral ossifications on the distal radial cartilages. The first distal radial to ossify is serially associated with proximal-middle radial 4 at 15.2 mm SL and by 15.5 mm SL (Fig. 22D) distal radial 5 has also started to ossify. Development continues posteriorly and by 17.8 mm distal radials 6 and 7 have also appeared. In adult specimens (436 mm SL; Fig. 24A), distal radials 4–8 are fully ossified as paired elements with a sliver of cartilage between them. Distal radial 3 does not ossify and instead remains cartilaginous even in adults.

Comparison with *Noturus gyrinus*. The most common sequence of ossification for this region in *Noturus gyrinus* is as follows: dorsal-fin spine 2 (7.2 mm SL) – dorsal-fin rays (7.3 mm SL) – dorsal-fin spine 1 (7.9 mm SL) – dorsal-fin proximal-middle radial 3 (8 mm SL) – dorsal-fin proximal-middle radial 2 (8.6 mm SL) – dorsal-fin proximal-middle radials (9 mm SL) – dorsal-fin proximal-middle radial 1 (10.2 mm SL) – dorsal-fin distal radials.

The dorsal-fin sequence of ossification was better resolved for *Noturus gyrinus* than *Ictalurus punctatus*. Dorsal-fin spine 2 ossifies before the remaining dorsal-fin rays in *N. gyrinus* while in *I. punctatus* they have the same fixed length. However, some individuals of *I. punctatus* did possess dorsal-fin spine 2 before the remaining dorsal-fin rays suggesting the same pattern of appearance. Additionally, dorsal-fin proximal-middle radial 2 ossifies before the remaining proximal-middle radials in *N. gyrinus* while in *I. punctatus* they appeared at the same time. The dorsal fin of *N. gyrinus* is very similar to that of *I. punctatus* with the only noted difference being the shape of dorsal-fin spine 2 which lacks anterior denticuli and posterior serrations in *N. gyrinus*.

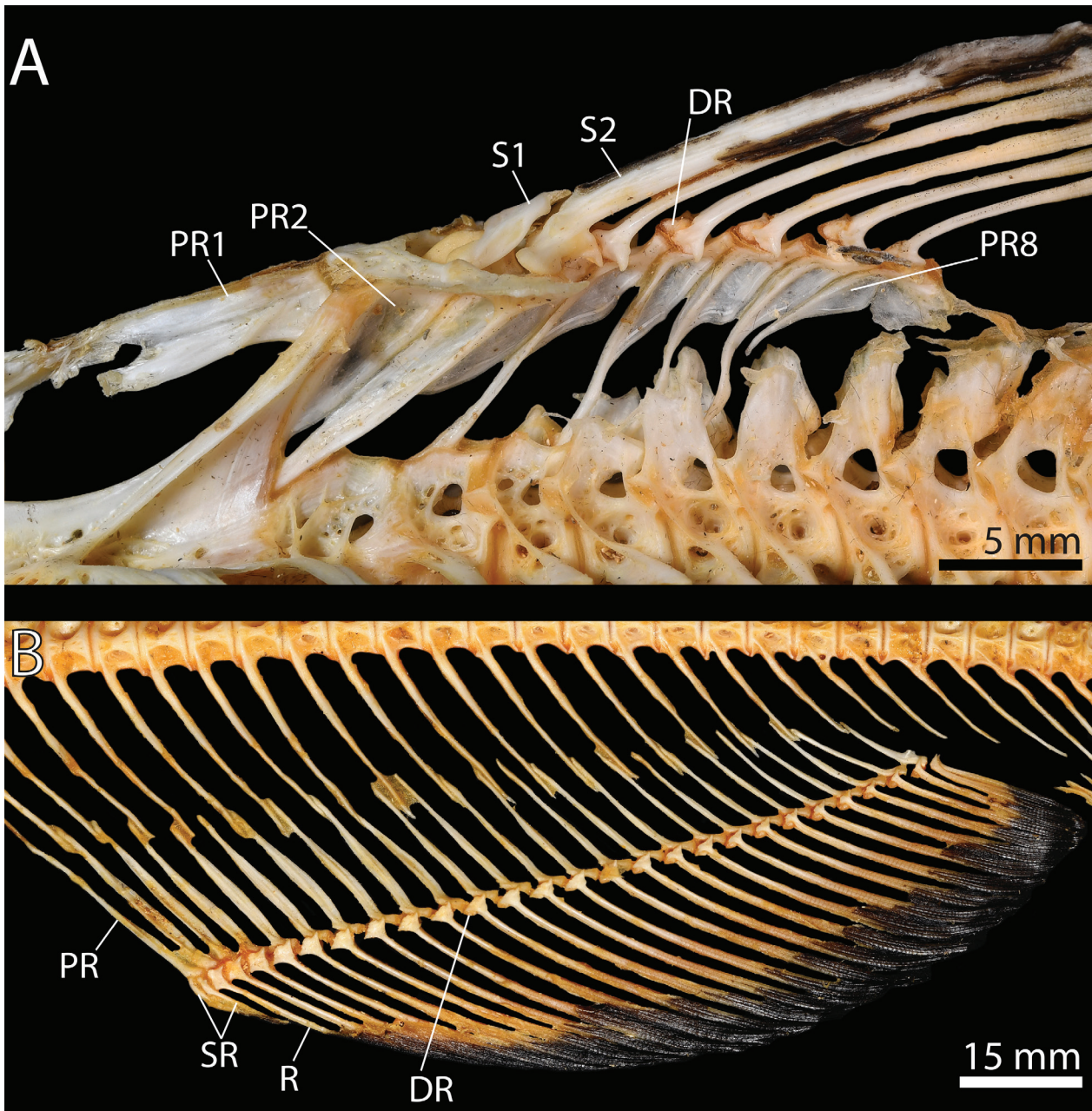


Figure 24. *Ictalurus punctatus*, specimen TCWC 20491.07, 436 mm SL (A) and TCWC 20491.08, 441 mm SL (B). **A** Dorsal-fin skeleton. **B** Anal-fin skeleton. Abbreviations: Dr, Distal radial; PR, Proximal-middle radial; R, Soft-fin ray; S, Dorsal-fin spine; SR, Supernumerary fin ray.

Anal fin

The most common sequence of ossification: anal-fin rays (11.4 mm SL) – anal-fin proximal-middle radials (13.4 mm SL) – anal-fin distal radials (21.2 mm SL). (Fig. 25)

Anal-fin rays. The anal-fin develops at approximately the same time as the dorsal fin with the first fin rays appearing in individuals as small as 10.9 mm SL. By 11.7 mm SL (Fig. 25A), 14 anal-fin rays are visible in the larval anal-fin fold and are serially associated with anal-fin proximal-middle radial cartilages 4–17. Of the 14 anal-fin rays present, those towards the middle of

the series are the most developed. At 13.1 mm SL (Fig. 25B), the anal fin possesses serially associated fin-rays on all of the anal-fin proximal-middle radial cartilages and a single supernumerary ray is associated with anal-fin proximal-middle radial 1. The larval anal-fin fold has regressed and the anal fin is now convex along its distal margin with the fin rays serially associated with anal-fin proximal-middle radial cartilages 8–12 being the longest. Anal-fin rays 5–24 are segmented distally. Shortly after (14.0 mm SL; Fig. 25C), individuals have a full complement of anal-fin rays (v.22–v.24) with all fin rays serially associated with anal-fin pterygiophores except for two supernumerary rays articulating with the anterodorsal margin of anal-fin proximal-middle radial 1 and the

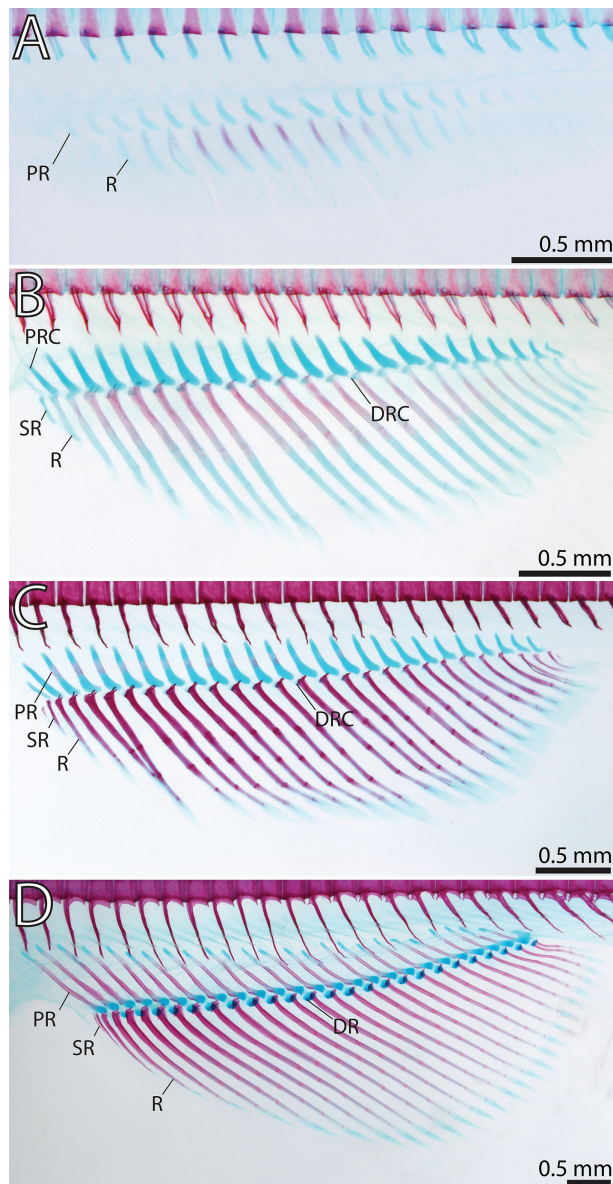


Figure 25. Ontogeny of the anal fin skeleton in *Ictalurus punctatus*. **A** 11.7 mm SL. **B** 13.2 mm SL. **C** 14.0 mm SL. **D** 20.1 mm SL. Abbreviations: DR, Distal radial; DRC, Distal radial cartilage; PR, Proximal-middle radial; PRC, Proximal-middle radial cartilage; R, Anal-fin ray; SR, Supernumerary fin ray.

last fin ray which along with the penultimate ray is also associated with the last proximal middle radial and last distal radial cartilage. By 20.1 mm SL (Fig. 25D), all of the anal-fin rays except the first supernumerary ray are segmented but none of the fin rays have started to branch. In some individuals, an additional splint-like third supernumerary ray forms anteriorly to the other two supernumerary rays (Fig. 24D); however, this fin ray is variably present and some adults possess only two supernumerary fin rays (Fig. 23B).

Anal-fin proximal-middle radials. The precursors of anal-fin proximal-middle radials first appear as small nodules of cartilage along the posteroventral midline of the body in some individuals as small as 10.1 mm SL

(Fig. 20A) and by 11.7 mm SL several of these cartilages have elongated and are slightly curved posteriorly at their distal margin (Fig. 20A). At 13.1 mm SL (Fig. 25B) the full complement of proximal-middle radial cartilages are present with those located more anteriorly typically being more elongate. The anal-fin proximal-middle radials start to ossify perichondrally around the middle portion of more proximal-middle radial cartilages 3–10 at 13.4 mm SL and by 14.0 mm SL (Fig. 25C) proximal-middle radials 3–17 are perichondrally ossified. All of the proximal-middle radials are ossified perichondrally by 14.8 mm SL and the posteriormost proximal middle radial possesses an anterodorsally projecting process, or anal-fin stay (*sensu* Weitzman 1962), at its posteriormost margin making the element axe-shaped. At 20.1 mm SL (Fig. 25D), all of the proximal-middle radials are endochondrally ossifying but remain cartilaginous at their proximal and distal tips. Also at this stage, flanges of membrane bone are forming on the anterior and posterior midlines of the first nine proximal-middle radials. In adult individuals (441 mm SL; Fig. 24B), the proximal middle radials have become more elongate, slender and no longer possess cartilage at their proximal tips. Anterior and posterior flanges of membrane bone can be seen on all of proximal-middle radials but are restricted to the distal half of the radials and are not as prominent as those of juvenile stages.

Anal-fin distal radials. The anal-fin distal radials first appear as small round cartilages between the proximal bases of the anal-fin ray hemitrichia in individuals as small as 12.2 mm SL (Fig. 20A). By 18 mm SL, there is a distal radial cartilage associated with each proximal-middle radial except for proximal-middle radial 1. At the same size, the distal radials start to form as two small lateral perichondral ossifications on the anterolateral margin of the distal radial cartilages and by 20.1 mm SL (Fig. 25D) distal radials 5–20 are present. Development of the distal radials continues bilaterally and by 44.9 mm SL all but the anteriormost two and posteriormost three distal radials are ossifying. In adults (441 mm SL; Fig. 24B) the distal radials are all ossified with each being composed of two lateral ossifications that are separated medially by a thin strip of cartilage.

Comparison with *Noturus gyrinus*. The most common sequence of ossification for this region in *Noturus gyrinus* is as follows: anal-fin rays (7.3 mm SL) – anal-fin proximal-middle radials (8.9 mm SL) – anal-fin distal radials.

No differences in the sequence of ossification were identified between *Noturus gyrinus* and *Ictalurus punctatus* in the anal fin. Only two differences were observed between *N. gyrinus* and *I. punctatus*. The first is that the anal-fin formula of *N. gyrinus* is iv.11–iv.13 compared to *I. punctatus* in which it is v.22–v.24. Additionally, *N. gyrinus* possesses a distal radial cartilage in serial association with the anteriormost proximal-middle radial unlike that of *I. punctatus*.

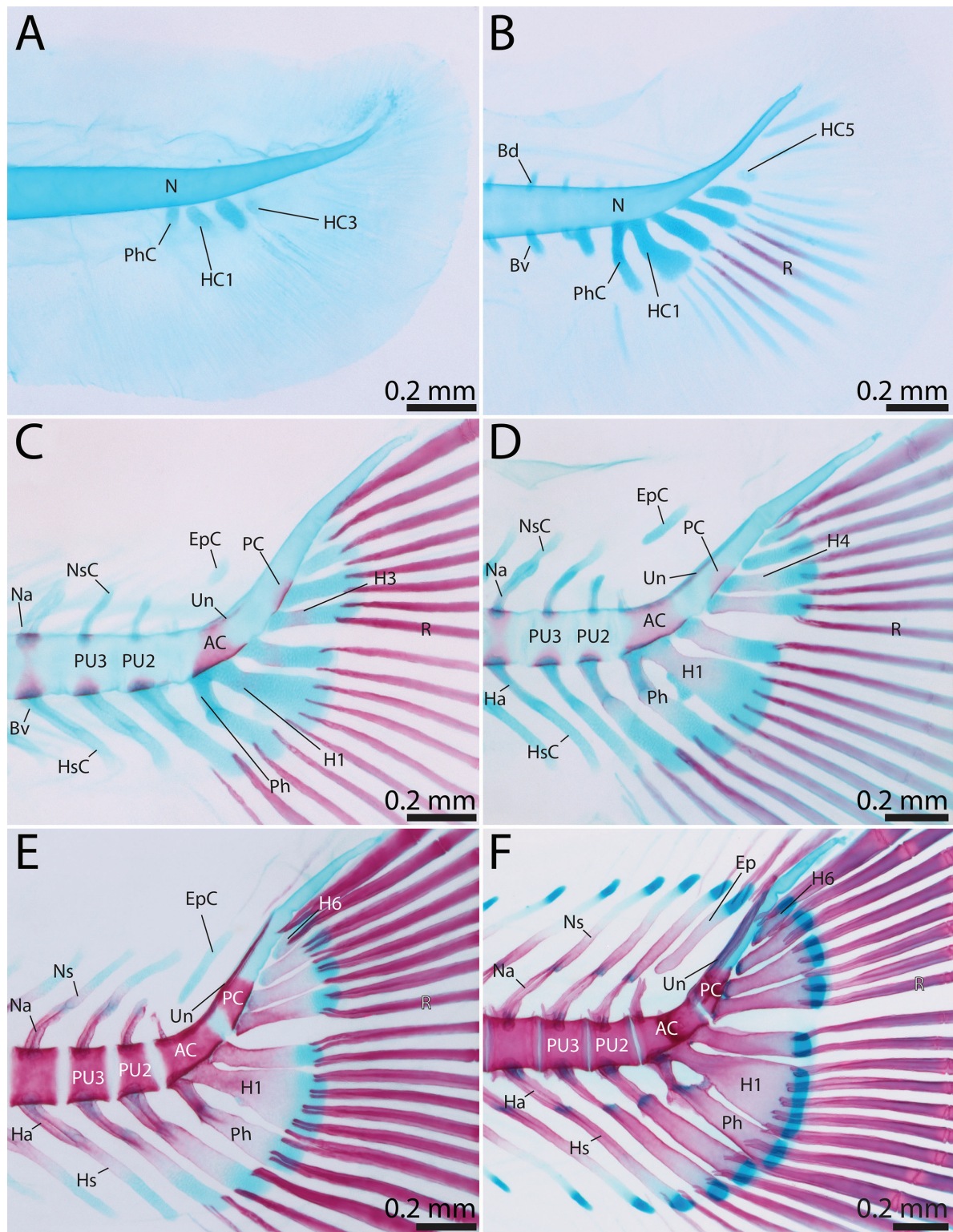


Figure 26. Ontogeny of the caudal-fin skeleton in *Ictalurus punctatus*. **A** 8.9 mm NL. **B** 9.7 mm NL. **C** 11.6 mm SL. **D** 11.9 mm SL. **E** 12.3 mm SL. **F** 15.0 mm SL. Abbreviations: AC, Anterior ural centrum; Bd, Basidorsal; Bv, Basiventral; Ep, Epural; EpC, Epural cartilage; H, Hypural; Ha, Hemal arch; HC, Hypural cartilage; Hs, Hemal spine; HsC, Hemal spine cartilage; Na, Neural arch; Ns, Neural spine; NsC, Neural spine cartilage; PC, Posterior ural centrum; Ph, Parhypural; PhC, Parhypural cartilage; PU, Preural centrum; R, Caudal-fin ray; Un, Unoneural.

Caudal fin and supporting skeleton

The most common sequence of ossification: principal caudal-fin rays (8.7 mm NL) – ventral procurrent caudal-fin rays (10.9 mm SL) – anterior ural centrum and

preural centrum 2 and 3 (11.7 mm SL) – posterior ural centrum and unoneural 1 (11.9 mm SL) – hemal arch of PU2 and PU3, hypurals 1, 2, 3, and 4, neural arch of PU2 and PU3 and parhypural (12 mm SL) – hemal spine of PU2 and PU3 (12.2 mm SL) – hypural 5 and dorsal pro-

current caudal-fin rays (12.5 mm SL) – neural spine PU3 (12.7 mm SL) – hypural 6 (12.8 mm SL) – epural (13.4 mm SL) (Fig. 26).

Principal caudal-fin rays. The first principal caudal-fin rays to form are associated with hypural cartilages 2 and 3 at 8.7 mm NL (Fig. 26A). Fin rays are continually added anteroventrally and posterodorsally and nearing the end of flexion (9.7 mm NL; Fig. 26B), the upper caudal-fin lobe possesses all eight principal caudal-fin rays and five fin rays support the lower caudal lobe. The full complement of principal caudal-fin rays (8+9) can be seen by 11.6 mm SL (Fig. 26C). At this stage the ventralmost principal caudal-fin ray articulates with the hemal spine cartilage of PU2 while the dorsalmost fin-ray in the upper caudal-fin lobe articulates with the developing hypural 6 cartilage. Both the dorsal- and ventralmost principal caudal-fin rays are larger than the remaining caudal fin-rays and by 15.0 mm SL (Fig. 26F) they are the longest fin-rays in the caudal fin and approximately twice the width of the other fin-rays. The length of the remaining principal caudal-fin rays decreases sequentially towards the middle of the fin, resulting in a distinctive forked caudal fin. By 15.5 mm SL, the two innermost fin rays in the upper and lower caudal-fin lobe are branching distally with all of the principal caudal-fin rays branched, excluding the dorsal- and ventralmost, by 20.1 mm SL. Additionally, the ventralmost principal caudal-fin ray has shifted to articulate with the parhypural. At this point, the caudal fin resembles the adult condition (436 mm SL; Fig. 27D).

Procurrent caudal-fin rays. The ventral procurrent rays are the first to appear with a single procurrent ray forming anterior to the ventralmost principal caudal-fin ray at 10.9 mm SL. The ventral procurrent rays are added anteriorly with two additional rays ossifying by 11.9 mm SL (Fig. 26D). At this size, a single dorsal procurrent fin ray is visible in some individuals anterodorsal to the notochord. Subsequent dorsal procurrent rays also develop in an anterior direction similarly to the ventral procurrent rays. Despite appearing later than the ventral procurrent rays, by 15.5 mm SL there are 12 procurrent rays dorsally and ventrally which articulate with the cartilaginous tips of the neural and hemal spines of PU2–PU6. The procurrent rays continue to form and decrease in size anteriorly until the adult condition is reached (16 ventral procurrent rays at 20.1 mm SL; 19 dorsal procurrent rays at 28.0 mm SL).

Anterior and posterior ural centra. The anterior ural centrum appears as a perichordal ossification of the notochord along the bases of the parhypural and hypurals 1 and 2 in individuals as small as 10.9 mm SL (fixed in development at 11.7 mm SL). The perichordal ossification expands dorsolaterally until the two sides meet at the distal midline forming a complete ring of bone around the notochord (11.6 mm SL; Fig. 26C). The posterior ural centrum appears around this stage as a small perichordal ossification along the connection of the notochord with hypurals 3 and 4. By 11.9 mm SL (Fig. 26D), the ante-

rior ural centrum has expanded into a cylinder of bone extending the length of the bases of the parhypural and hypurals 1 and 2. Additionally, a small rudimentary pair of basidorsals, which have begun to ossify perichondrally as neural arches, is now associated with the anterior ural centrum and it has fused with the single pair of uroneurals, which form the pleurostyle. The posterior ural centrum eventually surrounds the notochord (12.3 mm SL; Fig. 26E) and the anterior ural centrum has begun to fuse with the parhypural and hypurals 1 and 2. The small rudimentary neural arch has started to endochondrally ossify and possess a small pointed tip of membrane bone. By 15.0 mm SL (Fig. 26F), the anterior ural centrum has completed its fusion to the parhypural and hypurals 1 and 2 and the neural arch is endochondrally ossified but the two ossifications remain separate and do not form an arch. The posterior ural centrum is now fused with hypural 3 and by 17.8 mm SL, it has also fused with hypural 4. A close connection has formed between the posterior ural centrum and the pleurostyle but the elements do not fuse. At this stage, the dorsal and ventral prezygapophyses have formed on the anterior margin of the anterior ural centrum. In adults (436 mm SL; Fig. 27D) the anterior ural centrum, which is fused with uroneural 1, parhypural and hypurals 1 and 2, remains separate from the posterior ural centrum, which is fused with hypurals 3 and 4.

Preural centra 2 and 3. Preural centra 2 and 3 are the last centra in the vertebral column to ossify and first appear in individuals of 11.0 mm SL and their presence is fixed in development at 11.7 mm SL. Both centra originate as four separate perichordal ossifications around the base of the basidorsal and basiventral cartilages. Unlike preceding centra, the ossifications of PU2 and PU3 meet across the dorsal and ventral midline of the notochord first (11.9 mm SL; Fig. 21D) before later fusing laterally to form complete rings around the notochord (12.5 mm SL). The centra continue to increase in size until they abut the adjacent centra and at 15.0 mm SL (Fig. 26F) the dorsal and ventral pre- and postzygapophyses develop on the two centra. At 17.8 mm SL, ridges of membrane bone extend from the neural and hemal arches along the dorsolateral and ventrolateral margins of the centra spanning their length between the pre- and postzygapophyses and by 20.1 mm SL, PU2 and PU3 start to take on a hourglass shape that is typical of the adult condition.

Uroneural 1. The single pair of uroneurals originates as thin paired splints of membrane bone dorsolateral to the anterior ural centrum in individuals as small as 11.2 mm SL (Fig. 26C). The anterior margin of the uroneural is fused to the anterior ural centrum by 11.9 mm SL (Fig. 26D) forming the pleurostyle. Ontogenetically, the uroneural expands posterodorsally along the notochord until the posterior tip is in line with the dorsal margin of hypural 6 (12.3 mm SL; Figure 18E). By 15.0 mm SL (Fig. 26F), the uroneural extends further posterodorsally until it is approximately in line with the dorsal tips of the epural and neural spines supporting the procurrent caudal fin rays, and has become wider. The uroneural continues to

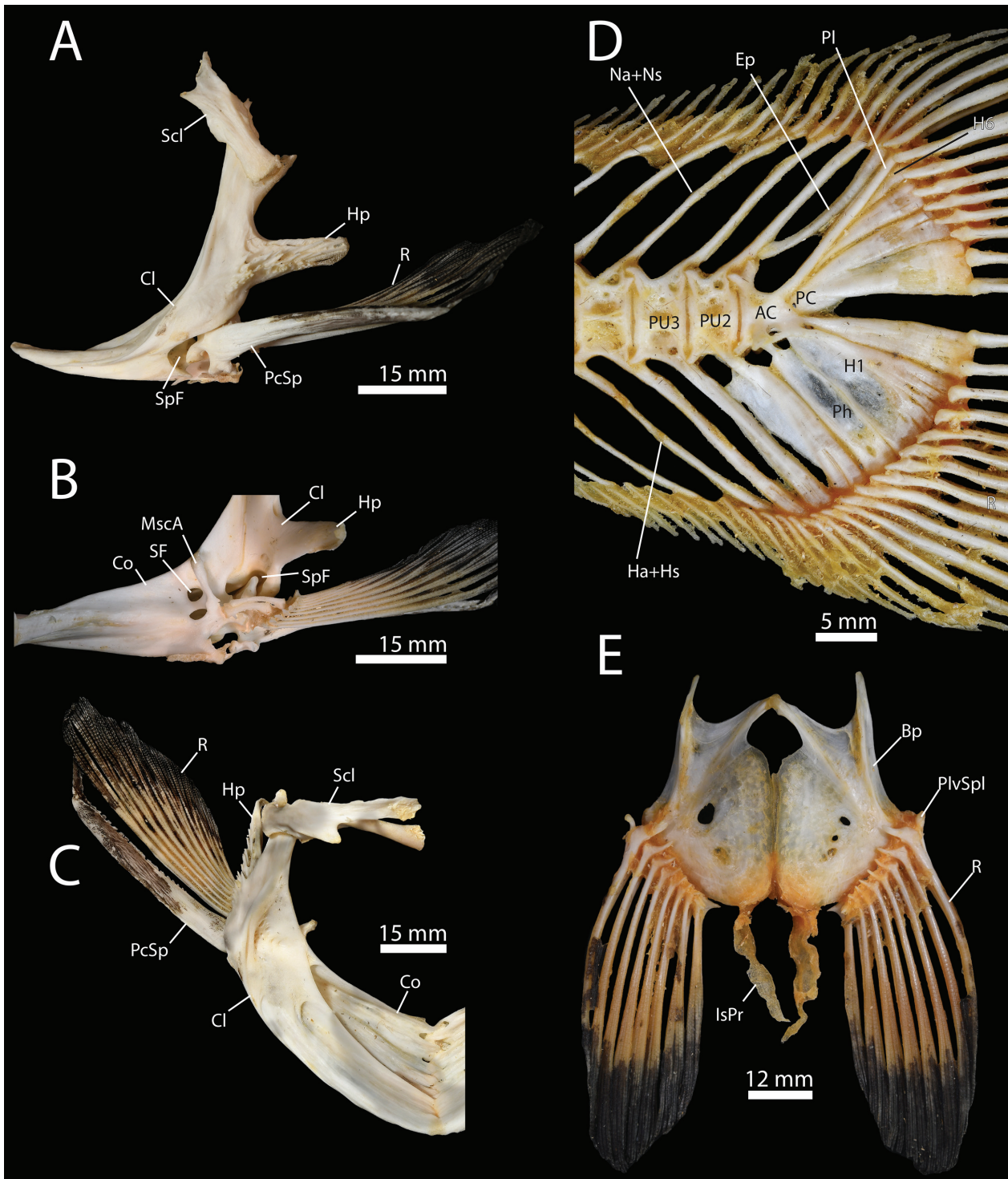


Figure 27. *Ictalurus punctatus*, specimen TCWC 20491.06, 426 mm SL (A), (B), (C), and TCWC 20491.07, 436 mm SL (D) and (E). **A** Dermal pectoral girdle in lateral view **B** Endoskeletal pectoral girdle in medial view **C** Pectoral girdle in dorsal view **D** Caudal skeleton in lateral view **E** Pelvic-girdle in ventral view. Abbreviations: AC, Anterior ural centrum; Bp, Basipterygium; Cl, Cleithrum; Co, coracoid; Ep, Epural; H, Hypural; Ha, Hemal arch; Hp, Humeral process; Hs, hemal spine; IsPr, Ischiac process; MscA, Mesocoracoid arch; Na, Neural arch; Ns, Neural spine; PC, Posterior ural centrum; PcSp, Pectoral-fin spine; Ph, Parhypural, Pl, Pleurostyle; PlvSpl, Pelvic splint; PU, Preural centrum; R, Soft fin ray; Scl, Supracleithrum; SF, Scapular foramen; SpF, Spinal fossa; U, Ural centrum.

grow in width but remains relatively unchanged in larger individuals. In adult individuals (436 mm SL; Fig. 27D), the left and right uroneurals meet each other across the midline and replace the notochord as the border between the dorsal and ventral portions of the caudal skeleton.

Hemal arches and spines of preural centra 2 and 3. The hemal arches of PU2 and PU3 are chondral bones that form from the basiventral cartilages of their respective centra. The basiventral of PU2 is larger and develops faster than the other basiventral cartilages. By 9.7 mm

NL (Fig. 26B) it already forms a complete arch and has developed a small hemal spine cartilage and in some individuals of 10.1 mm SL, it matches the parhypural cartilage in size. At this stage, the basiventral cartilages of PU3 form a complete arch and a neural spine cartilage has just started to form distally from the arch. The hemal arches are first observed in individuals of 11.2 mm SL as perichondral ossifications around the proximal base of the basiventals. Their ossification spreads ventrally to completely cover the basiventral cartilages at which point the hemal spines begin to ossify around the proximal end of their precursor cartilages (11.6 mm SL first appearance and fixed in development by 12.2 mm SL; Fig. 26E). The hemal arches and spines of PU2 and PU3 develop at approximately the same rate from this point on, with the perichondral ossification of the hemal spines spreading ventrally until only the distal tip of the hemal spine cartilages remains uncovered by perichondral bone (14.0 mm SL). By 15.0 mm SL (Fig. 26F) the hemal arches are completely endochondrally ossified and are connected anteriorly to the prezygapophyses. By 17.8 mm SL, the hemal spines are endochondrally ossifying and a small flange of membrane bone has formed on the anteroproximal edge of the hemal spine of PU2. This membranous flange continues to grow and in adults (436 mm SL; Fig. 27D) it is now triangular in shape and contacts the hemal spine of PU3 anteriorly.

Hypurals 1–6. The six hypurals are preformed in cartilage along the ventral end of the notochord. The cartilaginous precursors of hypurals 1 and 2 are the first skeletal elements to appear in the axial skeleton and were observed in the smallest specimen examined (7.7 mm NL). Hypural cartilage 3 appears at approximately the same time as the first caudal fin-rays are beginning to form (8.6 mm NL) as the tip of the notochord is just starting to curve dorsally. By 9.7 mm NL (Fig. 26B), just before flexion is complete, hypural cartilages 1–5 are present. At this stage, the proximal base of hypural 1 cartilage is now confluent with that of the parhypural. Distally, hypural 1 fans out into a triangular plate of cartilage that, at its widest, is approximately twice the width of the rod-like hypural 2–4 cartilages. Hypurals 1–4 begin to ossify perichondrally around the middle of their respective cartilages in individuals as small as 11.2 mm SL. Although hypurals 1–4 typically appear at the same size in development, there was one individual in which only hypurals 1 and 2 were present (11.7 mm SL) and two individuals in which hypurals 1–3 were observed (11.3 and 11.6 mm SL; Fig. 21C). This suggests that the ossification of the hypurals proceeds in an anterior to posterior direction. By the time the first hypurals begin to ossify, a sixth hypural cartilage has formed between hypural 5 cartilage and the notochord. The appearance of ossification among the hypurals continues posteriorly with hypurals 5 and 6 first appearing in individuals as small as 11.6 mm SL and 11.9 mm SL, respectively. Their perichondral ossifications expand proximally and distally along the hypural cartilages except for the distal tips, which serve as a point of articulation with the caudal-fin rays and remain fully cartilaginous (12.3 mm SL; Fig. 26E). At this point,

the bases of hypurals 1 and 2 along with the parhypural are continuous and have started to fuse with the underlying anterior ural centrum while hypurals 3 and 4 retain cartilage at their point of articulation with the posterior ural centrum. By 15.0 mm SL (Fig. 26F), all of the hypurals have started to endochondrally ossify and hypural 2 has developed a small anterior and posterior lamina of membrane bone. The fusion of hypurals 1 and 2 to the anterior ural centrum is complete and hypural 3 has fused to the posterior ural centrum. The hypurals start to take up their characteristic triangular shape by 17.8 mm SL and hypural 4 has fused to the posterior ural centrum. A small flange of membrane bone has formed laterally from the base of hypural 1 at the level of the ventral edge of the centra. At approximately this size, a large round region in the middle of hypural 1 is being resorbed creating a hole in the bone. At 41.2 mm SL, the flanges of membrane bone on hypural 1 have expanded further laterally and the hole in hypural 1 has started to fill in with membrane bone. In the adult condition (436 mm SL; Fig. 27D), the 6 hypurals are all in close contact with one another, excluding the diastema separating hypurals 2 and 3. The lateral flanges of bone on hypural 1 are fused with similar flanges on the parhypural forming the hypurapophysis, a continuous shelf of bone which serves as the origin of the hypochordal longitudinalis muscle. The large hole in hypural 1 is now completely filled in with a thin layer of membrane bone.

Neural arches and spines of preural centra 2 and 3.

The neural arches of PU2 and PU3 begin development as basidorsal cartilages associated with their respective centra (9.7 mm NL; Fig. 21B). They continue to grow dorsally until they meet and fuse across the dorsal midline where a median cartilaginous precursor to the neural spine forms (11.6 mm SL; Fig. 21C). The neural arches of PU2 and PU3 first appear in individuals of 11.2 mm SL as perichondral ossifications around the proximal base of the basidorsal cartilages. The perichondral ossifications expand dorsally to cover the basidorsal cartilages and shortly after (11.9 mm SL first appearance) the neural spines of PU2 and PU3 ossify proximally around their respective cartilaginous precursors. By 14.0 mm SL, the neural arches are endochondrally ossifying and the perichondral neural spines have spread dorsally, covering two-thirds of the neural spine cartilages. The neural arches are completely ossified endochondrally and possess small anterior membranous flanges that join with the anterior prezygapophyses (15.0 mm SL; Fig. 26F). At this point, the neural spines are completely ossified perichondrally, except for the distal tips, but retain a cartilaginous core. The neural arches develop a membranous connection to the postzygapophyses by 17.8 mm SL, at which point the neural spines have begun to endochondrally ossify. At 20.1 mm SL, the neural arches and spines of PU2 and PU3 are fully ossified endochondrally except for the distal tip in the latter, and resemble the adult condition.

Parhypural. The parhypural starts as a pair of cartilages shortly after the appearance of hypural 1 and 2 cartilages

(8.7 mm NL; Fig. 26A) which quickly form a complete arch and develop a median, hemal spine-like extension of cartilage by 9.7 mm NL (Fig. 26B). By this stage the base of the parhypural cartilage is confluent with the base of hypural 1 cartilage. The parhypural is a chondral bone that ossifies at approximately the same size as hypurals 1 and 2 and first appears in individuals as small as 11.2 mm SL. It originates as a perichondral ossification around the paired arches of the parhypural cartilage (Fig. 26D) and continues to expand proximally and distally until it covers the arch and the proximal base of the median extension of cartilage. By 12.3 mm SL (Fig. 26E), the parhypural, along with hypural 1 and 2 begin to fuse to the anterior ural centrum and most of the parhypural is covered in perichondral bone. A small flange of membrane bone extends from the anteroproximal edge of the parhypural by 14.0 mm SL and by 17.8 mm SL a large round portion the parhypural has started to be resorbed forming a hole. A small lateral nodule of bone has formed laterally on the middle of the arch and by 41.2 mm SL a shelf-like lamina of membrane bone extends from the nodule to the anterior ural centrum. At the same size, the flange of membrane bone on the anterior edge of the parhypural almost reaches the hemal spine of PU2 and the hole in the middle of the parhypural has begun to fill in with membrane bone. In the adult condition (436 mm SL; Fig. 27D), the parhypural sits tightly between the hemal spine of PU2 and hypural 1 and the hole in the parhypural has completely filled in with a thin layer of membrane bone. The shelf of membrane bone extending laterally from the arch of the parhypural has fused with a similar lateral process of hypural 1 and forms the hypurapophysis, the origin for the hypochordal longitudinal muscle of the caudal fin.

Epural. The epural is a chondral bone and the last skeletal element in the caudal skeleton to ossify. It first originates from a small cartilage which can be seen in individuals of 11.6 mm SL (Fig. 26C) and continues to elongate until it resembles a neural spine cartilage without a neural arch at 12.3 mm SL (Fig. 21E). The epural begins to ossify perichondrally around the ventral portion of the epural cartilage (13.4 mm SL) and by 14.0 mm SL it has expanded to cover the entire ventral third of the cartilage. By 15.0 mm SL (Fig. 26F), the epural cartilage is completely perichondrally ossified except for the distal tip which serves as a point of articulation for the posteriormost dorsal procurrent ray. The epural begins to endochondrally ossify and a small flange of membrane bone forms at the anteroventral midline of the bone by 17.8 mm SL. By 44.9 mm SL, the epural is completely endochondrally ossified and resembles the adult condition.

Comparison with *Noturus gyrinus*. The most common sequence of ossification for this region in *Noturus gyrinus* is as follows: principal caudal-fin rays (5.9 mm SL) – hypural 1 and 2 and anterior ural centrum (7 mm SL) – parhypural, dorsal and ventral procurrent caudal-fin rays (7.2 mm SL) – neural arch PU3, hypural 3 and posterior ural centrum (7.3 mm SL) – preural centrum 3 (7.6 mm SL) – hemal arch PU2 and PU3, hemal spine PU2 and

PU3, neural arch PU2 and hypural 4 (7.7 mm SL) – ural neural 1 (7.9 mm SL) – preural centrum 2 (8.3 mm SL) – neural spine PU3 (8.6 mm SL) – neural spine PU2 and hypural 5 (8.7 mm SL) – epural (9.8 mm SL)

The sequence of development of *Noturus gyrinus* has a two differences when compared to *Ictalurus punctatus*. The first difference is that the dorsal and ventral procurrent caudal-fin rays start to ossify at the same time in *N. gyrinus* while in *I. punctatus* the dorsal procurrent fin-rays start to ossify much later after most of the other elements of the caudal skeleton. The second major difference is that preural centra 2 and 3 appear later in development in *N. gyrinus*, not ossifying until after the two ural centra, the parhypural and hypurals 1–3 while in *I. punctatus* they are some of the first elements to ossify in the region at approximately the same time as the ural centra and earlier than the parhypural and hypurals. The caudal skeleton of *N. gyrinus* and *I. punctatus*, despite differing in their external appearance, are similar internally, with the only differences being in the total number of hypurals (5 in *N. gyrinus* vs. 6 in *I. punctatus*) and that there is not a well-developed shelf of bone for the origin of the hypochordal longitudinal muscle.

Pectoral girdle

The most common sequence of ossification: cleithrum (7.7 mm NL) – pectoral-fin rays (10.9 mm SL) – supracleithrum (11.4 mm SL) – coracoid (13.2 mm SL) – propterygium (13.9 mm SL) – pectoral-fin radial 3 and 4 (14.2 mm SL) (Fig. 28).

Cleithrum. The dermal cleithrum appears in individuals as small as 7.7 mm SL. It starts off as a slightly curved, thin split of bone just posterior to the cranium and anterodorsal to the yolk-sac. By 10.0 mm SL (Fig. 28A), the bone is ‘L’ shaped with its ventral third directed anteromedially. The bone is widest at its midpoint where it possesses a small rounded posterior extension with additional bone forming dorsal and medial to this widened portion. By 11.9 mm SL (Fig. 28B), the reduction of the yolk-sac has brought the left and right cleithra closer together but they do not make contact across the ventral midline. The bone has widened with laminae of bone extending both anterior and posterior to the original splint like ossification, which appears as a median ridge of bone. At 12.8 mm SL, the bone continues to widen at its center and its posterior edge now extends lateral to much of the scapulocoracoid cartilage. The humeral process is starting to form on the posterior edge just dorsal to the scapulocoracoid cartilage and a small process has formed on the posterodorsal most point of the bone. A posterolateral curved expansion of bone starts to form ventral to the humeral process (14.3 mm SL) and by 15.0 mm SL (Fig. 28D) it forms the spinal fossa, a groove on the posteromedial surface of the cleithrum for the articulation of the dorsal head of the pectoral-fin spine. Posteroventrally, the cleithrum meets the abductor coracoid lamina (*sensu* Fine et al. 1997) which along with the spinal fossa serves as part of the spine locking mechanism. At the same stage, the

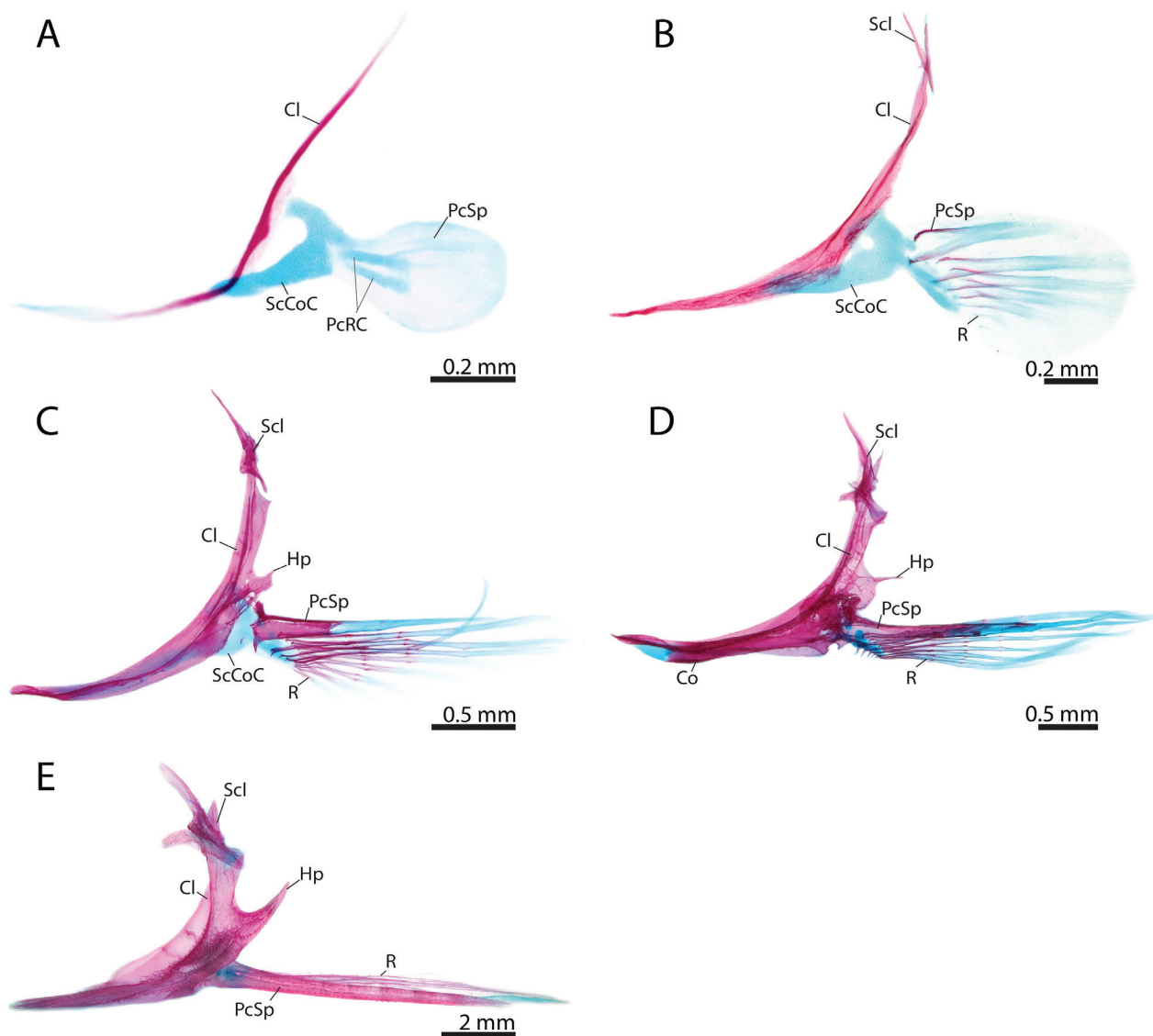


Figure 28. Ontogeny of the dermal pectoral girdle of *Ictalurus punctatus*. **A** 10.0 mm NL. **B** 11.8 mm SL. **C** 13.3 mm SL. **D** 15.0 mm SL. **E** 44.9 mm SL. Abbreviations: Co, Coracoid; Cl, Cleithrum; Hp, Humeral process; Pcl, Postcleithrum; PcRC, Pectoral radial cartilage; PcSp, Pectoral-fin spine; R, Pectoral-fin ray; ScCoC, Scapulocoracoid cartilage; Scl, Supracleithrum.

cleithrum joins its antimere ventrally and is attached firmly to the ventral arm of the coracoid via dense connective tissue. A small cartilage, herein referred to as the cleithral cartilage (Fig. 18), appears in a recess on the dorsal surface of the cleithrum. The cartilage is bordered anteriorly by the dorsal most tip of the cleithrum, posteriorly by the posterodorsal process and laterally by a lamina of bone extending between them. Dorsomedially, the cartilage is bordered by a ligament that connects the supracleithrum to the outer arm of the *os suspensorium*. At 21.5 mm SL, the ventral portion of the cleithrum is directed medially almost at a right angle to the dorsal half and forms a tight connection with its counterpart. The connections between coracoid and cleithrum are near inseparable and sculpturing is present over the entire surface of the bone at this stage. At 44.9 mm SL (Fig. 28E) the cleithrum is heavily ossified and the humeral process has become significantly larger. In adults (426 mm SL; Fig. 27A), the humeral process has become sculptured and possesses a series of spine-like projections on its surface.

Pectoral-Fin Rays. The pectoral fin is the second fin to develop in *I. punctatus* with the first two fin rays appearing at 10.9 mm SL. The anteriormost pectoral-fin ray which will become the pectoral-fin spine is approximately twice the size of subsequent fin rays and its dorsal hemitrichium is closely associated with the propterygium. Four more fin-rays have appeared by 12.0 mm SL and the first four are now segmented. The dorsal and ventral hemitrichia of the first segment of the anteriormost fin ray have started to fuse across the anterior edge and eight fin rays (including the spine) have formed. A second segment has fused to the spine proper and the propterygium has perichondrally ossified and is fused to the proximal head of the upper hemitrichium of the spine at 14.1 mm SL. At approximately the same time as a third segment is added to the spine proper (15.0 mm SL; Fig. 28D), the spine is now capable of locking. At this size, the tenth and final fin ray has just formed. By 15.9 mm SL the number of pectoral-fin rays equals that of the adult (i.9) and all fin rays are segmented. The pectoral-fin spine possesses serrations

along the posterior edge associated with each segment and the anterior margin has gained several denticuli (a more detailed account of pectoral-fin spine development is provided by Kubicek et al. 2019). In adult individuals (426 mm SL; Fig. 27A), the posterior serrations and anterior denticuli become more numerous and significantly smaller relative to the size of the pectoral-fin spine.

Supracleithrum. Whether this element is of compound origin (posttemporal+supracleithrum) or not has been a contentious subject in the past. Herein I refer to the element as the supraclithrum and further discuss the homology of this element below (see discussion). The dermal supraclithrum first appears as a thin splint of bone anterolateral to the dorsal tip of the cleithrum (10.9 mm SL; Fig. 28B). By 12.2 mm SL, an anteroventral process has started to form giving the bone a triangular shape and a medially directed process has appeared and extends anterior to the dorsal tip of the cleithrum. Ridges of bone arise on the lateral surface of the supraclithrum forming a trough around the lateral line sensory canal. Shortly after this (12.8 mm SL), the median process of the supraclithrum wraps around the cleithrum and is connected to the base of the chondrocranium via the newly formed Baudelot's ligament. The dorsal tip of the supraclithrum lies over the posterodorsal surface of the otic capsule and the roof of the lateral line sensory canal associated with the supraclithrum is fully enclosed in bone. At 15.0 mm SL (Fig. 28D), the medial process continues to lengthen replacing Baudelot's ligament with bone. Posteroventrally, the supraclithrum extends laterally to the posterodorsal process of the cleithrum strengthening its connection with the latter bone. Additionally, a ligament connecting the supraclithrum to the outer arm of the *os suspensorium* extends dorsal to the cleithrum and cleithral cartilage. Anteriorly, a lamina of membrane bone has formed between the dorsal tip of the bone and the anteroventral process which almost reaches the posterolateral surface of the chondrocranium. By 21.5 mm SL, Baudelot's ligament has been entirely replaced by the medial process of the supraclithrum except for a small portion between the process and the basioccipital. The anteroventral process reaches and lies ventral to the lateral lamina of membrane bone of the pterotic and the dorsal arm overlies the epioccipital. At 44.9 mm SL (Fig. 28E), the supraclithrum has changed only in size and its lateral surface has become sculptured. The tip of the dorsal arm forms an attachment to and is covered by the accessory posttemporal and in adult individuals, it sits firmly in a fossa formed by the epioccipital, supraoccipital and accessory posttemporal.

Coracoid. Whether this element is of compound origin (scapula+coracoid) or not has been previously undetermined. Herein I refer to the element as the coracoid and further discuss the homology of this bone in the discussion. The coracoid first appears as a perichondral ossification around the proximal end of the ventral arm of the scapulocoracoid cartilage (12.6 mm SL). By 13.1 mm SL (Fig. 29A), the ventral portion of the ventral arm of the

scapulocoracoid cartilage has widened and the coracoid spreads posterodorsally around the scapular foramen (enabling passage of a branch of the pterygial nerve) to the anterodorsal most point of the scapulocoracoid cartilage. At this size, a small ridge of membrane bone is present on the concave margin of the scapulocoracoid cartilage dorsal to the ventral arm. A small projection of membrane bone extends from the posterior edge of the coracoid on the lateral surface of the scapulocoracoid cartilage. By 14.1 mm SL, the coracoid has started to spread down the ventral arm and over the posterior surface of the scapulocoracoid cartilage. The ventral arm of the coracoid rotates roughly 90 degrees with dorsal and ventral edges of smaller stages making up the posterior and anterior margins respectively. Two membranous processes, one at both the dorsal and ventral most tip of the posterior edge, extend towards each other on the medial side of the bone. The projection of membrane bone on the lateral surface of the coracoid extends anteriorly towards the posteroventral corner of the cleithrum and by 15.0 mm SL (Fig. 29B) it reaches and forms a tight connection with the cleithrum forming the abductor coracoid lamina of the spine locking mechanism. At this stage the coracoid extends over the entirety of the scapulocoracoid cartilage except for the anteroventral tip of the ventral arm, the posterodorsal margin at the point of articulation with the propterygium, as well as the tip of the scapular process (*sensu* Brousseau 1976), which articulates with the complex distal radial cartilage. The ventral arm has widened considerably, increasing the area of contact with its antimerere. The lamina of bone originating on the posterodorsal edge of the ventral arm extends to its tip where it overlaps slightly with its counterpart across the midline. A second ridge of laminar bone is present on the ventral surface of the bone extending from the posteroventral most point towards the midlength of its anterior edge. The medial membranous processes of the dorsal and ventral tips of the posterior margin of the coracoid continue to grow towards each other and by 16.2 mm SL, these processes have fused together forming the mesocoracoid arch. The coracoid has started to endochondrally ossify and forms a weakly interdigitated suture with its counterpart across the midline. At 21.2 mm SL, the entire bone is endochondrally ossified and the tip of the ventral arm is more heavily sutured with its antimerere, resembling the adult condition. The coracoid and cleithrum have strengthened their connection and an interdigitating suture is forming at the point of contact between the cleithrum and the abductor coracoid lamina (426 mm SL; Fig. 27A).

Pectoral-Fin Radials. Two small pectoral radial cartilages are present by 10.0 mm SL (Fig. 29D), although they remain connected by a thin layer of cartilage distally and proximally where they are continuous with the scapulocoracoid cartilage. By 11.0 mm SL (Fig. 29E) the two pectoral radial cartilages are separated from the scapulocoracoid cartilage and have fully differentiated into independent cartilages. The complex pectoral distal radial cartilage has appeared at the base of pectoral-fin ray 2 and is confluent with the scapular process of the scapulo-

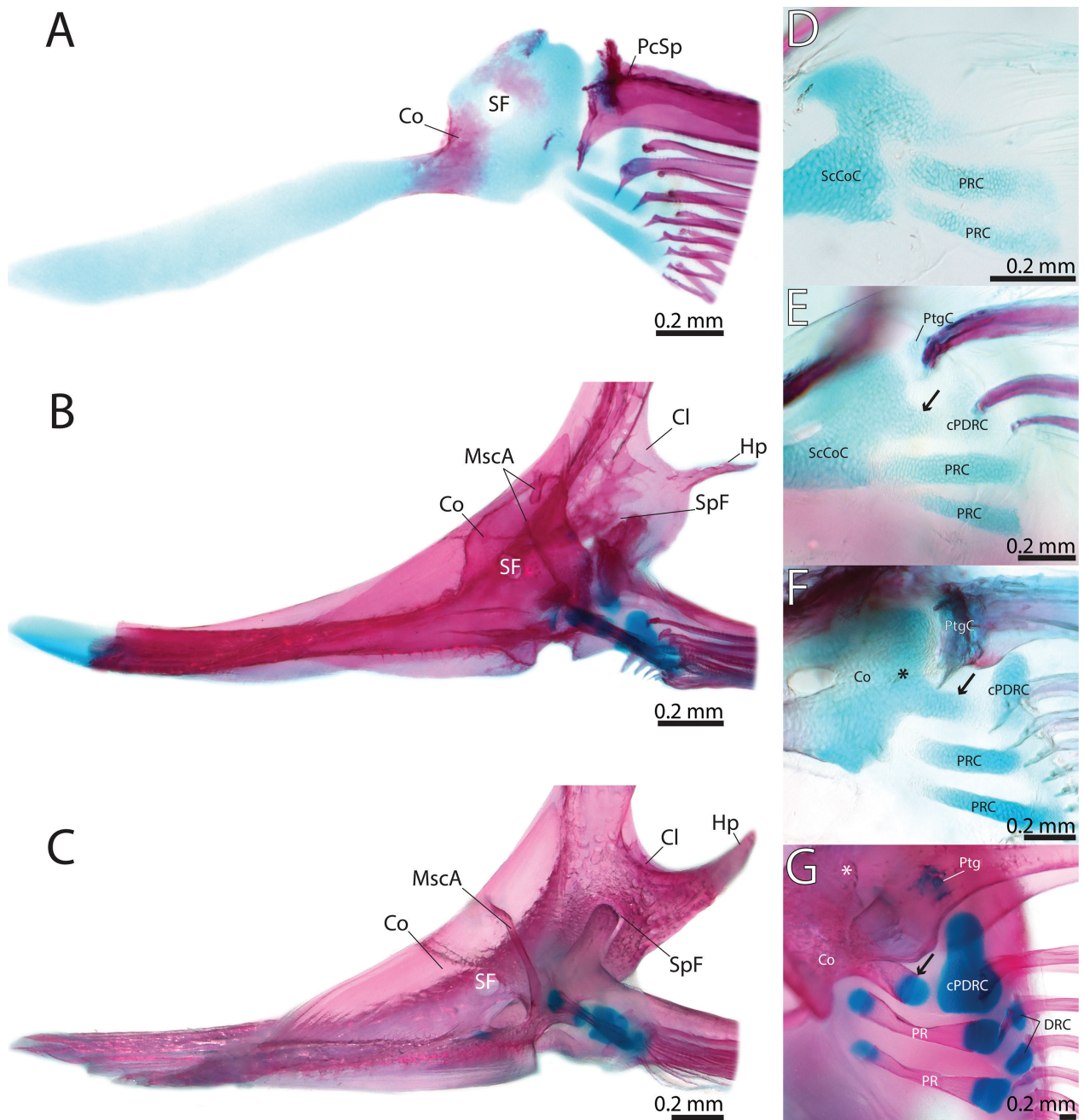


Figure 29. Ontogeny of the endoskeletal pectoral girdle (A-C, scapulocoracoid; D-G, pectoral radials) of *Ictalurus punctatus* **A** 13.3 mm SL. **B** 15.0 mm SL. **C** 44.9 mm SL. **D** 10.0 mm NL. **E** 10.8 mm SL. **F** 12.9 mm SL. **G** 44.9 mm SL. Asterisk indicates abductor coracoid lamina. Black arrows indicates scapular process of Coracoid. Abbreviations: Co, Coracoid; CI, Cleithrum; cPDRC, complex pectoral distal radial cartilage; DRC, distal radial cartilage; Hp, Humeral process; MscA, Mesocoracoid arch; PcSp, Pectoral-fin spine; PR, Pectoral radial; PRC, Pectoral radial cartilage; Ptg, Propterygium; PtgC, Propterygial cartilage; ScCoC, Scapulocoracoid cartilage; SF, Scapular foramen; SpF, Spinal fossa.

coracoid cartilage. Both pectoral-radial cartilages start to perichondrally ossify around their midline in individuals as small as 13.2 mm SL. By this size, the complex pectoral distal radial cartilage has separated from, and now articulates with, the scapular process. At 16.2 mm SL, the perichondral ossification covers all but the distal and proximal tips of the two radials. The complex pectoral distal radial cartilage extends anteriorly into the posterior edge of the spine where it articulates with a remnant of the propterygial cartilage and two distal radials have formed distal to the pectoral radials. In a stage resembling

the adult (44.9 mm SL; Fig. 29G), the pectoral radials are endochondrally ossified and possess lateral flanges of membrane bone and the complex pectoral distal radial remains cartilaginous.

Comparison with *Noturus gyrinus*. The most common sequence of ossification for this region in *Noturus gyrinus* is as follows: cleithrum (5.4 mm NL) – pectoral-fin rays (6.4 mm SL) – supracleithrum (7.0 mm SL) – coracoid (8.3 mm SL) – propterygium (9.9 mm SL) – pectoral-fin radial 3+4 (11.1 mm SL).

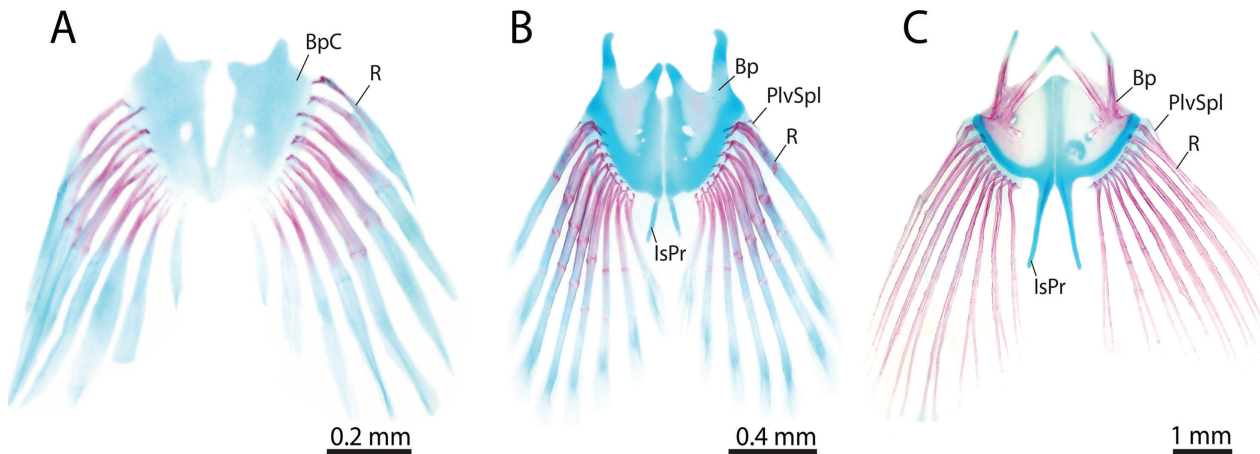


Figure 30. Ontogeny of the pelvic girdle of *Ictalurus punctatus*. **A** 13.3 mm SL. **B** 15.0 mm SL. **C** 44.9 mm SL. Abbreviations: Bp, Basipterygium; BpC, Basipterygial cartilage; PlvSpl, Pelvic splint; R, Pelvic-fin ray.

No differences in the sequence of ossification were identified between *Noturus gyrinus* and *Ictalurus punctatus* in the pectoral girdle. The pectoral girdle of *N. gyrinus* and *I. punctatus* are similar, except for the shape of the pectoral-fin spine, which lacks posterior serrations and anterior denticuli in *N. gyrinus*, and the pectoral-fin radials, in which there is only a single pectoral-radial element in *N. gyrinus* which is a compound element consisting of pectoral radials 3 and 4.

Pelvic girdle

The most common sequence of ossification: pelvic-fin rays (12.3 mm SL) – basipterygium (15.0 mm SL) (Fig. 30).

Pelvic-Fin Rays. The pelvic fin is the last of the fins to develop with fin rays first appearing in individuals of 11.9 mm SL on the posterolateral margin of the yolk-sac. By 12.6 mm SL, resorption of the yolk-sac has resulted in the fins sitting in their normal position on the ventral margin of the body anterior to the anus. At this size, five small fin rays are present but remain unsegmented. At 14.1 mm SL, the number of pelvic-fin rays equals that of adults (i.7) and all eight fin rays are segmented. A small pelvic splint (not included in the ossification sequence) has appeared on the lateral margin of the fin by 15.9 mm SL.

Basipterygium. The basipterygium starts as a perichondral ossification of the basipterygial cartilage between the anterior foramen and the anterior edge of the cartilage (14.5 mm SL; Fig. 30B). By 16.2 mm SL, the ossification has spread to cover most of the basipterygial cartilage excluding the posterior margin (which serves as a point of articulation for the pelvic-fin rays), the ischiac processes, and the medial margin (where it abuts its counterpart), and the tips of the anterior lateral and medial processes. Laminae of membrane bone have formed on either side of the anterior processes by 21.5 mm SL. At 44.9 mm SL (Fig. 30C), the basipterygium is endochondrally ossifying and the surface of the bone near the base of the anterior processes is lightly sculptured. In adults (436

mm SL; Fig. 27E), membrane bone has filled in approximately two-thirds of the gap between the anterior lateral and medial processes.

Comparison with *Noturus gyrinus*. The most common sequence of ossification for this region in *Noturus gyrinus* is as follows: pelvic-fin rays (8.3 mm SL) – basipterygium (10.4 mm SL).

No differences in the sequence of ossification were identified between *Noturus gyrinus* and *Ictalurus punctatus* in the pelvic girdle. The pelvic girdle of *N. gyrinus* and *I. punctatus* are similar, except for the ischiac processes which are much shorter and the outer edge of the basipterygia which reaches approximately half the distance of the lateral anterior process in *N. gyrinus*.

Discussion

Skeletal development in *Ictalurus punctatus* and *Noturus gyrinus*

The development of the skeleton in *Ictalurus punctatus* and *Noturus gyrinus* occurred over a relatively short period of growth, with all elements of the skeleton (excluding the dorsal- and anal-fin distal radials in *N. gyrinus*) present by 22.4 and 14.1 mm SL, respectively. Dorsal- and anal-fin distal radials, which are present in the adult stage of *N. gyrinus* (41.5 mm SL, TCWC 15438.13), are absent from the developmental series compiled for this study suggesting that these elements form later in development, at sizes larger than that of the material examined herein (max size 26.4 mm SL). Elements of the skeleton typically appeared at smaller sizes in *N. gyrinus* compared to *I. punctatus*, which is not surprising given that the former is much smaller than the latter and it is generally observed that smaller bodied species develop faster than closely related, larger bodied species (Reiss 1989; Block and Mabee 2012; Kubicek and Conway 2016). Comparison of the sequences generated for *I. punctatus* (Fig. 1)

and *N. gyrinus* (Fig. 2) revealed differences in the order of appearance of particular bones (e.g., the prootic is the 38th bone to appear in the overall sequence for *I. punctatus* vs. 74th in *N. gyrinus*); however, when looking at the sequence of development by region (e.g., the neurocranium) these differences disappear (e.g., the prootic is the first bone of the otic region to appear in both species; Fig. 3–4) except for preural centra 2 and 3, which are the 41st and 42nd bones to appear in *I. punctatus* and the 79th and 55th bones to appear in the whole skeleton, and in the vertebral column are the 12th and 13th in *I. punctatus* and the 26th and 24th bones in *N. gyrinus*.

Intraspecific variation in *Ictalurus punctatus* and *Noturus gyrinus*

Low levels of intraspecific variation in the total number of certain serial elements were observed in both species. In *I. punctatus*, having 11 post-Weberian ribs associated with vertebrae 5–15 was the most common condition although in a small number of individuals (n=11) an additional 12th rib associated with vertebra 16 was observed. The majority of individuals examined had 20 abdominal vertebrae and 31 caudal vertebrae although individuals with 19 abdominal centra and 30 or 32 caudal centra were observed, resulting in a total vertebral count ranging from 49–52. Variation in the presence of a neural spine on PU2 was also observed. The majority of individuals possess a neural spine associated with PU2 (Fig. 26F); however, in some individuals PU2 only had a neural arch without a spine (Fig. 26E). In *N. gyrinus*, the number of post-Weberian ribs, starting at vertebra 5, varied between seven and nine in total with seven being the most commonly observed condition (n=45), followed by eight (n=39). The number of centra also varied with the most commonly observed condition being 13 abdominal vertebrae and 28 caudal vertebrae. The number of abdominal vertebrae observed ranged from 13–15 and the number of caudal vertebrae ranged from 26–30 with a total observed range of 40–43 vertebrae. The neural spine associated with PU2 was also variably present in *N. gyrinus* with the majority of the individuals possessing it. In addition to elements of the vertebral column, variation was also observed in the number of branchiostegal rays and hypurals present in individuals of *N. gyrinus*. In a small number of individuals (n=16) an additional branchiostegal ray was observed anterior to the remaining nine branchiostegal rays (asymmetry of this element was also observed in a single individual, in which it was present on the right side only). Most individuals of *N. gyrinus* have five hypurals; however, in a few individuals a sixth hypural is present and ossified. The intraspecific variation observed here for *N. gyrinus* in the total number of vertebrae, branchiostegal rays and hypurals was also reported by Taylor (1969). However, the variation observed for the post-Weberian ribs (seven to nine) differed from the six reported by Taylor as the most commonly observed count. The rib associated with vertebra five is typically much smaller than those associated with more posterior vertebrae and

fuses in development with the corresponding parapophysis (Fig. 15C,D and Fig. 16C,D). Although intraspecific variation in the presence of an autogenous rib on vertebra five has been reported in adult individuals of other ictalurids (Grande and Lundberg 1988), none of the individuals of either species examined retained a separate rib at larger sizes (>15.0 mm SL in *I. punctatus* and >10.0 mm SL in *N. gyrinus*). As a result, it is possible that this element was overlooked by Taylor (1969) due to its relatively brief development as an autogenous element before fusing to the parapophysis or that it was excluded from the total count, as he also excluded vertebra five from his vertebral counts.

Comparison of skeletal development with other Otophysans

Although there have been numerous studies of skeletal development in otophysans, most of these have focused only on a subsection of the skeleton (e.g., cranium and paired fins, post-cranial skeleton, Weberian apparatus; Kindred 1919; Bamford 1948; Cubbage and Mabee 1996; Bird and Mabee 2003; Britz and Hoffman 2006). Studies that provide information on the development of the entire skeleton are available for only three other otophysans, the cypriniforms *Danio rerio* (Cubbage and Mabee 1996; Bird and Mabee 2003) and *Enteromius holotaenia* (Conway et al. 2017), and the characiform *Salminus brasiliensis* (Mattox et al. 2014). In the following section I compare the ossification sequence data collected herein with that available for the *D. rerio*, *E. holotaenia* and *S. brasiliensis*. Due to the similarity between the sequence of ossification compiled for *Ictalurus punctatus* and *Noturus gyrinus*, I focus here only on the sequence compiled for *I. punctatus*. Some skeletal elements found in other otophysans are not present in ictalurids (and vice versa) so only those elements present in all four otophysan species were compared.

***Danio rerio* and *Enteromius holotaenia*.** In the ethmoid region, the nasal is the first bone to appear in *Ictalurus punctatus* and appears much earlier in the entire sequence of ossification compared to *D. rerio* and *E. holotaenia*, in which it does not appear until much later in development and is the last bone in the region to appear. The lateral ethmoid appears later in *I. punctatus*, being the third bone to appear in the region, while it is the first bone to appear in the ethmoid region of *D. rerio* and is present much earlier in the entire sequence of ossification. *E. holotaenia* does not exhibit this shift in lateral ethmoid development and instead, the first bone of the ethmoid region to appear is the vomer compared to it being the last bone to appear in this region in *I. punctatus*. In the otic region, the dermopterotic is the second element of the region to appear in *I. punctatus*, after the prootic and before the autopterotic and autosphenotic. In the cypriniforms, the dermopterotic is the last element to appear in the region and is one of the last to appear in the overall sequence of ossification.

In the suspensorium of *Ictalurus punctatus*, both the hyomandibular and endopterygoid appear much later in the regional sequence as well as the entire ossification sequence when compared to that of *Danio rerio*, in which both ossifications represent some of the first bones to appear in the sequence of ossification. Unfortunately, in *Enteromius holotaenia* the smallest individual observed had already 14 bones which included many of the elements of the hyopalatine arch, jaws, and opercular series so it is not possible to compare the sequence of development in most of this region. Among the elements of the branchial arches, ceratobranchial 5 ossifies later in *I. punctatus*, being the 62nd element to ossify while in the cypriniforms it is one of the first bones to appear. In *I. punctatus*, basibranchials 2 and 3 are among the last elements of the skeleton with the hypobranchials being the only other elements of the branchial arches to ossify later. In *E. holotaenia* the basibranchials appear much earlier in the sequence and before several other branchial arch elements. The sequence of ossification of the elements of the hyoid bar of *I. punctatus* differ from *E. holotaenia* in the earlier appearance of the urohyal and interhyal and the later appearance of the dorsal hypohyal. The urohyal is the third element of the region to appear in *I. punctatus* while it is the second to last to appear in *E. holotaenia*. The interhyal appears at approximately the same time as the posterior ceratohyal in *I. punctatus* but well after all other elements of the hyoid bar in *E. holotaenia*. The dorsal hypohyal is one of the last elements to appear in *I. punctatus* while in *E. holotaenia* it ossifies before approximately two-thirds of the skeleton.

In the post-cranial skeleton, the pectoral- and dorsal-fin rays appear early in the ossification sequence of *Ictalurus punctatus* while in the cypriniforms they ossify much later in the entire sequence of ossification. In the case of the procurrent caudal-fin rays, the ventral-procurrent caudal-fin rays of *I. punctatus* appear very early in the sequence of ossification while the dorsal-procurrent caudal-fin rays appear much later in the overall sequence. In *Danio rerio* and *Enteromius holotaenia*, both the dorsal and ventral procurrent caudal-fin rays appear at approximately the same time in the middle of the sequence. It is also worth noting that in *I. punctatus* the fin rays associated with all fins (except for the pelvic fin) ossify before the endoskeletal elements of the caudal fin, while in the cypriniforms most of the caudal skeleton is ossified before any of the other fin rays start to develop. In the vertebral column the most notable difference between *I. punctatus* and the cypriniforms is the early appearance of the parapophyses, which start to ossify before all of the post-Weberian centra in *I. punctatus*, but do not start to ossify until almost the entire vertebral column (excluding some of the hemal and neural spines and ural centrum 2) has formed in *D. rerio* and *E. holotaenia*. The outer arm of the *os suspensorium* is the second of the Weberian elements to ossify in *I. punctatus* while in *D. rerio* and *E. holotaenia* it is the second to last, just before the *claustrum*. Additionally, the *intercalarium*, inner arm of the *os suspensorium*, *scaphium* and *tripus* all start to ossify slightly later in the overall sequence of *I. punctatus*

when compared to that of the two cypriniforms. The centra associated with the caudal skeleton (preural centra 2 and 3 and the two ural centra) appeared earlier in the sequence of ossification of *I. punctatus* before the Weberian ossicles and some of the hemal and neural arches; in *E. holotaenia* these centra were some of the last elements of the vertebral column to ossify.

***Salminus brasiliensis*.** In the cranial skeleton, the nasal and dermopterotic appeared much earlier in the regional sequences of ossification as well as that of the whole skeleton in *Ictalurus punctatus* compared to *S. brasiliensis*. Likewise, the hyomandibular and endopterygoid appeared much later in *I. punctatus* while both appeared very early in the sequence of *S. brasiliensis*. The gill rakers of *I. punctatus* do not appear until after all of the ceratobranchials and epibranchials are ossified while in *S. brasiliensis* the gill rakers ossified very early in development, before ceratobranchial 4 or any of the epibranchials had appeared. Additionally, the interhyal in *I. punctatus* appears at the same time as the posterior ceratohyal and before the dorsal hypohyal. This is slightly earlier in the overall sequence compared to *S. brasiliensis* in which it forms towards the end of the sequence, well after the other elements of the hyoid bar had ossified.

In the postcranial skeleton, the pectoral-fin rays and the parapophyses showed the same pattern of appearing much earlier in the sequence of *Ictalurus punctatus* when compared to *Salminus brasiliensis*. The ventral procurrent caudal-fin rays appear much earlier in *I. punctatus* while the dorsal procurrent caudal-fin rays appear at roughly the same place in the sequence as *S. brasiliensis*. Neural arches 3 and 4 also appear much earlier in the sequence of *I. punctatus*, ossifying before most of elements of the vertebral column while in *S. brasiliensis* they do not ossify until after most of the vertebral column is present. Finally, like what was observed in the comparison with *E. holotaenia*, the four centra supporting the caudal skeleton appear much earlier in the sequence of ossification of *I. punctatus* while in *S. brasiliensis* they were some of the last elements of the vertebral column to appear.

Differences shared between *Danio rerio*, *Enteromius holotaenia* and *Salminus brasiliensis*. The relative timing of appearance for bony skeletal elements varied between *Ictalurus punctatus* and the three non-siluriform otophysans. Most of this variation was restricted to only slight shifts in the relative position of skeletal elements in comparisons of either regional or the entire sequences. However, several major differences were observed between the ossification sequence compiled for *I. punctatus* and those for all three non-siluriform otophysan species, several of which were consistent across all three comparisons. In the neurocranium, elements associated with the cephalic lateral line canals (e.g., nasal, dermopterotic) all appear much earlier in the development of *I. punctatus*. This also applies to the lacrimal, another element associated with the cephalic lateral line sensory system, which is one of the first elements to appear in *I. punctatus* but does not make an appearance until much later in devel-

opment in the three other species of otophysans. The hyomandibular and endopterygoid also appear later in the sequence of ossification of *I. punctatus*.

In the post-cranial skeleton, the pectoral-fin rays, ventral procurrent caudal-fin rays, and the parapophyses all appear very early in the sequence of ossification compiled for *Ictalurus* compared to the three non-siluriform otophysans. Of particular interest is the much earlier appearance of the pectoral-fin rays in the two ictalurids, which are the 21st or the 11th bones to appear in the sequence of *I. punctatus* and *Noturus gyrinus*, respectively, versus the 100th to 125th in the three non-siluriform otophysans. The anteriormost pectoral-fin ray of most catfishes is modified into a robust lockable spine that exhibits a remarkable amount of morphological variation (e.g., Reed 1924; Vanscoy et al. 2015; Kubicek et al. 2019). A similar shift is observed in the dorsal-fin rays, which also possesses fin-rays modified into spines, when compared to the two cypriniforms, but not in comparison to the characiform *Salminus brasiliensis*.

Although the aforementioned differences in the appearance of ossifications were consistently observed in comparisons between *Ictalurus punctatus* and the three non-siluriform otophysans, it is not possible to tell whether these consistent patterns are due to chance, as variation exists throughout the entire ossification sequence of these taxa, or if these differences in the timing of appearance of these elements could be derived characters of ictalurids or even Siluriformes. In other groups of vertebrates (e.g., amphibians, squamates, birds, and mammals; Harrington et al. 2013; Werneburg and Sánchez-Villagra 2015; Carril and Tambussi 2017; Sánchez-Villagra et al. 2008), shifts in the relative timing of developmental events, or sequence heterochrony, has been shown to be connected with major changes in morphology, life-history and function (e.g., the earlier development of the cranial and forelimb skeleton in marsupial vs. placental mammals; Goswami et al. 2009; Keyte and Smith 2010). Given that certain elements, like the pectoral-fin spine, appear to be significantly shifted in the development of catfishes, an examination of sequence heterochrony between siluriforms and non-siluriform otophysans could help to clarify if these elements vary in their relative position due to chance or if the early appearance of these elements is the product of heterochrony.

Homology

Supraoccipital. In the posterodorsal surface of the neurocranium, teleosts typically possess a pair of parietals, dermal bones which form via intramembranous ossification in the dermis, and a single median supraoccipital, a chondral bone which ossifies around and replaces a portion of the otic capsule cartilage. Unlike teleosts, siluriforms only possess a single median bone in this region which is hypothesized to result from the fusion of the parietals and the supraoccipital (Arratia and Gayet 1995) and is commonly referred to as the parieto-supraoccipital (a term coined by Arratia 1987). Prior to 1948, the pari-

etal was hypothesized either: (1) to be absent in catfishes with the supraoccipital extending anteriorly on either side of the postcranial fontanelle to occupy the space left in its absence (McMurrich 1884); or (2) to have fused with the supraoccipital (Kindred 1919), forming a compound element. Evidence of a fusion between these two elements was first reported by Bamford (1948) in a developmental study of the cranium in the ariid catfish *Ariopsis felis*. Using serial sections of a limited series of specimens (six individuals ranging from 8–50 mm), Bamford described the supraoccipital as originating from two pairs of separate ossifications, the more posterior pair of which would become chondroid bone in a larger stage. These elements would proceed to fuse on either side of the postcranial fontanelle, forming a single pair of elements before subsequently fusing across the midline into the single ‘U’-shaped element observed in adults (e.g., see figures 4 and 6; Bamford 1948). As a result, Bamford (1948) interpreted the supraoccipital in *A. felis* to be a compound element composed of two separate pairs of ossifications, the parietal and a paired supraoccipital, the latter of which is a median bone in other teleosts. A small paired element interpreted to represent the parietal has also been reported in juvenile individuals of the trichomycterids *Hatcheria* and *Bullockia* (Arratia et al. 1978; Arratia and Menu-Marque 1981). This small paired element is located between the supraoccipital, frontal and autosphenotic and is reported to subsequently fuse to the supraoccipital in adult individuals. In addition to these reported cases of fusion, Arratia and Gayet (1995) argued that the elements that surround and suture with the ‘supraoccipital’ of catfishes are also those elements that surround and suture with the parietals and supraoccipital in other teleosts, providing an additional line of circumstantial evidence in support of the compound nature of this element.

At no point in the development of the supraoccipital in *Ictalurus punctatus* and *Noturus gyrinus* was fusion between dermal and chondral ossifications observed (see description of supraoccipital development in *I. punctatus*; Fig. 31). In both species, development of the supraoccipital starts as a paired perichondral ossification of the dorsal margin of the otic capsule on either side of the posterior fontanelle (Fig. 31A). As development continues, an anterior extension of membrane bone forms from the perichondral ossification of the supraoccipital on the edge of the otic capsule (13.2 mm SL, Fig. 31B) and shortly after, the pair of ossifications fuse across the midline, along the posterior border of the cranial fontanelle (14.1 mm SL, Fig. 31C). The anterior extensions of this now median ossification widen and continue to expand anteriorly until they meet and suture with the paired frontal, at which point the bone resembles the adult condition (15.4 mm SL, Fig. 31D). Given that this element arises through endochondral ossification of the otic capsule and tectum synoticum, it is interpreted herein to represent a highly modified supraoccipital and the parietals are absent. This hypothesis is supported by studies of the Clariidae (Adriaens and Verraes 1998), Callichthyidae (Huysentruyt et al. 2011), Heteropneustidae (Srinivasachar 1958), and

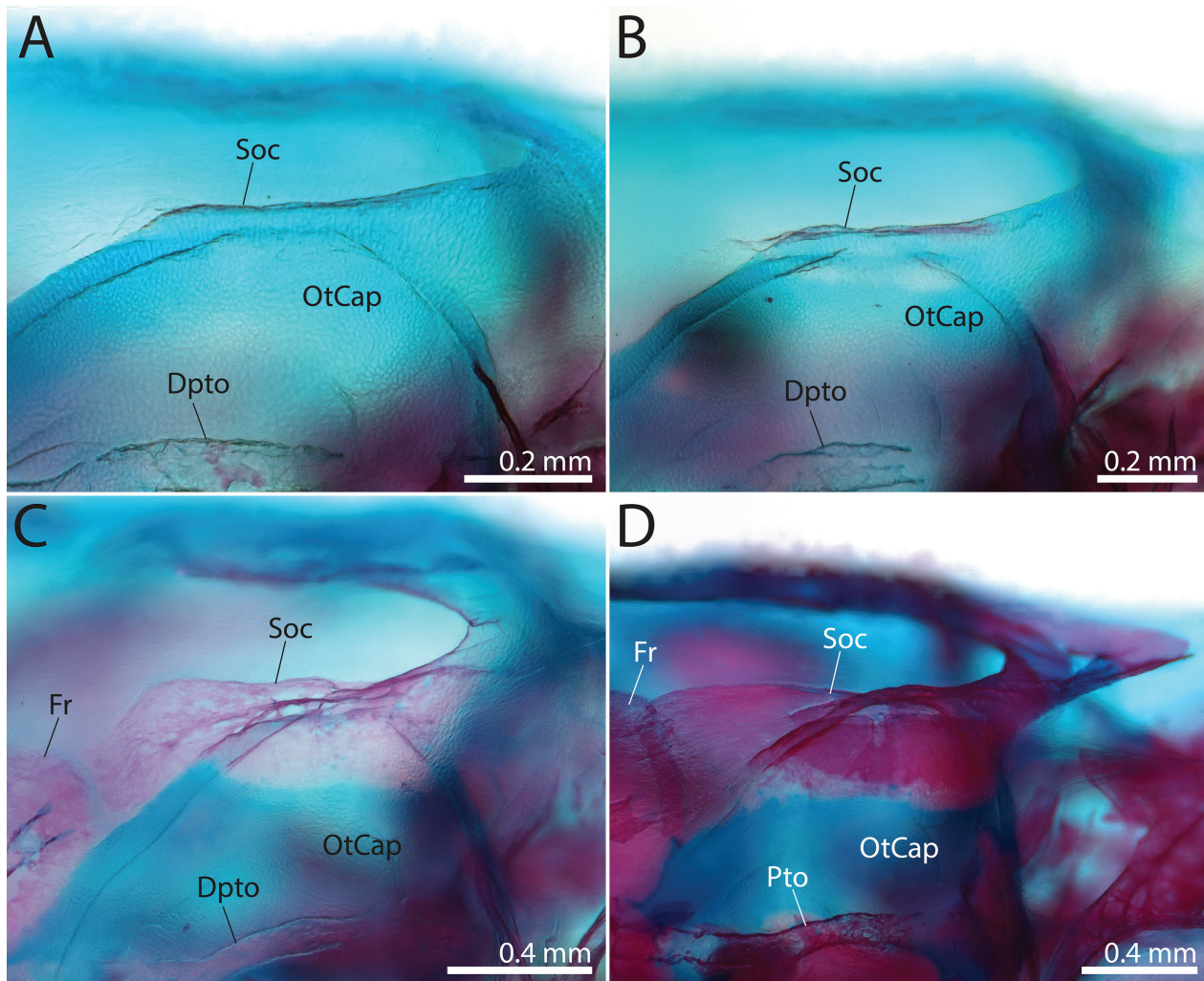


Figure 31. Ontogeny of the supraoccipital of *Ictalurus punctatus*. **A** 12.7 mm SL. **B** 13.2 mm SL. **C** 14.1 mm SL. **D** 15.4 mm SL. Abbreviations: Dpto, Dermopterotic; Fr, Frontal; OtCap, Otic capsule; Pto, Pterotic; Soc, Supraoccipital.

Loricariidae (Geerinckx et al. 2007) in which the absence of a separate parietal during development was also noted. The origin of the chondral supraoccipital as a paired ossification is consistent with what has been reported for *Ariopsis felis* (Bamford 1948) and *Ancistrus cf. triradiatus* (Geerinckx et al. 2007), which appears to be a mode of development unique to catfishes. Although Bamford (1948) reported the supraoccipital as a compound element resulting from fusion of two separate pairs of elements (i.e., parietal and supraoccipital), it should be noted that he only observed two separate pairs of ossifications in a single specimen (14.0 mm; fig. 6 of Bamford 1948) via serial sections and not observation of entire three-dimensional specimens, which would have had an impact on his interpretation. In the next largest specimen illustrated (17.5 mm; Fig. 4 of Bamford 1948) there are only two ossifications which meet medially at the posterior border of the cranial fontanelle, similar to that observed herein for *I. punctatus* and *N. gyrinus* (Fig. 31C). Given the limited sample size, as well as the other examples of the supraoccipital originating as a single pair of ossification centers mentioned above, Bamford's conclusion of a fused parietal and supraoccipital in *A. felis* should be put into doubt until further supporting evidence for such fu-

sion is obtained. The way in which the supraoccipital develops may vary across catfishes as only a single center of ossification was reported for this bone in *Heteropneustes fossilis* (Srinivasachar 1958) and *Corydoras paleatus* (Huysentruyt et al. 2011).

Supracleithrum. In teleosts, the dermal component of the pectoral-girdle is typically comprised of three elements (cleithrum, supraclathrum, and posttemporal). Siluriformes differ from this condition in that they possess only two major dermal bones in the pectoral-girdle, the cleithrum and an upper element of the pectoral girdle which has previously been interpreted as: (1) the posttemporal (Herrick 1901; Kindred 1919; Bamford 1948; Alexander 1965); (2) the supraclathrum (Regan 1911; Hubbs and Miller 1960; Taylor 1969; Lundberg 1975); or (3) a compound element resulting from fusion of the posttemporal and supraclathrum (Fink and Fink 1981; Arratia 1987). The first of these hypotheses is based solely on this upper element being the point of articulation between the pectoral-girdle and the neurocranium, a position typically occupied by the posttemporal in teleosts. The second hypothesis is based on the insertion of Baudelet's ligament on the upper element, while this prominent

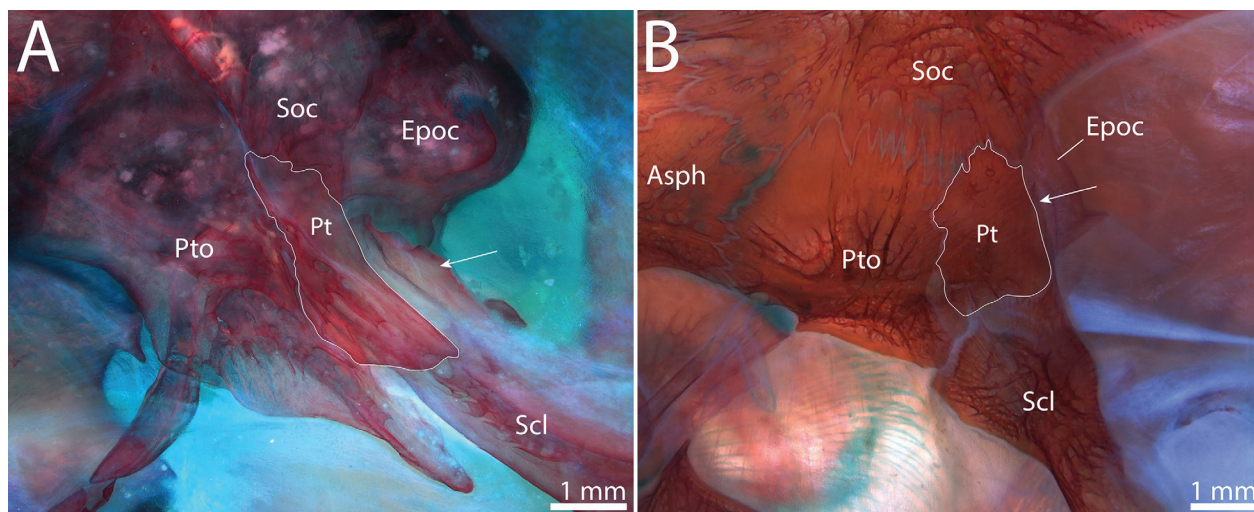


Figure 32. Skeletal elements associated with the articulation of the cranium and pectoral girdle. **A** *Diplomystes papillosus*, CAS 81539, 118 mm SL. **B** *Cranoglanis boudierius*, CAS 69758, 97.0 mm SL. Arrows indicate anterodorsal tip of supracleithrum. Abbreviations: Asph, Autosphenotic; Epoc, Epioccipital; Pt, Posttemporal; Pto, Pterotic; Scl, Supracleithrum; Soc, Supraoccipital.

ligament inserts on the supracleithrum in other teleosts. The proposed compound nature of this upper shoulder girdle element was originally suggested by Fink and Fink (1981) because it possessed both of the previously mentioned characteristics in combination with the absence of ontogenetic material that could clarify whether or not this element originated from a single ossification center or two ossification centers. The compound origin hypothesis of Fink and Fink (1981) has become the most widely adopted of the three, with the element commonly referred to as the posttemporo-supracleithrum, a term coined by Arratia (1987).

In the developmental series of the two species of ictalurids examined herein, the upper element of the pectoral-girdle originates from a single ossification that forms lateral to the dorsal tip of the cleithrum and no evidence of fusion during the ontogeny of this element was observed (Fig. 28). This corroborates what has previously been observed in the development of *Clarias gariepinus* (Adriaens and Verraes 1998) and *Ancistrus cf. triradiatus* (Geerinckx et al. 2007), and refutes the hypothesis of Fink and Fink (1981) that the upper element of the pectoral girdle in catfishes represents a compound element resulting from the ontogenetic fusion of the supracleithrum and the posttemporal. Of the two remaining hypotheses, homology of the upper element of the shoulder girdle with the supracleithrum is the best supported given the insertion of Baudelot's ligament on the medial surface of the element, a relationship only observed with the supracleithrum in other teleosts (Fink and Fink 1981; Patterson and Johnson 1995). Additionally, the supracleithrum in other otophysans appears relatively early in development compared to other skeletal elements, including the posttemporal (Cubbage and Mabee 1996; Britz and Conway 2009; Mattox et al. 2014; Conway et al. 2017). In taxa in which one of the three major dermal bones of the pectoral girdle is lost, it is always the posttemporal (Conway and Britz 2007; Britz & Conway 2009, 2016; Conway 2011;

Conway et al. 2017). Fink and Fink (1981) recognized this in the proposal of their compound origin hypothesis as they stated the upper element of the pectoral girdle "...comprises the supracleithrum, the ossified Baudelot's ligament, and perhaps also the posttemporal" implying some degree of uncertainty about the incorporation of the posttemporal. The only evidence provided by Fink and Fink (1981) for the fusion of the posttemporal is the presence of a dorsal arm in the upper element of the catfish shoulder girdle that is similar to that of the posttemporal of other teleosts; to explain this condition, however, they also mention the possibility of a dorsal expansion of the supracleithrum to take the typical place of the posttemporal. As a consequence of my developmental results, I interpret the upper element of the pectoral-girdle in catfishes to represent a supracleithrum that has become modified by expanding anterodorsally and ossifying along Baudelot's ligament to resemble the general appearance and occupy the typical location of the posttemporal of non siluriform teleosts.

Posttemporal and Extrascapular. In teleosts, the posterior portion of the cranium that connects to the pectoral girdle typically possesses an extrascapular which carries the sensory canal from the posttemporal to the neurocranium. Catfishes, unlike most teleosts, exhibit variation in the number, shape and relationship of bones in this region (summarized in Table 1) and as a result, the homology of these dermal elements has remained uncertain. Before discussing the homology of the elements found in *Ictalurus punctatus* and *Noturus gyrinus*, homology of the bones in this region across catfishes must first be addressed. The most common condition observed across members of the order (21 species, 18 families; Fig. 32), including the morphologically most primitive *Diplomystes*, is the possession of a single plate-like dermal bone that is sutured to the pterotic and supraoccipital, articulates with the supracleithrum, and bears a portion of the postotic sensory can-

Table 1. Summary of diversity in the elements of the cranio-pectoral articulation of catfish species examined.

Family	Species	Cranio-Pectoral Articulation
Loricarioidea		
Astroblepidae	<i>Astroblepus</i> sp.	Posttemporal absent; Supracleithrum attached directly to the pterotic.
Callichthyidae	<i>Megalechis thoracata</i>	Posttemporal absent; Supracleithrum attached directly to the pterotic.
	<i>Dianema longibarbis</i>	Posttemporal absent; Supracleithrum attached directly to the pterotic.
	<i>Corydoras melini</i>	Posttemporal absent; Supracleithrum attached directly to the pterotic.
	<i>Corydoras panda</i>	Posttemporal absent; Supracleithrum attached directly to the pterotic.
Loricariidae	<i>Ancistrus</i> sp.	Posttemporal absent; Supracleithrum attached directly to the pterotic.
	<i>Pareiorhaphis vestigipinnis</i>	Posttemporal absent; Supracleithrum attached directly to the pterotic.
Nematogenyidae	<i>Nematogenys inermis</i>	Posttemporal absent; Supracleithrum articulates directly with the pterotic.
Scoloplacidae	<i>Scoloplax empousa</i>	Posttemporal absent; Supracleithrum attached directly to the pterotic.
Trichomycteridae	<i>Henonemus</i> sp.	Posttemporal absent; Supracleithrum articulates directly with the pterotic.
	<i>Trichomycterus punctulatus</i>	Posttemporal absent; Supracleithrum articulates directly with the pterotic.
	<i>Potamoglanis hasemani</i>	Posttemporal absent; Supracleithrum articulates directly with the pterotic.
Diplomystoidea		
Diplomystidae	<i>Diplomystes chilensis</i>	Posttemporal present as a plate-like bone between the supracleithrum and pterotic.
Siluroidea		
Amblycipitidae	<i>Amblyiceps cerinum</i>	Posttemporal present as a simple canal ossification between the supracleithrum and pterotic.
	<i>Amblyiceps mangois</i>	Posttemporal present as a simple canal ossification between the supracleithrum and pterotic.
	<i>Liobagrus somjinensis</i>	Posttemporal present as a simple canal ossification between the supracleithrum and pterotic.
Amphiliidae	<i>Amphilius uranoscopus</i>	Posttemporal absent; Supracleithrum forms part of skull roof.
Anchariidae	<i>Ancharius fuscus</i>	Posttemporal present as a plate-like bone between the supracleithrum and pterotic.
Ariidae	<i>Ariopsis felis</i>	Posttemporal present as a plate-like bone between the supracleithrum and pterotic.
	<i>Ariopsis seemanni</i>	Posttemporal present as a plate-like bone between the supracleithrum and pterotic.
	<i>Bage marinus</i>	Posttemporal present as a plate-like bone between the supracleithrum and pterotic.
Aspredinidae	<i>Bunocephalus</i> sp.	Posttemporal present as a simple canal ossification between the supracleithrum and pterotic.
	<i>Pseudobunocephalus lundbergi</i>	Posttemporal absent; Supracleithrum forms part of skull roof.
Auchenipteridae	<i>Tatia intermedia</i>	Posttemporal absent; Supracleithrum forms part of skull roof.
	<i>Trachycorystes</i> sp.	Posttemporal absent; Supracleithrum forms part of skull roof.
Auchenoglanididae	<i>Auchenoglanis occidentalis</i>	Posttemporal present as a plate-like bone between the supracleithrum and pterotic.
Austroglanididae	<i>Austroglanis gilli</i>	Posttemporal present as a plate-like bone between the supracleithrum and pterotic.
Bagridae	<i>Pseudomystus siamensis</i>	Posttemporal present as a plate-like bone between the supracleithrum and pterotic.
Cetopsidae	<i>Cetopsis coecutiens</i>	Posttemporal present as a plate-like bone between the supracleithrum and pterotic.
	<i>Helogenes marmoratus</i>	Posttemporal absent; Supracleithrum articulates directly with the pterotic.
Chacidae	<i>Chaca chaca</i>	Posttemporal absent; Supracleithrum articulates directly with the pterotic.
Clariidae	<i>Clarias batrachus</i>	Posttemporal absent; Supracleithrum forms part of skull roof.
	<i>Clarias garipepinus</i>	Posttemporal absent; Supracleithrum forms part of skull roof.
Claroteidae	<i>Chrysichthys mabusi</i>	Posttemporal present as a plate-like bone between the supracleithrum and pterotic.
Cranoglanididae	<i>Cranoglanis boudierus</i>	Posttemporal present as a plate-like bone between the supracleithrum and pterotic.
Doradidae	<i>Ossancora punctata</i>	Posttemporal absent; Supracleithrum forms part of skull roof.
	<i>Platydoras armatulus</i>	Posttemporal absent; Supracleithrum forms part of skull roof.
Heptateridae	<i>Goeldiella eques</i>	Posttemporal present as a plate-like bone between the supracleithrum and pterotic.
Heteropneustidae	<i>Heteropneustes fossilis</i>	Posttemporal absent; Supracleithrum forms part of skull roof.
Horabagradae	<i>Horabagrus brachysoma</i>	Posttemporal present as a plate-like bone between the supracleithrum and pterotic.
Ictaluridae	<i>Ameiurus melas</i>	Posttemporal and Accessory Posttemporal present between supracleithrum and pterotic.
	<i>Ictalurus furcatus</i>	Posttemporal and Accessory Posttemporal present between supracleithrum and pterotic.
	<i>Ictalurus punctatus</i>	Posttemporal and Accessory Posttemporal present between supracleithrum and pterotic.
	<i>Noturus flavus</i>	Posttemporal absent; Supracleithrum articulates directly with the pterotic.
	<i>Noturus gyrinus</i>	Posttemporal present as a simple canal ossification between the supracleithrum and pterotic.
	<i>Pylodictis olivaris</i>	Posttemporal present as a plate-like bone between the supracleithrum and pterotic.
Kryptoglanididae	<i>Kryptoglanis shajii</i>	Posttemporal absent; Supracleithrum articulates directly with the pterotic.
Malapteruridae	<i>Malapterurus oguensis</i>	Posttemporal absent; Supracleithrum articulates directly with the pterotic.

Family	Species	Cranio-Pectoral Articulation
Mochokidae	<i>Chiloglanis</i> sp.	Posttemporal absent; Supracleithrum forms part of skull roof.
	<i>Euchilichthys</i> sp.	Posttemporal absent; Supracleithrum forms part of skull roof.
	<i>Microsynodontis</i> sp.	Posttemporal absent; Supracleithrum forms part of skull roof.
Pangasiidae	<i>Pangasius macronema</i>	Posttemporal present as a plate-like bone between the supracleithrum and pterotic.
Pimelodidae	<i>Pimelodus pictus</i>	Posttemporal present as a plate-like bone between the supracleithrum and pterotic.
Plotosidae	<i>Plotosus lineatus</i>	Posttemporal present as a plate-like bone between the supracleithrum and pterotic.
Pseudopimelodidae	<i>Microglanis</i> cf. <i>iheringi</i>	Posttemporal present as a plate-like bone between the supracleithrum and pterotic.
	<i>Microglanis poecilus</i>	Posttemporal present as a plate-like bone between the supracleithrum and pterotic.
Ritidae	<i>Rita rita</i>	Posttemporal present as a plate-like bone between the supracleithrum and pterotic.
Schilbeidae	<i>Parailia congica</i>	Posttemporal absent; Supracleithrum articulates directly with the pterotic.
	<i>Parailia pellucida</i>	Posttemporal absent; Supracleithrum articulates directly with the pterotic.
	<i>Schilbe intermedius</i>	Posttemporal present as a plate-like bone between the supracleithrum and pterotic.
Siluridae	<i>Silurus asotus</i>	Posttemporal absent; Supracleithrum articulates directly with the pterotic.
	<i>S. glanis</i>	Posttemporal absent; Supracleithrum articulates directly with the pterotic.
	<i>Wallago attu</i>	Posttemporal absent; Supracleithrum articulates directly with the pterotic.
Sisoridae	<i>Glyptothorax lampris</i>	Posttemporal absent; Supracleithrum forms part of skull roof.
	<i>Parachiloglanis</i>	Posttemporal absent; Supracleithrum articulates directly with the pterotic.
	<i>Pseudolaguvia kapuri</i>	Posttemporal absent; Supracleithrum forms part of skull roof.

nal as it passes from the supraoccipital to the pterotic. This suggests that this condition is plesiomorphic at the level of Siluriformes, with subsequent modifications occurring in derived members throughout the order (see Table 1). This single dermal bone has been variably referred to as either the posttemporal (Regan 1911; Hubbs and Miller 1960; Lundberg 1975; Slobodian and Pastana 2018) or the extrascapular (Herrick 1901; Allis 1904; Bamford 1948; Fink and Fink 1981; Arratia and Gayet 1995); however, homology of this element has remained unclear.

To date, there are three hypotheses of the homology of elements in this region: (1) the plate-like bone represents the posttemporal and the extrascapular is lost (Lundberg 1975); (2) the plate-like bone represents the posttemporal and the extrascapular has fused with the pterotic in most catfishes (Slobodian and Pastana 2018); and (3) the plate-like bone represents the extrascapular and the posttemporal has fused with the supracleithrum (Fink and Fink 1981; Arratia and Gayet 1995). The hypothesized homology of the plate-like bone with the posttemporal is based on Lundberg's (1975) interpretation of the sensory canal homology in this region and the osteological relationships of the canal. Lundberg (1975) concluded that the extrascapular was lost and the portion of the sensory canal typically carried by the extrascapular of teleosts (excluding the supratemporal canal which is absent in catfishes) was incorporated into or closely associated with the pterotic. This conclusion was based on the location of a posterolateral branch of the otic sensory canal, also known as the pterotic branch (Coombs et al. 1988). Slobodian and Pastana (2018) also hypothesized that the plate-like element is homologous with the posttemporal. Their view was based on the number and arrangement of neuromasts in the sensory canal, which were not directly observed by Slobodian and Pastana (2018), and they disagreed with the hypothesis that the extrascapular is lost. Finally, evidence to support the homology of the plate-like bone as the extrascapular was first provided by Fink and Fink (1981) and includes: (1) the lack of a prominent

dorsal arm typical of the posttemporal in nonsiluriform otophysans; and (2) the fact that the extrascapular of Gymnotiformes, the sister group to catfishes, is immovably articulated to the cranium. Fink and Fink (1981) postulated that the latter could be a feature of the Siluriphysi. In addition to these two factors, Fink and Fink (1981) and Arratia and Gayet (1995) disagreed with Lundberg's (1975) interpretation of pterotic branch homology, which they provided as evidence to contradict the posttemporal hypothesis. Surprisingly, most of the evidence used in the homology assessment of the plate-like element has been based on the sensory canals and neuromasts in this region, with little attention paid to the ossification itself or its association with other bones in the region.

In the 21 species of catfishes examined in the present study that possess the plate-like element, the bone always shares the same relationship with the surrounding elements of the neurocranium. The bone is sutured to the pterotic and the supraoccipital anterolaterally and anteromedially, respectively. Posteriorly, it overlays and forms a firm connection to the anterodorsal tip of the supracleithrum via dense connective tissue (Fig. 32). This firm connection between the plate-like element and the supracleithrum is similar to that shared between the posttemporal and supracleithrum of most teleosts, not the extrascapular. The lack of a prominent dorsal arm on the plate-like element was cited as evidence for the plate-like bone being homologous to the extrascapular; however, a plate-like posttemporal which lacks a prominent dorsal arm is found among the Otophysi in some cypriniformes (e.g., *Danio rerio*, Cubbage and Mabee 1996). Additionally, Fink and Fink (1981) suggested that the immovable articulation of the extrascapular in gymnotiforms may represent a shared feature with catfishes. However, it is unclear exactly what Fink and Fink (1981: p. 333) meant by "immovably articulated" as they do not describe it in detail, explain how it differs from the extrascapular attachment of other otophysans and it is also not illustrated in their figures. It is worth noting that in Gymnotiformes,

the attachment of the extrascapular to the neurocranium is variable and has been reported to be either fused to the neurocranium or remain as an independent element (Lundberg and Mago-Leccia 1986; Albert 2001; Dutra et al. 2021) in different species. Also, the absence of the posttemporal is rare across teleosts having been reported to be absent in a single genus of miniature Gonorynchiformes (*Grasseichthys*; Britz and Moritz 2007), three genera of miniature Cypriniformes (*Danionella*, *Paedocypris* and *Sundadanio*; Conway and Britz 2007; Britz and Conway 2009, 2016), certain stomiiforms of the families Sternoptychidae (Baird 1971) and Stomiidae (Fink 1985), the miniature synbranchiforms of the family Chaudhuriidae (Britz and Kottelat 2003) and gymnodont tetraodontiforms of the families Tetraodontidae and Diodontidae (Tyler 1980). All of this information taken together supports the hypothesis that the plate-like bone is homologous to the posttemporal, as suggested by Lundberg (1975) and Slobodian and Pastana (2018), not to the extrascapular. Additionally, the relationship between the sensory canal and the bones in this region match that described by Lundberg (1975), although I did not examine enough material to be able to comment on the homology of the pterotic branch among otophysans or its reliability in determining homology of osteological elements of the region.

Neither *Ictalurus punctatus* or *Noturus gyrinus* possess the plesiomorphic condition described above for catfishes; however, the single plate-like posttemporal likely represents the plesiomorphic condition of the family as this condition is also exhibited by the Cranoglanididae (Fig. 32B), the hypothesized sister group to Ictaluridae (Diogo 2004; Hardman 2005); †*Astephus* sp., a hypothesized stem ictalurid (Lundberg 1975; Grande and Lundberg 1988); as well as *Pylodictis olivaris*, an extant ictalurid. This suggests that the conditions in *I. punctatus* and *N. gyrinus* are both derived within the family. *Noturus gyrinus* possesses a single canal ossification with no underlying lamina of bone, a condition which appears to have evolved multiple times across Siluriformes (Table 1). As a result, this element is typically considered to be homologous to the single plate-like bone characteristic of the plesiomorphic condition of catfishes, a conclusion I agree with. The condition found in *I. punctatus* is rare among catfishes, and to my knowledge has only been observed in ictalurid catfishes of the genera *Ictalurus* and *Ameiurus*. Members of these genera possess two small bones in this region, one of which bears the sensory canal between the supraclithrum and the pterotic and the other one being plate-like. To date only a few studies (Allis 1904; Lundberg 1975; Arratia and Gayet 1995; Slobodian and Pastana 2018) have attempted to address the homology of these two elements in these ictalurids. Among these studies, two hypotheses have been proposed for the canal bearing bone: (1) it is homologous to the extrascapular (Arratia and Gayet 1995; Slobodian and Pastana 2018); or (2) it is homologous to the canal ossification of the posttemporal that has separated from the adjacent laminar portion of the posttemporal (Lundberg 1975). The homology of the additional-plate like bone is even less

certain, with each study reaching a different conclusion. This bone has been interpreted as either the parietal (Allis 1904), a laminar portion of the posttemporal separate from the adjacent canal bearing ossification (Lundberg 1975), a *de novo* ossification (Arratia and Gayet 1995), or the posttemporal in its entirety (Slobodian and Pastana 2018). Given the presence of a canal-bearing and an additional dermal bone in this region when compared to the remaining siluriforms, the homology of these two elements in *Ictalurus* and *Ameiurus* remains uncertain.

In the developmental series of *Ictalurus punctatus* examined herein, the canal bearing element is the first of the two elements to appear (~12.8 mm SL; Figs 5C, 6C) as a canal ossification lateral to the posterior margin of the chondrocranium. The additional plate-like bone appears later (~15.1 mm SL; Fig. 34A) as a thin sliver of bone at the anterior margin of the dorsal tip of the supraclithrum. As development continues, the additional plate-like bone covers and forms a close connection to the dorsal-tip of the supraoccipital and the canal ossification obtains an extension of laminar bone (Fig. 34B). Both proceed to expand until, in the adult skeleton (Fig. 8; Fig. 34C), the two elements become sutured to each other and the surrounding cranial elements and constitute a portion of the cranial roof. Together, both elements form the roof of the fossa which receives the dorsal tip of the supraclithrum, and occupy the same topographical region of the neurocranium as the posttemporal in the plesiomorphic condition of catfishes.

Based on the developmental series of *Ictalurus punctatus* examined herein, in addition to the association and location of the two elements in adult specimens, I narrow down the homology of these bones to two hypotheses: (1) the canal bearing element is homologous to the posttemporal and the additional plate-like bone represents a *de novo* ossification; or (2) the single posttemporal present in the plesiomorphic condition has become fragmented and is represented by two separate ossifications. Regardless of the hypothesis, the canal bearing element is interpreted as either the whole or part of the posttemporal due to it carrying the same sensory canal ossification as that observed in the single plate-like posttemporal of the plesiomorphic condition. This conclusion is in agreement with those of both Lundberg (1975) and Arratia and Gayet (1995), with the present hypothesis only differing from the latter in that they interpret the single-plate like element in the plesiomorphic condition of catfishes as the extrascapular rather than the posttemporal as concluded herein. The additional plate-like bone, despite occupying approximately the same area as the parietal in other ostariophysans and sharing relationships with several of the same elements, exhibits a topological relationship with the supraclithrum. This includes both the additional plate-like bone's origin of ossification, and eventual connection to the anterodorsalmost tip of the supraclithrum, which are not observed between the parietal and supraclithrum in other teleosts. This relationship between the additional plate-like element and the supraclithrum, however, is the same as that observed between the single plate-like posttemporal in its plesiomorphic condition (as

e.g., in *Diplomystes*, Fig. 32A) and the supracleithrum. This relationship and the position that both elements together occupy, match that of the single plate-like posttemporal and thus support the hypothesis that these two elements represent a posttemporal that has become fragmented into two separate ossification centers. However, there is simply not enough evidence in the material examined here to reject the possibility that the additional plate-like bone may represent a *de novo* ossification, which has assumed a relationship with the supracleithrum that matches the plesiomorphic relationship between the posttemporal and the anterodorsal tip of the supracleithrum in other catfishes. Based on this information, I suggest the term accessory posttemporal for the additional plate-like bone in *Ictalurus* and *Ameiurus*.

Finally, it is worth mentioning that the examination of the canal neuromasts in this region of select catfishes (Fig. 33) refutes Slobodian and Pastana's (2018) hypothesis that the canal bearing element in some ictalurids is homologous to the extrascapular. I also challenge their conclusion that number and arrangement of canal neuromasts are not variable between species of catfishes and therefore can be used to accurately determine the homology of the underlying bones, the basis for their homology proposition. Slobodian and Pastana (2018) posited that all catfishes that possess a single plate-like posttemporal (plesiomorphic condition) have three canal neuromasts associated with the pterotic, compared to other otophysans, which possess two neuromasts in the pterotic and a third in the extrascapular. Due to canal ossifications typically originating around canal neuromasts (e.g., see Webb and Shirey 2003) and the presence of the additional neuromast in the pterotic, they concluded that the extrascapular was not lost but instead fused to the pterotic. In contrast to their own hypothesis, Slobodian and Pastana (2018: Fig. 3) labeled the single element in this position of the neurocranium of *Pimelodella bockmanni* as the extrascapular rather than the posttemporal.

In ictalurids in which two elements are present in this region, Slobodian and Pastana (2018) inferred that the canal bearing element is the extrascapular, which remains an independent element based on the possession of the third neuromast of the postotic canal, and that the additional-plate like bone represents a posttemporal that has lost its connection to the sensory canal. Slobodian and Pastana's (2018) hypothesis was based not on their own observation of neuromasts directly but rather on the previous work of Allis (1904), Collinge (1895) and Herrick (1901), as well as the authors' assumption that "...lateral-line branches emerge between each lateral-line neuromast...". Interestingly, Allis's (1904) work was based primarily on the adult skeleton of *Ameiurus nebulosus*, which possesses the derived condition described above for *Ictalurus punctatus*, not the plesiomorphic condition observed in other catfishes. The other species directly observed by Allis, *Silurus glanis*, also does not possess the plesiomorphic condition but rather the pterotic articulates directly with the upper element of the shoulder girdle and there is no intervening element. Upon examination of the canal neuromasts in this area in a small number of cat-

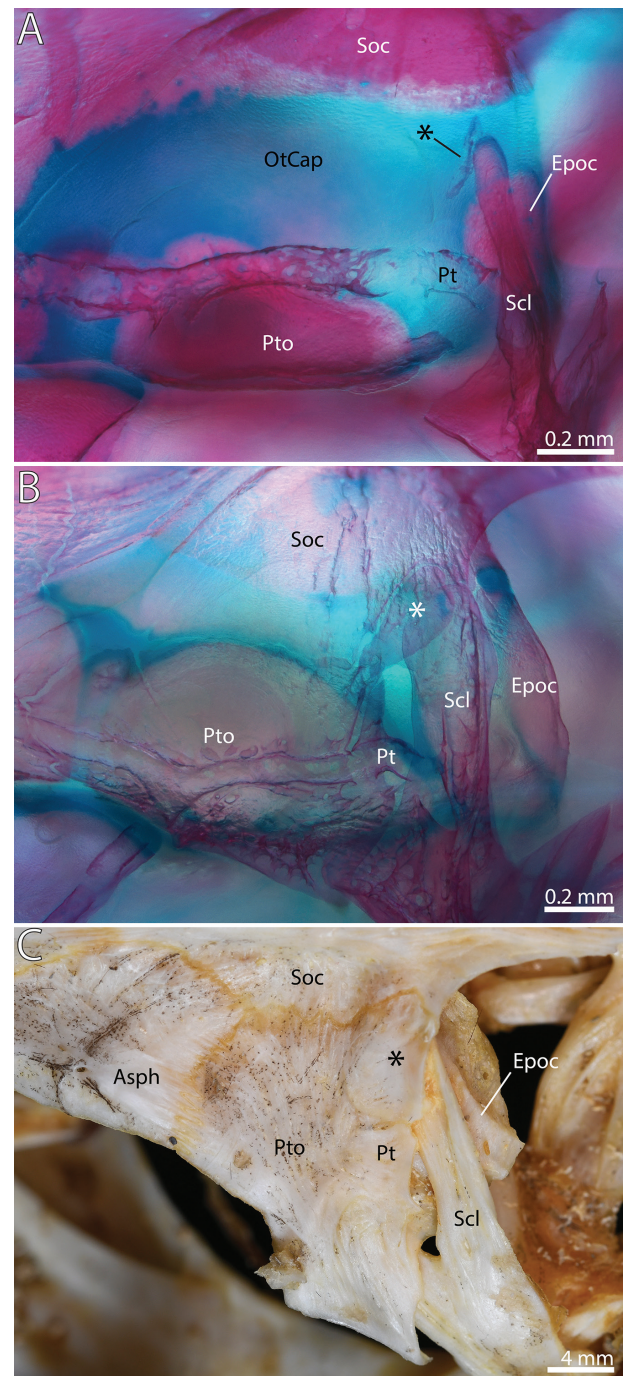


Figure 33. Ontogeny of the cranial bones associated with the articulation of the pectoral girdle of *Ictalurus punctatus*. **A** 15.4 mm SL. **B** 44.9 mm SL. **C** 441 mm SL. Abbreviations: *, Accessory posttemporal; Asph, Autosphenotic; Epoc, Epioccipital; Pt, Posttemporal; Pto, Pterotic; Scl, Supracleithrum; Soc, Supraoccipital.

fishes it is apparent that Slobodian and Pastana's (2018) hypothesis falls apart. I found that two species with the plesiomorphic plate-like posttemporal, *Pimelodus pictus* (Fig. 33A) and *Pylodictis olivaris* (Fig. 33B), that would be expected to have three neuromasts in their pterotic according to the hypothesis of Slobodian and Pastana (2018), do not, but rather differ in their number of canal neuromasts: three in *Pi. pictus* vs. two in *Py. olivaris*. Several studies on the cephalic lateral line canal system of

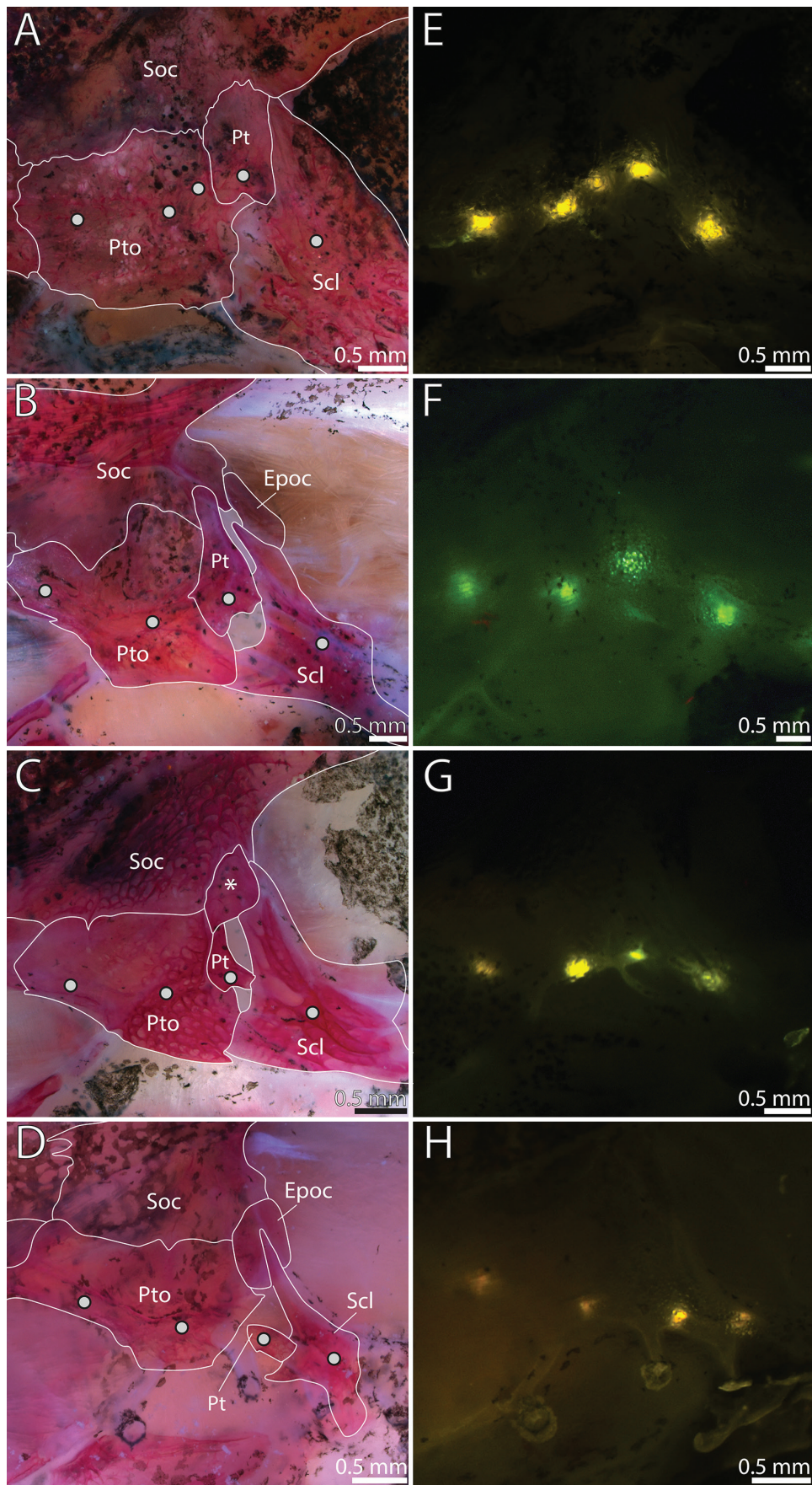


Figure 34. Neuromasts and associated cranial bones of select catfishes *Pimelodus pictus* (TCWC 20491.12, 42.0 mm SL; A,E), *Pylodictis olivaris* (TCWC 20490.04, 56.0 mm SL; B, F), *Ictalurus punctatus* (TCWC 20490.02, 60.0 mm SL; C, G) and *Noturus gyrinus* (TCWC 20490.03, 27.0 mm SL; D, H). **A–D** Cranial bones stained with alizarin red S. White dots correspond to canal neuromasts of E–H. **E–H** Canal neuromasts stained using 4-Di-2-ASP following Nakae et al. (2012). Abbreviations: *, Accessory posttemporal; Epoc, Epioccipital; Pt, Posttemporal; Pto, Pterotic; Scl, Supracleithrum; Soc, Supraoccipital.

non-catfishes have shown that the number of neuromasts between lateral-line branches (or pores) of a canal may be lower or higher than one (e.g., see figure 1 in Klein et al. 2013; figure 2 in Sumi et al. 2015; figs. 2, 6, 10 in Sato et al. 2017; figs. 2, 4 in Nakae et al. 2021). These facts refute Slobodian and Pastana's (2018) assumption that there is always one neuromast between two lateral-line branches. Additionally, *Py. olivaris* has the same number of canal neuromasts as the other ictalurids examined (*Ictalurus punctatus*, *Noturus gyrinus*, and *Ameiurus melas*; Fig. 33), despite the interspecific variation in these elements among members of the family. This suggests that neuromast number and the condition of associated bones in the skeleton are independent of one another and cannot be used on their own as the sole criterion to establish bone homology.

Coracoid. In teleosts, the scapulocoracoid cartilage typically gives rise to three separate ossifications, the dorsal scapula, ventral coracoid and medial mesocoracoid. The single endoskeletal element in the pectoral-girdle of catfishes has previously been assumed to represent the product of ontogenetic fusion between the three endochondral ossifications, based on comparisons of the adult skeleton (Stark 1930; Alexander 1966). Arratia (2003b), based on examination of a small developmental series of *Ictalurus punctatus*, observed only a single ossification within the scapulocoracoid cartilage, though in the supporting figure this ossification was shown to cover much of the lateral face of the cartilage. As reported by Arratia (2003b), in the material studied herein the element originates from a single center of ossification within the scapulocoracoid cartilage. Ossification starts in the *pars coracoidea* around the ventral arm of scapulocoracoid cartilage, which corresponds to the typical location of the coracoid in other teleosts. The ossification proceeds to spread posterodorsally to surround the portion of the scapulocoracoid cartilage in which the scapula typically ossifies, adjacent to the foramen for the passage of a branch of the pterygial nerve. A separate mesocoracoid is absent in both of the species of ictalurid examined herein and instead the 'mesocoracoid' arch forms from two separate extensions of the single ossification of the scapulocoracoid cartilage, one dorsal and one ventral, which meet and fuse. Given that only a single center of ossification is ever observed in the scapulocoracoid cartilage, there is no evidence for ontogenetic fusion between the scapula and the coracoid. Since ossification of this single element originates on the ventral arm of the *pars coracoidea*, a position occupied by the coracoid of other teleosts, it is herein interpreted in catfishes as being homologous to the coracoid which has expanded to also occupy the space of the scapula and mesocoracoid.

Dorsal-fin Spine 2. The soft dorsal-fin rays of teleosts typically consist of two separate segmented hemitrichia, the proximal bases of which articulate directly with the lateral surface of the distal radial that is in serial association with that fin ray. In many catfishes, the hemitrichia

and developing distal segments of the second dorsal-fin ray fuse into a lockable dorsal-fin spine. The proximal base halves of this dorsal-fin spine are also fused across the midline, and rather than articulating with a typical distal radial, form a foramen through which an ossified ring-like process of proximal-middle radial 3 passes, establishing in the dorsal-fin spine a "chain-link" articulation (*sensu* Bridge 1896). It has previously been hypothesized that the modification to the proximal base of the second dorsal-fin spine in catfishes is the result of fusion between the lateral hemitrichia and medial distal radial 2 in order to form the foramen through which the ring-like process of proximal radial 3 passes (Alexander 1966; Ballen and de Pinna 2021). At no point in the development of *Ictalurus punctatus* or *Noturus gyrinus* was a distal radial observed between the hemitrichial bases of dorsal-fin spine 2. Instead, medially directed processes which originate from the anteroproximal base of each hemitrichium, meet and fuse medially to form the foramen through which the ring-like process passes. Based on this observation, it is apparent that dorsal-fin distal radial 2 is lost and the "chain-link" articulation of catfishes is the result of modifications to the base of dorsal-fin spine 2 and proximal-middle radial 3.

Urohyal. The urohyal of teleosts is a median bone that originates in the tendons of the sternohyoideus muscle as a single ossification. The urohyal of catfishes differs from that of other teleosts in that it originates as two separate ossification centers, which fuse during development into a single element (Arratia and Schultze 1990). Additionally, the urohyal of loricarioid catfishes is a compound element of the tendon ossification of a typical siluriform urohyal and an ossification of the anterior basibranchial copula cartilage (Arratia and Schultze 1990; Geerinckx et al. 2007). Arratia and Schultze (1990) also interpreted this fusion as occurring in siluriform catfishes based on the observation of 'chondroid bone' fused to the dorsal portion of the urohyal in skeletonized material of adult individuals of ictalurids. This led them to refer to the element as the 'parurohyal' and proposed that it represented a synapomorphy of Siluriformes. In the developmental series examined herein for *Ictalurus punctatus* and *Noturus gyrinus*, the urohyal does originate as paired ossifications in the tendons of the sternohyoideus muscles, which later fuse into a single median element (see description of urohyal development in *I. punctatus*). As it develops, the urohyal forms a close articulation with the anterior tip of the anterior basibranchial copula; however, no ossification or subsequent fusion between the two elements was observed. Additionally, in adult individuals of *I. punctatus* (426–441 mm SL), no signs of 'chondroid bone' were observed in the cup-shaped process which articulates with the anterior basibranchial copula. As a result, the urohyal of ictalurids is comprised only of tendon bone, similar to the typical teleost condition, and does not represent a compound element as previously reported by Arratia and Schultze (1990). This may suggest that the compound nature of the urohyal in catfishes is restricted

to loricarioid catfishes, although more information on the development of this element across catfishes is required before any more general conclusions can be made.

Lacrimal. The infraorbital elements of teleosts are typically comprised of plates of dermal bone that carry the infraorbital sensory canal. In catfishes, the infraorbitals differ from the typical condition in that they are greatly reduced, represented by only simple tube-like ossifications around the infraorbital canal, except for the anteriormost infraorbital element. This bone has a laminar portion that carries the ossified canal. Homology of this anteriormost element still remains uncertain. Previous studies have referred to it as either infraorbital 1, or the lacrimal (Bamford 1948; Lundberg 1982), the antorbital (Arratia & Huaquín 1995), or as a compound element resulting from the fusion of the lacrimal and the antorbital (Kindred 1919; de Pinna et al. 2020). The anteriormost element of the infraorbital sensory canal in *Ictalurus punctatus* (Fig. 11) and *Noturus gyrinus* originates from a single ossification center that will make up part of the canal portion of this element. As the bone develops the canal becomes enclosed and an anterior and posterior projection of bone extend from the canal ossification forming the laminar portion of this element. At no point during development of this bone was there evidence of fusion between an autogenous canal and the laminar portion of bone, refuting the hypothesis that the element is compound in nature. Given that the canal ossification appears first, with the laminar portion subsequently developing from the canal ossification, the anterior element of the infraorbital series of catfishes is herein interpreted to represent the lacrimal and the antorbital is lost.

Acknowledgements

This study represents part of my doctoral dissertation conducted at Texas A&M University, under the direction of K. W. Conway. I would like to thank all members of my dissertation committee (including K. O. Wine-miller, G. Voelker, C. D. Marshall, and R. Britz) for their helpful advice and comments which have greatly improved the contents of this dissertation. I am grateful to B. Brown (AMNH), M. Sabaj (ANSP), O. Crimmen (BMNH), D. Catania (CAS), C. Dillman (CUMV), C. McMahan (FMNH), A. Bentley (KU), R. Feeney (LACM), H. Prestridge (TCWC), P. Harris (UAIC), D. Nelson (UMMZ), and J. Williams (USNM) for the loan of specimens and/or assistance with specimen curation. I also thank D. Gatlin III and B. Ray for providing access to eggs of *Ictalurus punctatus*, R. O'Hanlon, C. Mynatt, K. W. Conway, and A. K. Pinion for help in the collection of *Noturus gyrinus*. Additional thanks to K. W. Conway for help with histological sectioning, neuromast staining, and photography of skeletal preparations. I would also like to thank G. Mattox for critical comments and J. Lundberg for discussions that helped to improve the quality of this manuscript. Finally, I thank K. W. Conway and R. Britz for critical advice and countless discussions concerning all aspects of this study. This research was possible with funding from Texas A&M Agrilife Research (TEX09452 to K. W. Conway) and represents publication number 1664 of the TAMU BRTC and publication 08 of the TAMU Aquarium Research Facility.

References

- Adriaens D, Verraes W (1998) Ontogeny of the osteocranium in the African catfish, *Clarias gariepinus* Burchell (1822) (Siluriformes: Clariidae): ossification sequence as a response to functional demands. *Journal of Morphology* 235: 183–237. [https://doi.org/10.1002/\(SICI\)1097-4687\(199803\)235:3<183::AID-JMOR2>3.0.CO;2-8](https://doi.org/10.1002/(SICI)1097-4687(199803)235:3<183::AID-JMOR2>3.0.CO;2-8)
- Albert JS (2001) Species diversity and phylogenetic systematics of American knifefishes (Gymnotiformes, Teleostei). *Miscellaneous Publications of the Museum of Zoology University Michigan* 190: 1–127.
- Alexander RMcN (1966) Structure and function in the catfish. *Journal of Zoology* 148: 88–152. <https://doi.org/10.1111/j.1469-7998.1966.tb02943.x>
- Allis EP (1904) The latero-sensory canals and related bones in fishes. *Internationale Monatsschrift für Anatomie und Physiologie* 21: 401–503.
- Arratia G (1987) Description of the primitive family Diplomystidae (Siluriformes, Teleostei, Pisces): morphology, taxonomy and phylogenetic implications. *Bonner Zoologische Monographien* 24: 1–120
- Arratia G (1992) Development and variation of the suspensorium of primitive Catfishes (Teleostei: Ostariophysii) and their phylogenetic relationships. *Bonner Zoologische Monographien* 32: 1–149.
- Arratia G (2003a) Catfish head skeleton—an overview. In: Arratia G, Kapoor BG, Chardon M, Diogo R (Eds) *Catfishes*, vol.1. Science Publishers, Enfield, 3–46.
- Arratia G (2003b) The siluriform postcranial skeleton—an overview. In: Arratia G, Kapoor BG, Chardon M, Diogo R (Eds) *Catfishes*, vol.1. Science Publishers, Enfield, 121–158.
- Arratia G, Gayet M (1995) Sensory canals and related bones of tertiary siluriform crania from Bolivia and North America and comparison with recent forms. *Journal of Vertebrate Paleontology* 15: 482–505. <https://doi.org/10.1080/02724634.1995.10011243>
- Arratia G, Huaquín L (1995) Morphology of the lateral line system and of the skin of diplomystids and certain primitive loricarioid catfishes and systematic and ecological considerations. *Bonner Zoologische Monographien* 36: 1–110.
- Arratia G, Menu-Marque S (1981) Revision of the freshwater catfishes of the genus *Hatcheria* (Siluriformes, Trichomycteridae) with commentaries on ecology and biogeography. *Zoologischer Anzeiger* 207: 88–111.
- Arratia G, Schultze HP (1990) The urohyal: development and homology within osteichthyans. *Journal of Morphology* 203: 247–282. <https://doi.org/10.1002/jmor.1052030302>
- Arratia G, Schultze HP (1991) Palatoquadrate and its ossifications: development and homology within osteichthyans. *Journal of morphology* 208: 1–81. <https://doi.org/10.1002/jmor.1052080102>
- Arratia G, Chang GA, Menu-Marque SM, Rojas MG (1978) About *Bullockia* gen. nov., *Trichomycterus mendozensis* n. sp. and revision of the family Trichomycteridae (Pisces, Siluriformes). *Studies on Neotropical Fauna and Environment* 13: 157–194. <https://doi.org/10.1080/01650527809360539>
- Baird RC (1971) The systematics, distribution, and zoogeography of the marine hatchetfishes (family Sternoptychidae). *Bulletin of the Museum of Comparative Zoology* 142: 1–522.
- Ballen GA, de Pinna MC (2021) A standardized terminology of spines in the order Siluriformes (Actinopterygii: Ostariophysii). *Zoological Journal of the Linnean Society* 194: 601–625. <https://doi.org/10.1093/zoolinnean/zlab008>

- Ballen GA, Pastana MN, Peixoto LA (2016) A new species of *Farlowella* (Siluriformes: Loricariidae) of the *F. nattereri* species-group from the rio Xingu basin, Mato Grosso, Brazil, with comments on *Farlowella jauruensis*, a poorly-known species from the upper rio Paraguai basin. *Neotropical Ichthyology* 14: 517–524. <https://doi.org/10.1590/1982-0224-20160046>
- Bamford TW (1948) Cranial development of *Galeichthys felis*. *Proceedings of the Zoological Society of London* 118: 364–391. <https://doi.org/10.1111/j.1096-3642.1948.tb00383.x>
- Barbieri LR, dos Santos RP, Andreato JV (1992) Reproductive biology of the marine catfish, *Genidens genidens* (Siluriformes, Ariidae), in the Jacarepaguá Lagoon system, Rio de Janeiro, Brazil. *Environmental Biology of Fishes* 35: 23–35. <https://doi.org/10.1007/BF00001154>
- de Beer GR (1937) The development of the vertebrate skull. Clarendon Press, Oxford, 552 pp.
- Bird NC, Mabee PM (2003) Developmental morphology of the axial skeleton of the zebrafish, *Danio rerio* (Ostariophysi: Cyprinidae). *Developmental Dynamics* 228: 337–357. <https://doi.org/10.1002/dvdy.10387>
- Birindelli JL, Sousa LM, Pérez MHS (2008) New species of thorny catfish, genus *Leptodoras* Boulenger (Siluriformes: Doradidae), from Tapajós and Xingu basins, Brazil. *Neotropical Ichthyology* 6: 465–480. <https://doi.org/10.1590/S1679-62252008000300020>
- Block AJ, Mabee PM (2012) Development of the mandibular, hyoid arch and gill arch skeleton in the Chinese barb *Puntius semifasciolatus*: comparisons of ossification sequences among Cypriniformes. *Journal of Fish Biology* 81: 54–80. <https://doi.org/10.1111/j.1095-8649.2012.03307.x>
- Bridge TW (1896) The mesial fins of ganoids and teleosts. *Zoological Journal of the Linnean Society* 25: 530–602. <https://doi.org/10.1111/j.1096-3642.1896.tb00400.x>
- Bridge TW, Haddon AC (1893) Contributions to the anatomy of fishes. II. The airbladder and Weberian ossicles in the siluroid fishes. *Philosophical Transactions of the Royal Society of London B* 184: 66–333. <https://doi.org/10.1098/rsp1.1889.0038>
- Britz R, Conway KW (2009) Osteology of *Paedocypris*, a miniature and highly developmentally truncated fish (Teleostei: Ostariophysi: Cyprinidae). *Journal of Morphology* 270: 389–412. <https://doi.org/10.1002/jmor.10698>
- Britz R, Conway KW (2016) *Danionella dracula*, an escape from the cypriniform Bauplan via developmental truncation?. *Journal of morphology* 277: 147–166. <https://doi.org/10.1002/jmor.20486>
- Britz R, Hoffmann M (2006) Ontogeny and homology of the claustra in otophysan Ostariophysi (Teleostei). *Journal of Morphology* 267: 909–923. <https://doi.org/10.1002/jmor.10447>
- Britz R, Johnson GD (2012) Ontogeny and homology of the skeletal elements that form the sucking disc of remoras (Teleostei, Echeneidae). *Journal of Morphology* 273: 1353–1366. <https://doi.org/10.1002/jmor.20063>
- Britz R, Kottelat M (2003) Descriptive osteology of the family Chaudhuriidae (Teleostei, Synbranchiiformes, Mastacembeloidei), with a discussion of its relationships. *American Museum Novitates* 2003(3418): 1–62. [https://doi.org/10.1206/0003-0082\(2003\)418<0001:DOOTFC>2.0.CO;2](https://doi.org/10.1206/0003-0082(2003)418<0001:DOOTFC>2.0.CO;2)
- Britz R, Moritz T (2007) Reinvestigation of the osteology of the miniature African freshwater fishes *Cromeria* and *Grasseichthys* (Teleostei, Gonorynchiformes, Kneriidae), with comments on kneriid relationships. *Zoosystematics and Evolution* 83: 3–42. <https://doi.org/10.1002/mmzn.200600016>
- Britz R, Kakkassery F, Raghavan R (2014) Osteology of *Kryptoglanis shajii*, a stygobitic catfish (Teleostei: Siluriformes) from Peninsular India with a diagnosis of the new family Kryptoglanidae. *Ichthyological Exploration of Freshwaters* 24: 193–207.
- Brown BA, Ferraris CJ (1988) Comparative osteology of the Asian catfish family Chacidae: with the description of a new species from Burma. *American Museum Novitates* 1988(2907): 1–16.
- Carril J, Tambussi CP (2017) Skeletogenesis of *Myiopsitta monachus* (Psittaciformes) and sequence heterochronies in Aves. *Evolution & Development* 19: 17–28. <https://doi.org/10.1111/ede.12211>
- Calegari BB, Vari RP, Reis RE (2019) Phylogenetic systematics of the driftwood catfishes (Siluriformes: Auchenipteridae): a combined morphological and molecular analysis. *Zoological Journal of the Linnean Society* 187: 661–773. <https://doi.org/10.1093/zoolinnean/zlz036>
- Carvalho TP, Reis RE (2020) A New Miniature Species of *Acanthobunocephalus* (Siluriformes: Aspredinidae) from the Lower Purus River Basin, Amazon Basin, Brazil. *Copeia* 108: 347–357. <https://doi.org/10.1643/CI-19-309>
- Chranilov NS (1927) Beiträge zur Kenntnis des Weber'schen Apparates der Ostariophysi. 1. vergleichend-anatomische Übersicht der Knochenelemente des Weber'schen Apparates bei Cypriniformes. *Zoologische Jahrbücher, Abteilung für Anatomie* 49: 501–597.
- Coburn MM, Grubich PG (1998) Ontogeny of the Weberian apparatus in the armored catfish *Corydoras paleatus* (Siluriformes: Callichthyidae). *Copeia* (1998): 301–311. <https://doi.org/10.2307/1447426>
- Collinge WE (1895) On the sensory canal system of fishes. Teleostei – Suborder A. Physostomi. *Proceedings of the Zoological Society of London* 2: 274–298.
- Conway KW, Britz R (2007) Sexual dimorphism of the Weberian apparatus and pectoral girdle in *Sundadanio axelrodi* (Ostariophysi: Cyprinidae). *Journal of Fish Biology* 71: 1562–1570. <https://doi.org/10.1111/j.1095-8649.2007.01646.x>
- Conway KW, Kubicek KM, Britz R (2017) Morphological novelty and modest developmental truncation in *Barboides*, Africa's smallest vertebrates (Teleostei: Cyprinidae). *Journal of Morphology* 278: 750–767. <https://doi.org/10.1002/jmor.20670>
- Conway KW, Kubicek KM, Britz R (2021) Extreme evolutionary shifts in developmental timing establish the miniature *Danionella* as a novel model in the neurosciences. *Developmental Dynamics* 250: 601–611. <https://doi.org/10.1002/dvdy.280>
- Coombs S, Janssen J, Webb JF (1988) Diversity of lateral line systems: evolutionary and functional considerations. In: Atema J, Fay RR, Pospner AN, Tavolga WN (Eds) *Sensory biology of aquatic animals*, Springer, New York, 553–593.
- Copp GH, Robert Britton J, Cucherousset J, García-Berthou E, Kirk R, Peeler E, Stakénas S (2009) Voracious invader or benign feline? A review of the environmental biology of European catfish *Silurus glanis* in its native and introduced ranges. *Fish and Fisheries* 10: 252–282. <https://doi.org/10.1111/j.1467-2979.2008.00321.x>
- Cubbage CC, Mabee PM (1996) Development of the cranium and paired fins in the zebrafish *Danio rerio* (Ostariophysi, Cyprinidae). *Journal of Morphology* 229: 121–160. [https://doi.org/10.1002/\(SICI\)1097-4687\(199608\)229:2<121::AID-JMOR1>3.0.CO;2-4](https://doi.org/10.1002/(SICI)1097-4687(199608)229:2<121::AID-JMOR1>3.0.CO;2-4)
- Cumplido N, Allende ML, Arratia G (2020) From Devo to Evo: patterning, fusion and evolution of the zebrafish terminal vertebra. *Frontiers in Zoology* 17: 1–17. <https://doi.org/10.1186/s12983-020-00364-y>
- Diogo R (2004) Morphological Evolution, Adaptations, Homoplasies, Constraints, and Evolutionary Trends: Catfishes as a Case Study on

- General Phylogeny and Macroevolution. Science Publishers, Enfield, 491 pp.
- Dutra GM, Peixoto LAW, Abrahão VP, Wosiacki WB, Menezes NA, de Santana CD (2021) Morphology-based phylogeny of Eigenmanniinae Mago-Leccia, 1978 (Teleostei: Gymnotiformes: Sternopygidae), with a new classification. *Journal of Zoological Systematics and Evolutionary Research* 59: 2010–2059. <https://doi.org/10.1111/jzs.12535>
- Egge JJD (2007) The osteology of the stonecat, *Noturus flavus* (Siluriformes: Ictaluridae), with comparisons to other siluriforms. *Alabama Museum of Natural History Bulletin* 25: 71–89.
- Fink SV, Fink WL (1981) Interrelationships of the ostariophysan fishes (Teleostei). *Zoological Journal of the Linnean Society* 72: 297–353. <https://doi.org/10.1111/j.1096-3642.1981.tb01575.x>
- Fink WL (1985) Phylogenetic interrelationships of the stomiid fishes (Teleostei: Stomiiformes). *Miscellaneous Publications Museum of Zoology University of Michigan* 171: 1–127.
- Fricke R, Eschmeyer WN, Fong JD (2022) Species by Family/Subfamily. (<http://research.calacademy.org/research/ichthyology/catalog/SpeciesByFamily.asp>). Electronic version accessed 08 April 2022
- Friel JP, Lundberg JG (1996) *Micromyzon akamai*, gen. et sp. nov., a small and eyeless banjo catfish (Siluriformes: Aspredinidae) from the river channels of the lower Amazon basin. *Copeia* (1996): 641–648. <https://doi.org/10.2307/1447528>
- Fukushima M, Kohno H, Fujita K, Taki, Y (1992) Ontogenetic development of the Weberian apparatus in the bitterling, *Rhodeus ocellatus ocellatus*. *Journal of the Tokyo University of Fisheries* 79: 195–200.
- Geerinckx T, Brunain M, Adriaens D (2007) Development of the osteocranium in the suckermouth armored catfish *Ancistrus cf. tri-radiatus* (Loricariidae, Siluriformes). *Journal of Morphology* 268: 254–274. <https://doi.org/10.1002/jmor.10515>
- Goswami A, Weisbecker V, Sánchez-Villagra MR (2009) Developmental modularity and the marsupial-placental dichotomy. *Journal of Experimental Zoology Part B: Molecular and Developmental Evolution* 312: 186–195. <https://doi.org/10.1002/jez.b.21283>
- Grande L, Lundberg JG (1988) Revision and redescription of the genus *Astephus* (Siluriformes: Ictaluridae) with a discussion of its phylogenetic relationships. *Journal of Vertebrate Paleontology* 8: 139–171. <https://doi.org/10.1080/02724634.1988.10011694>
- Grande T, Shardo JD (2002) Morphology and development of the postcranial skeleton in the channel catfish *Ictalurus punctatus* (Ostariophysii: Siluriformes). *Field Museum of Natural History* 1518: 1–30.
- Hardman M (2005) The phylogenetic relationships among non-diplomyxid catfishes as inferred from mitochondrial cytochrome b sequences; the search for the ictalurid sister taxon (Otophysi: Siluriformes). *Molecular phylogenetics and evolution* 37: 700–720. <https://doi.org/10.1016/j.ympev.2005.04.029>
- Harrington SM, Harrison LB, Sheil CA (2013) Ossification sequence heterochrony among amphibians. *Evolution & Development* 15: 344–364. <https://doi.org/10.1111/ede.12043>
- Herrick CJ (1901) The cranial nerves and cutaneous sense organs of the North American silurid fishes. *Journal of Comparative Neurology and Psychology* 11: 177–249.
- Hilton EJ, Johnson GD (2007) When two equals three: developmental osteology and homology of the caudal skeleton in carangid fishes (Perciformes: Carangidae). *Evolution & Development* 9: 178–189. <https://doi.org/10.1111/j.1525-142X.2007.00148.x>
- Hoffmann M, Britz R (2006) Ontogeny and homology of the neural complex of otophysan Ostariophysii. *Zoological Journal of the Linnean Society* 147: 301–330. <https://doi.org/10.1111/j.1096-3642.2006.00220.x>
- Hubbs CL, Miller RR (1960) *Potamarius*, a new genus of ariid catfishes from the fresh waters of Middle America. *Copeia* (1960): 101–112. <https://doi.org/10.2307/1440202>
- Huysentruyt F, Adriaens D (2005) Descriptive osteology of *Corydoras aeneus* (Siluriformes: Callichthyidae). *Cybio* 29: 261–73.
- Huysentruyt F, Geerinckx T, Brunain M, Adriaens D (2011) Development of the osteocranium in *Corydoras aeneus* (Gill, 1858) Callichthyidae, Siluriformes. *Journal of Morphology* 272: 573–582. <https://doi.org/10.1002/jmor.10935>
- Ichiyanagi T, Kohno H, Fujita K (1997) Ontogenetic development of the Weberian ossicles in the bagrid catfish, *Pseudobagrus ichikawai*. *Journal of the Tokyo University of Fisheries* 84: 93–97.
- Jansen G, Devaere S, Weekers PHH, Adriaens D (2006) Phylogenetic relationships and divergence time estimate of African anguilliform catfish (Siluriformes: Clariidae) inferred from ribosomal gene and spacer sequences. *Molecular Phylogenetics and Evolution* 38: 65–78. <https://doi.org/10.1016/j.ympev.2005.09.011>
- Johnels AG (1957) The mode of terrestrial locomotion in *Clarias*. *Oikos* 8: 122–129. <https://doi.org/10.2307/3564996>
- Johnson GD (1983) *Niphon spinosus*: a primitive epinepheline serranid, with comments on the monophyly and intrarelationships of the Serranidae. *Copeia* (1983): 777–787. <https://doi.org/10.2307/1444346>
- Johnson GD, Washington BB (1987) Larvae of the Moorish idol, *Zanclus cornutus*, including a comparison with other larval acanthuroids. *Bulletin of Marine Science* 40: 494–511.
- Kaatz, IM, Stewart DJ, Rice AN, Lobel PS (2010) Differences in pectoral fin spine morphology between vocal and silent clades of catfishes (order Siluriformes): ecomorphological implications. *Current Zoology*, 56: 73–89. <https://doi.org/10.1093/czoolo/56.1.73>
- Katano O, Saitoh K, Koizumi A (1988) Scatter-spawning of the catfish, *Silurus asotus*. *Japanese Journal of Ichthyology* 35: 203–211. <https://doi.org/10.11369/jji1950.35.203>
- Keyte AL, Smith KK (2010) Developmental origins of precocial forelimbs in marsupial neonates. *Development* 137: 4283–4294. <https://doi.org/10.1242/dev.049445>
- Kiernan JA (1990) *Histological and histochemical methods: Theory and practice*. Pergamon Press, New York, 571 pp.
- Kindred J (1919) *The skull of Ameiurus*. Illinois Biological Monograph, 5: 1–120.
- Klein A, Münz H, Bleckmann H (2013) The functional significance of lateral line canal morphology on the trunk of the marine teleost *Xiphister atropurpureus* (Stichaeidae). *Journal of comparative physiology A* 199: 735–749. <https://doi.org/10.1007/s00359-013-0834-6>
- Kubicek KM, Conway KW (2016) Developmental osteology of *Sciaenops ocellatus* and *Cynoscion nebulosus* (Teleostei: Sciaenidae), economically important sciaenids from the western Atlantic. *Acta Zoologica* 97: 267–301. <https://doi.org/10.1111/azo.12122>
- Kubicek KM, Britz R, Conway KW (2019) Ontogeny of the catfish pectoral-fin spine (Teleostei: Siluriformes). *Journal of Morphology* 280: 339–359. <https://doi.org/10.1002/jmor.20947>
- Lundberg JG (1975) Homologies of the upper shoulder girdle and temporal region bones in catfishes (Order Siluriformes), with comments on the skull of the Helogeneidae. *Copeia* (1975), 66–74. <https://doi.org/10.2307/1442407>
- Lundberg JG (1975) The fossil catfishes of North America. *University of Michigan Museum of Paleontology, Papers on Paleontology* 11: 1–51.

- Lundberg JG (1982) The comparative anatomy of the toothless blindcat, *Trogloglanis pattersoni* Eigenmann, with a phylogenetic analysis of the ictalurid catfishes. Miscellaneous Publications of the Museum of Zoology University Michigan 163: 1–85.
- Lundberg JG, Baskin JN (1969) The caudal skeleton of the catfishes, order Siluriformes. American Museum Novitates 1969(2398): 1–49.
- Lundberg JG, Mago-Leccia F (1986) A review of *Rhabdolichops* (Gymnotiformes, Sternopygidae), a genus of South American freshwater fishes, with descriptions of four new species. Proceedings of the Academy of Natural Sciences of Philadelphia 138: 53–85.
- Lundberg JG, Hendrickson DA, Luckenbill KR, Mariangeles AH (2017) *Satan's* skeleton revealed: a tomographic and comparative osteology of *Satan eurystomus*, the subterranean Widemouth Blindcat (Siluriformes, Ictaluridae). Proceedings of the Academy of Natural Sciences of Philadelphia 165: 117–173. <https://doi.org/10.1635/053.165.0108>
- Lundberg JG, Sullivan JP, Rodiles-Hernández R, Hendrickson DA (2007) Discovery of African roots for the Mesoamerican Chiapas catfish, *Lacantunia enigmatica*, requires an ancient intercontinental passage. Proceedings of the Academy of Natural Sciences of Philadelphia 156: 39–53. [https://doi.org/10.1635/0097-3157\(2007\)156\[39:DOARFT\]2.0.CO;2](https://doi.org/10.1635/0097-3157(2007)156[39:DOARFT]2.0.CO;2)
- Mabee PM, Trendler TA (1996) Development of the cranium and paired fins in *Betta splendens* (Teleostei: Percomorpha): intraspecific variation and interspecific comparisons. Journal of Morphology 227: 249–287. [https://doi.org/10.1002/\(SICI\)1097-4687\(199603\)227:3<249::AID-JMOR1>3.0.CO;2-1](https://doi.org/10.1002/(SICI)1097-4687(199603)227:3<249::AID-JMOR1>3.0.CO;2-1)
- Maehata M (2007) Reproductive ecology of the Far Eastern catfish, *Silurus asotus* (Siluridae), with a comparison to its two congeners in Lake Biwa, Japan. Environmental Biology of Fishes, 78: 135–146. <https://doi.org/10.1007/s10641-006-9083-7>
- Mayden RL, Burr BM, Dewey SL (1980) Aspects of the life history of the Ozark madtom, *Noturus albater*, in southeastern Missouri (Pisces: Ictaluridae). American Midland Naturalist 104: 335–340. <https://doi.org/10.2307/2424874>
- Mattox GM, Britz R, Toledo-Piza, M (2014) Skeletal development and ossification sequence of the characiform *Salminus brasiliensis* (Ostariophysi: Characidae). Ichthyological Exploration of Freshwaters, 25: 103–158.
- Mattox GM, Britz R, Toledo-Piza, M (2016) Osteology of *Priocharax* and remarkable developmental truncation in a miniature Amazonian fish (Teleostei: Characiformes: Characidae). Journal of Morphology, 277: 65–85. <https://doi.org/10.1002/jmor.20477>
- McMurrich JP, (1884) On the osteology of *Amiurus catus* (L.) gill. Zoologisches Anzeiger 168: 296–299.
- Mistri A, Kumari U, Mittal S, Mittal AK (2018) Morphological specializations of the epidermis of an angler catfish *Chaca chaca* (Siluriformes, Chacidae) in relation to its ecological niche: A scanning electron microscopic investigation. Microscopy research and technique 81: 439–448. <https://doi.org/10.1002/jemt.22996>
- Nakae M, Asaoka R, Wada H, Sasaki K (2012) Fluorescent dye staining of neuromasts in live fishes: an aid to systematic studies. Ichthyological research, 59: 286–290. <https://doi.org/10.1007/s10228-012-0274-2>
- Nakae M, Kuroki M, Sato M, Sasaki K (2021) The lateral line system and its innervation in the Japanese eel *Anguilla japonica* (Teleostei: Elopomorpha: Anguillidae). Journal of Morphology, 282: 863–873. <https://doi.org/10.1002/jmor.21353>
- Nelson JS, Grande TC, Wilson MV (2016) Fishes of the World (5th ed.). John Wiley & Sons, Hoboken, 752 pp.
- Patterson C (1977) Cartilage bones, dermal bones and membrane bones, or the exoskeleton versus the endoskeleton. In: Andrews SM, Miles RS, Walker AD (Eds) Problems in Vertebrate Evolution. London: Academic Press, 77–121.
- Patterson C, Johnson GD (1995) The intermuscular bones and ligaments of teleostean fishes. Smithsonian Contributions to Zoology 559: 1–85.
- Paxton CGM (1997) Shoaling and activity levels in *Corydoras*. Journal of Fish Biology 51: 496–502. <https://doi.org/10.1111/j.1095-8649.1997.tb01507.x>
- Pinon AK, Siegel DS, Britz R, Martínez-García R, Álvarez-González CA, Conway KW (2021) The larval attachment organ of the tropical gar *Atractosteus tropicus* Gill, 1863 (Lepisosteiformes: Lepisosteidae). Journal of Fish Biology 99: 418–424. <https://doi.org/10.1111/jfb.14733>
- de Pinna MCC, Ng HH (2004) The second urol centrum in Siluriformes and its implication for the monophyly of superfamily Sisoroidea (Teleostei, Ostariophysi). American Museum Novitates, 2004: 1–23. [https://doi.org/10.1206/0003-0082\(2004\)437<0001:TSUCIS>2.0.CO;2](https://doi.org/10.1206/0003-0082(2004)437<0001:TSUCIS>2.0.CO;2)
- de Pinna MCC, Winemiller KO (2000) A new species of *Ammoglanis* (Siluriformes: Trichomycteridae) from Venezuela. Ichthyological Exploration of Freshwaters 11: 255–264.
- de Pinna MCC, Ferraris Jr CJ, Vari RP (2007) A phylogenetic study of the Neotropical catfish family Cetopsidae (Osteichthyes, Ostariophysi, Siluriformes), with a new classification. Zoological Journal of the Linnean Society 150: 755–813. <https://doi.org/10.1111/j.1096-3642.2007.00306.x>
- de Pinna MCC, Reis V, Britski H (2020) A new species of *Trichogenes* (Siluriformes, Trichomycteridae), with a discussion on the homologies of the anterior orbital bones in trichomycterids and other lorricarioids. American Museum Novitates 2020(3951): 1–27. <https://doi.org/10.1206/3951.1>
- Rao KS, Lakshmi K (1984) Head skeleton of the marine catfish *Arius tenuispinis* Day (Osteichthyes: Siluriformes, Ariidae). Journal of Morphology 181: 221–238. <https://doi.org/10.1002/jmor.1051810208>
- Reed HD (1924) The morphology and growth of the spines of siluroid fishes. Journal of Morphology 38: 431–451. <https://doi.org/10.1002/jmor.1050380306>
- Regan CT (1911) LXV.—The classification of the Teleostean fishes of the order Ostariophysi.—2. Siluroidea. Journal of Natural History 8: 553–577. <https://doi.org/10.1080/00222931108693067>
- Reiss JO (1989) The meaning of developmental time: a metric for comparative embryology. The American Naturalist 134: 170–189. <https://doi.org/10.1086/284974>
- Reynolds JD (1971) Biology of the small pelagic fishes in the New Volta Lake in Ghana: I. schooling and migrations. Hydrobiologia 38: 79–91. <https://doi.org/10.1007/BF00036795>
- Rodiles-Hernández R, Hendrickson DA, Lundberg JG, Humphries JM (2005) *Lacantunia enigmatica* (Teleostei: Siluriformes) a new and phylogenetically puzzling freshwater fish from Mesoamerica. Zootaxa 1000: 1–24. <https://doi.org/10.11646/zootaxa.1000.1.1>
- Sabaj MH (2020) Codes for natural history collections in ichthyology and herpetology. Copeia 108: 593–669. <https://doi.org/10.1643/ASIHCODONS2020>
- Sánchez-Villagra MR, Goswami A, Weisbecker V, Mock O, Kuratani S (2008) Conserved relative timing of cranial ossification patterns in early mammalian evolution. Evolution & Development 10(5): 519–530. <https://doi.org/10.1111/j.1525-142X.2008.00267.x>

- Sato M, Asaoka R, Nakae M, Sasaki K (2017) The lateral line system and its innervation in *Lateolabrax japonicus* (Percoidae: *incertae sedis*) and two apogonids (Apogonidae), with special reference to superficial neuromasts (Teleostei: Percomorpha). *Ichthyological Research*, 64: 308–330. <https://doi.org/10.1007/s10228-016-0568-x>
- Schultze HP, Arratia, G (2013) The caudal skeleton of basal teleosts, its conventions, and some of its major evolutionary novelties in a temporal dimension. *Mesozoic Fishes* 5: 187–246.
- Slobodian V, Pastana MN (2018) Description of a new *Pimelodella* (Siluriformes: Heptapteridae) species with a discussion on the upper pectoral girdle homology of Siluriformes. *Journal of Fish Biology* 93: 901–916. <https://doi.org/10.1111/jfb.13795>
- Sørensen W (1890) Om Forbeninger i Svømmeblaeren, Pleura og Aortas Vaeg og Sammelsmeltning deraf med Hvirvelsøjlen saerlig hos Siluroiderne, samt de saakaldte Weberske Knoglers Morfologi. *Det Kongelige Danske Videnskabernes Selskabs Skrifter*, 6 Raekke, Naturvidenskabelig og Matematisk Afdeling VI 2: 1–88.
- Srinivasachar HR (1958) Development of the skull in catfishes. V. Development of skull in *Heteropneustes fossilis* (Bloch). *Proceedings of the National Institute of Sciences India* 24B: 165–190.
- Starks EC (1930) The primary shoulder girdle of the bony fishes. Stanford University Publications, University Series, Biological Sciences 6: 147–239.
- Sumi K, Asaoka R, Nakae M, Sasaki K (2015) Innervation of the lateral line system in the blind cavefish *Astyanax mexicanus* (Characidae) and comparisons with the eyed surface-dwelling form. *Ichthyological Research* 62: 420–430. <https://doi.org/10.1007/s10228-015-0458-7>
- Tavolga WN (1962) Mechanisms of sound production in the ariid catfishes *Galeichthys* and *Bagre*. *Bulletin of the American Museum of Natural History* 124: 1–30. <http://hdl.handle.net/2246/1211>
- Taylor WR (1967) An enzyme method of clearing and staining small vertebrates. *Proceedings of the United States National Museum* 122: 1–17.
- Taylor WR (1969) A revision of the catfish genus *Noturus* Rafinesque with an analysis of higher groups in the Ictaluridae. *Bulletin of the United States National Museum* 282: 1–315.
- Taylor WR, Van Dyke GC (1985) Revised procedures for staining and clearing small fishes and other vertebrates for bone and cartilage study. *Cybiurn* 9: 107–119.
- Tencatt LFC, Ohara WM (2016) Two new species of *Corydoras* Lacépède, 1803 (Siluriformes: Callichthyidae) from the rio Madeira basin, Brazil. *Neotropical Ichthyology* 14(1): 139–154. <https://doi.org/10.1590/1982-0224-20150063>
- Tyler JC (1980) Osteology, phylogeny, and higher classification of the fishes of the order Plectognathi (Tetraodontiformes). NOAA (National Oceanic and Atmospheric Administration) Technical Report NMFS (National Marine Fisheries Service) Circular 434: 1–422.
- Vanscoy T, Lundberg JG, Luckenbill KR (2015) Bony ornamentation of the catfish pectoral-fin spine: comparative and developmental anatomy, with an example of fin-spine diversity using the Tribe Brachyplatystomini (Siluriformes, Pimelodidae). *Proceedings of the Academy of Natural Sciences of Philadelphia* 164: 177–212. <https://doi.org/10.1635/053.164.0107>
- Vigliotta TR (2008) A phylogenetic study of the African catfish family Mochokidae (Osteichthyes, Ostariophysi, Siluriformes), with a key to genera. *Proceedings of the Academy of Natural Sciences of Philadelphia* 157: 73–136. [https://doi.org/10.1635/0097-3157\(2008\)157\[73:APSOTA\]2.0.CO;2](https://doi.org/10.1635/0097-3157(2008)157[73:APSOTA]2.0.CO;2)
- Walker MB, Kimmel CB (2007) A two-color acid-free cartilage and bone stain for zebrafish larvae. *Biotechnic & Histochemistry* 82: 23–28. <https://doi.org/10.1080/10520290701333558>
- Webb JF, Shirey JE (2003) Postembryonic development of the cranial lateral line canals and neuromasts in zebrafish. *Developmental Dynamics* 228: 370–385. <https://doi.org/10.1002/dvdy.10385>
- Weitzman SH (1962) The osteology of *Brycon meeki*, a generalized characid fish, with an osteological definition of the family. *Stanford Ichthyological Bulletin* 8: 1–77.
- Werneburg I, Sánchez-Villagra MR (2015) Skeletal heterochrony is associated with the anatomical specializations of snakes among squamate reptiles. *Evolution* 69: 254–263. <https://doi.org/10.1111/evo.12559>